Zirconia-Supported Iron-Based Fischer-Tropsch Catalysts

Influence of Pressure and Potassium on Structure and Catalytic Properties

Fe/ZrO_2 Fischer-Tropsch Katalysatoren

Invloed van Druk en Kalium op Struktuur
en Katalytische Eigenschappen

(met een samenvatting in het Nederlands)

Proefschrift

ter verkrijging van de graad van doctor aan de Universiteit Utrecht op gezag van de rector magnificus, Prof. dr. W.H. Gispen, ingevolge het besluit van het College voor Promoties in het openbaar te verdedigen
op donderdag 10 mei 2001 des middags te 12:45 uur
door

Frans Richard van den Berg

Geboren op 14 mei 1972 te Ijsselmuiden

Promotor: Prof.dr.ir. J.W. Geus
verbonden aan de faculteit Scheikunde van de Universiteit Utrecht

Co-promotor: Dr. A.M. van der Kraan
verbonden aan het Interfacultair Reactor Instituut van de TU Delft

The Shell Research and Technology Center, Amsterdam is gratefully acknowledged for financially supporting the research described in this thesis.

‘La sperienza non falla mai, ma sol fallano i nostri giudizi promettendosi di quella effetto tale che in e nostri experimenti causati non sono.’

Niccolò Machiavelli 1469-1527

‘De ervaring bedriegt nooit, slechts onze beoordeling faalt als ze een dusdanig effect verwacht dat niet veroorzaakt is in onze experimenten.’

voor Elize
voor Gioia

CIP-GEGEVENS KONINKLIJKE BIBLIOTHEEK, DEN HAAG

Berg, Frans Richard van den

Zirconia-Supported Iron-Based Fischer-Tropsch Catalysts: Influence of Pressure and Potassium on Structure and Catalytic Properties / Frans R. van den Berg – Utrecht: Universiteit Utrecht, Faculteit Scheikunde
Thesis Universiteit Utrecht. – With ref. – With summary in Dutch
ISBN 90-393-2705-X
Subject headings: Fischer-Tropsch synthesis/ iron / zirconia / light olefins / ethene / propene / heterogeneous catalysis

Contents

1

General Introduction

1.1 Introduction

1.1.1 Historical background

Before World War II the production of industrial organic compounds was mainly based on coal. Coking of coal leads to coal tar, which provides aromatic compounds, and a gas, which contains ethylene and propylene besides hydrogen, carbon monoxide and other compounds. For a period of time before World War II research concentrated on the production of chemicals from acetylene. A range of processes has been developed to produce organic compounds, such as, acrylonitrile and monovinylchloride, from acetylene. However, the energy-intensive production of acetylene from calcium carbide asking is too expensive. The development of alternative processes for the production of acetylene, such as, the Wulff process, has also not been successful [4].

After World War II large amounts of light hydrocarbons became available in the U.S.A. due to the increasing consumption of natural gas for raising thermal energy. The low content of higher hydrocarbons of many natural gas deposits in the U.S.A. is sufficient to provide the chemical industry in the U.S.A. with a cheap feedstock for the production of light olefins. Consequently huge steam crackers have been installed to thermally dehydrogenate light hydrocarbons to olefins, while olefins became the feedstock of choice for a large range of organic chemicals. In Europe – where initially the consumption of gasoline for transport purposes was relatively low, since export of gasoline to the U.S.A. was legally prohibited – (light virgin) naphta was employed as a feedstock to produce light olefins in very large naphta-steam crackers. Presently also condensates from natural gas (e.g., from Algeria) are being processed in European naphta-steam crackers as well as gasoil to produce light olefins [4].

Olefins are presently one of the most important feedstocks to produce chemicals. Some important examples are polyethylene, polypropylene, and polyvinylchloride as well as special elastomers, which are being manufactured from ethylene and propylene. Acrylonitril (the fibre intermediate for another important polymer) is produced from propylene and ammonia. Also acetaldehyde and vinylacetate are being manufactured from ethylene. Finally, we mention the production of ethylene oxide, from which a wide range of chemicals is prepared, by selective oxidation of ethylene.

Although the production of light olefins from condensates of natural gas and naphta has been considerably optimised and exhibits the great advantage of

being executed in very large units, an alternative cheap feedstock can offer large advantages. The most obvious alternative feedstock is methane, which is abundantly available at sites globally more widely distributed than crude oil reserves. Hydrocarbons – produced from methane through an intermediate conversion into hydrogen and carbon monoxide – are an interesting feedstock for naphta(-steam) crackers. However, direct production of light olefins from hydrogen and carbon monoxide is much more attractive. This thesis therefore deals with the production of (light) olefins from carbon monoxide and hydrogen.

1.1.2 The Fischer-Tropsch Synthesis

The conversion of synthesis gas or syngas, a mixture of CO and H_2, into mainly hydrocarbons is known as the Fischer-Tropsch synthesis. This synthesis is named after Franz Fischer and Hans Tropsch, who published about the production of hydrocarbons over cobalt catalysts already in the early twenties [1-3]. To produce liquid transport fuels from coal, which is abundantly available in Germany in contrast to crude oil, much research was performed on the Fischer-Tropsch process before World War II. Just for the beginning of World War II it was found that at pressures of 15 to 20 bar iron can also be employed as a catalyst. However, the standard Fischer-Tropsch catalyst used during the war to produce transport fuels from coal was based on cobalt supported by Kieselguhr and containing thorium oxide and magnesia as promotors. Two different processes for the production of liquid hydrocarbons from coal were employed during World War II. Besides the Fischer-Tropsch process, which generally operates at temperatures from 423 to 573 K and pressures up to about 20 bar, the direct hydrogenation of coal with hydrogen to liquid hydrocarbons was performed in the Bergius process. The latter process was performed at 773 K and a hydrogen pressure of no less than 700 bar.

After World War II South Africa, that also has much coal and no crude oil, set up Fischer-Tropsch plants that are still successfully operated. Sasol, the South African company that is operating the coal gasification and Fischer-Tropsch plants, executes the Arge process and the Synthoil process. With the Arge process higher boiling hydrocarbons, such as diesel oil or waxes, are produced. This process is performed in a fixed bed reactor with a supported copper-iron catalyst, for example. The Synthoil process generates lower boiling hydrocarbons such as gasoline, acetone and alcohols. In the Synthoil process the iron-based catalyst, which is analogous to the double-promoted iron catalyst used in the ammonia synthesis, is recirculated. The synthesis gas, the mixture of carbon monoxide and

hydrogen, for the Fischer-Tropsch units is produced in large Lurgi gasifiers, in which the coal is gasified in a moving bed by reaction with steam and oxygen.

Since the Fischer-Tropsch synthesis is much more expensive than products (or derivatives) obtained by oil refineries, the synthesis is not able to compete with the oil refineries. For this reason, the interest for the Fischer-Tropsch process has increased enormously in the past decades. Nowadays, the production of liquid hydrocarbons from methane instead of coal is considered. First of all, production of liquid fuels from methane leads to a lower dependence on crude oil, the reserves of which are concentrated in a limited number of areas in the world. Another important reason for the production of liquid fuels from methane is limitation of the emission of carbon dioxide by flaring of methane being released during the production of crude oil. The synthesis gas is produced by partial oxidation or catalytic partial oxidation, in which methane reacts with pure oxygen to carbon monoxide and hydrogen. When heat generated by the reaction of methane with oxygen is employed to provide the heat of the reaction of methane and steam, the process is known as autothermal reforming. In the production of synthesis gas for the ammonia synthesis, the heat of the reaction of steam with methane is generated out of the reactor and transferred to the reactants mainly by radiation. The conventional methane-steam reforming process, however, provides a gas flow of which the hydrogen-to-carbon monoxide ratio is too elevated for the Fischer-Tropsch process, which calls for a molar hydrogen-to-carbon monoxide ratio slightly larger than about 2.

Presently, Koninklijke/Shell operates a gas-phase Fischer-Tropsch process, in which the considerably heat of the reaction is removed through the walls of a very large number of fairly thin metal tubes. The technology is taken from that of the production of ethylene oxide, in which a reactor is employed having about 20,000 tubes of a length of about 20 m. The Koninklijke/Shell process, the Shell middle distillate synthesis or SMDS process [6], is executed in Maleysia, where natural gas is abundantly available. To suppress the formation of methane as much as possible, the SMDS process produces initially high molecular waxes which are subsequently thermally cracked to diesel fuel. Presently, Koninklijke/Shell is seriously considering the construction of a second, considerably larger SMDS plant. Other companies, first of all Sasol, but also for instance Exxon, Statoil and Chevron, are aiming at a liquid-phase process in which the catalyst is suspended within the liquid resulting from the Fischer-Tropsch reaction. With a liquid the heat of the reaction can be transferred more easily out of the reactor. However, separation of the catalyst from the reaction products and prevention of an ongoing reaction of hydrogen remaining in the filter cake of the catalyst to undesired

methane are problems with the liquid-phase process. With the technical application of a liquid-phase Fischer-Tropsch process, Sasol – which has a very long-standing experience with this process – has made the greatest progress.

The Fischer-Tropsch reaction is represented in the following equations,

$$n\,CO + (2n+1)\,H_2 \longrightarrow C_nH_{2n+2} + n\,H_2O \quad (1.1)$$

$$n\,CO + 2n\,H_2 \longrightarrow C_nH_{2n} + n\,H_2O \quad (1.2)$$

in which Equation 1.1. relates to the production of paraffins and Equation 1.2 to that of olefins. Alcoholic products can also be formed either as by-products or as main product depending on the catalytically active metal and the pressure. A whole range of products with different lengths of the carbon chain can be obtained. The conventional fuel names and compositions known from crude oil refinery processes are listed in Table 1.1.

Table 1.1 *Conventions of fuel names and composition [4].*

Name	Synonyms	Components
Fuel gas		C_1-C_2
LPG		C_3-C_4
Gasoline		C_5-C_{12}
Naphtha		C_8-C_{12}
Kerosene	Jet Fuel	C_{11}-C_{13}
Diesel	Fuel oil	C_{13}-C_{17}
Middle distillates	Light gas oil	C_{10}-C_{20}
Soft wax		C_{19}-C_{23}
Medium wax		C_{24}-C_{35}
Hard wax		C_{35+}

Two important side reactions generally also proceed during the process, *viz.*, the water gas shift conversion reaction and the Boudouard reaction. The former involves reaction of carbon monoxide with water, which is formed during the reaction (Equation 1.1 and 1.2), to hydrogen and carbon dioxide.

$$CO + H_2O \rightleftharpoons CO_2 + H_2 \quad (1.3)$$

The water gas shift conversion can be favourable for the Fischer-Tropsch synthesis starting with CO-rich synthesis gas as is obtained from gasification of

coal or heavy oil fractions through partial oxidation (H_2/CO molar ratio approximately 1). The water gas shift conversion raises the H_2/CO ratio. In contrast, synthesis gas or syngas produced from natural gas initially already possesses a high H_2/CO ratio. Hence, the hydrogen-to-carbon monoxide ratio can become undesirably elevated due to the water gas shift conversion [5].

The second side reaction mentioned above is the Boudouard reaction. This reaction occurs preferably on the active metal surface and involves the conversion of carbon monoxide into carbon dioxide leaving carbon behind on the surface (Equation 1.4)

$$2\ CO \longrightarrow CO_2 + C. \qquad (1.4)$$

The carbon deposition can eventually lead to deactivation by, for example, blocking of active sites, disintegration of the catalyst bodies or plugging of the reactor by formation of very strong carbon fibrils.

The most commonly known active metals employed to predominantly produce paraffins and/or olefins in the Fischer-Tropsch process are Ni, Fe, Co and Ru. The metals exhibit some distinct differences in catalytic behavior. On nickel surfaces the ratio of adsorbed hydrogen and carbon is relatively high, which results in the production of mainly methane [27]. Moreover, at higher temperatures methane is exclusively produced. Analogous to nickel-based catalysts, Ru-based catalysts display predominantly reaction to methane. Among the four metals mentioned, ruthenium is the most active catalyst and, accordingly, Ru is already active at temperatures as low as 423 K. However, its high price and low abundance excludes industrial application. In contrast, cobalt catalysts have been employed commercially for a long period of time to provide long-chain hydrocarbons (mainly paraffinic products). Subsequent hydrocracking of the waxes formed leads to highly pure, desirable products [6, 7].

Also iron-based catalysts are commercially utilised for the production of hydrocarbons [8, 9]. Since the H/C at the surface is relatively low, the hydrogenation activity is low. Hence both olefins and paraffins can be formed selectively. For this reason iron is the most suitable metal to catalyse the formation of lower olefins (C_2-C_4). In the following the considerations for lower olefin production are discussed, particularly focussing on thermodynamics, kinetics, process conditions and required catalyst properties.

1.2 Thermodynamic considerations

Thermodynamics indicates that a compromise must be found between the formation of light olefins and that of two undesired products, *viz.*, methane and carbon [10-12]. Small-chain hydrocarbon products become more favourable at higher temperatures. Consequently, under Fischer-Tropsch conditions, the favourable methane is predicted to be the predominant product. As indicated, at higher temperatures the selectivity to methane will increase. Above Furthermore, carbon deposition according to the Boudouard reaction will contribute increasingly to the equilibrium composition with increasing temperature.

Thermodynamics also predicts that at equilibrium predominantly paraffins are present. However, under normal reaction conditions equilibrium is attained only slowly enabling the formation of olefins. The rate at which the thermodynamic equilibrium is established depends on the properties of the used catalyst and on the reaction conditions [10-12]. Before these parameters are dealt with, a kinetic model will be described. This model will provide insight in the maximum selectivity of light (C_2-C_4) products.

1.3 Anderson-Schulz-Flory distribution

Anderson was the first to introduce a kinetic model for the Fischer-Tropsch reaction [13]. This model was deduced from a polymerisation model proposed by Schulz [14] and Flory [15]. Nowadays, it is referred to as the Anderson-Schulz-Flory (ASF) mechanism. Initially, CO and H_2 are dissociatively adsorbed on the active surface and, after recombination, a CH_2-species results. Starting from C_1, CH_2 building blocks can be continuously inserted, eventually resulting in a C_n species at the surface. The hydrocarbon chain can be terminated by either hydrogenation leading to alkanes or hydrogen abstraction resulting in alkenes. The chain growth probability (α) for a CH_2 monomer insertion to a hydrocarbon chain is defined as the ratio of the propagation rate (k_p) and the sum of the propagation and termination (k_t) rates (Equation 1.5).

$$\alpha = \frac{k_p}{k_p + k_t} \qquad (1.5)$$

It is empirically established that α is generally independent on the chain size [11]. However, for very small chains, *i.e.* C_1 and C_2, the independence is not obeyed [16].

The Anderson-Schulz-Flory distribution is described by the following Equation.

$$\log(\frac{W_n}{n}) = 2\log(\ln(\alpha)) + n\log\alpha \qquad (1.6)$$

In this formula W_n is the weight fraction of chains with n carbons and n represents the carbon number. When the logarithm of the relative weight fraction ($\log(W_n/n)$ is plotted against the carbon number, the chain growth probability can be determined from the slope of the straight line.

The ASF distribution allows us to calculate the maximum C_2 to C_4 fraction, which can be formed during reaction. This is visualised in Figure 1.1, in which α is plotted against the selectivity. From this Figure it can be seen that the maximum selectivity to methane is reached at very low values for α. The maximum C_2-C_4 fraction is found at an α-value of approximately 0.5. The maximum production of C_2-C_4 hydrocarbons is about 56% of the total yield. As already mentioned C_1 and C_2 normally do not follow the ASF distribution kinetics; the methane fraction is somewhat higher and the C_2 fraction is lower than predicted by the model [16].

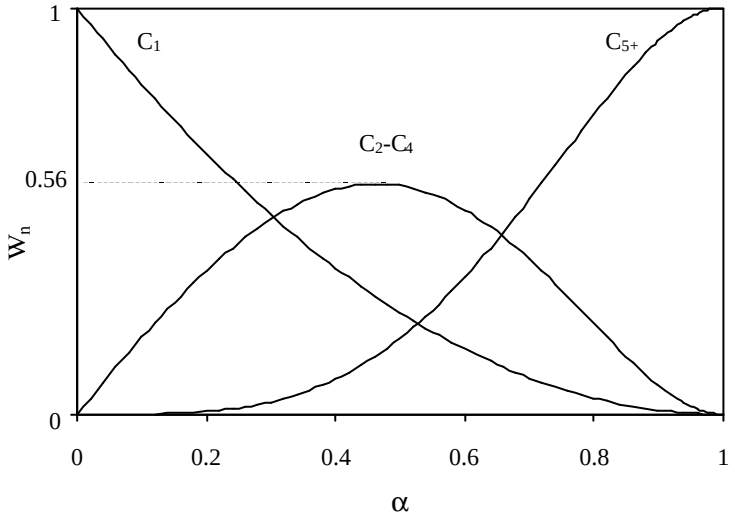

Figure 1.1 Product selectivity of ASF distribution limits

The aforementioned maximum is an important restriction to the maximal light olefin production. The parameters influencing the olefin selectivity will be discussed in the following sections. These parameters can be divided in two types *viz.* process variables and catalyst parameters. The former will be dealt with first.

1.4 Process variables

In literature, process variables, like pressure, temperature, H_2/CO ratio and space velocity, are known to influence the olefin selectivity [11, 12, 16, 17]. The selectivity to olefins increases at low pressure, high temperature, low H_2/CO ratio and high space velocity. At low total pressures, establishment of the thermodynamic equilibrium will proceed more slowly, while at equilibrium mainly paraffins are present (*vide supra*). As thermodynamic considerations as described previously indicate, that at high temperatures the formation of shorter chains, and especially of methane, is favoured. Experimentally this phenomenon is always observed. The formation of shorter hydrocarbons is attributed to a higher hydrogenation activity resulting in a decrease of α. Changing the H_2/CO ratio leads to different proportion of both adsorbed hydrogen and surface-carbon. At a lower ratio the hydrogenation activity will decrease resulting in a higher olefin selectivity. A larger space velocity generally leads to a lower conversion level, which results in an improvement of the olefin selectivity.

1.5 Catalyst properties

Next to process variables, the morphology and chemical structure of the catalyst used can also enhance the olefin selectivity [11, 16, 18]. The basicity of the catalyst, the dispersion of the active metal, and the interaction of the active species with the support can raise the selectivity to olefins. In the following, these factors will be discussed subsequently.

From the experience with the catalyst for the dehydrogenation of ethylbenzene to styrene, the iron oxide-chromium oxide catalyst, it is known that the presence of potassium oxide on oxidic surfaces suppresses the deposition of carbon. Accordingly, the presence of potassium oxide on the surface of the zirconia support may prevent the migration of carbonaceous material from the iron surface to the surface of the support. Potassium oxide on the surface of zirconia thus may raise the amount of carbon on or within the surface of the supported iron particles

and, hence, decrease the hydrogenation activity and increase the selectivity to olefins. Consequently, longer hydrocarbon chains will be produced.

Another possibility to change the chemisorption properties of H_2 and CO is adjusting the dispersion of the iron phase. When the diameter of the iron particles is smaller than 5 nm the H_2/CO ratio at the surface will decrease. The effect of the size of the iron particles is due to the fact that foreign atoms can penetrate in between metal surface atoms much more readily with small particles. With extended metal close-packed surface penetration of foreign atoms in between the metal surface atoms asks for lifting of metal atoms to positions above the surface, which leads to loss of intermetallic bonding energy. With small metal surfaces on small metal particles, the metal surface atoms can shift sidewards without an appreciable loss in intermetallic bonding energy. Accordingly, dissociation of carbon monoxide – which calls for penetration of carbon and oxygen atoms in between the metal surface atoms – will be promoted on very small metal particles. For this reason, on small metal particles the ratio of adsorbed hydrogen and carbon atoms will be relatively low, which leads to a higher olefin selectivity. An additional reason to prefer small iron particles for a catalyst aimed at a high production of olefins is the fact that small metal particles are not liable to be encapsulated by graphite layers and to induce the growth of carbon nanofibers. Nucleation of graphite does not proceed on the very small flat planes of small metal particles, while graphite layers cannot assume the high curvature of the surface of small metal particles.

The last property to be mentioned here is the interaction of the metal phase with the support. According to Ponec [18], the carrier can change the geometry of the active phase or it can create new centres which have different chemical properties. A possibility mentioned in his article is migration of a reduced titania species onto the surface of (titania-supported) precious metal catalysts, which has been generally accepted as the cause of the strong metal-support interaction.

1.6 Research Strategy

As discussed in the previous paragraph the ability to produce light olefins is heavily dependent on the catalyst design. The active metal, the support, the dispersion and the promotor employed determine the design of a catalyst.

As the active metal, iron is chosen for its ability to dissociatively adsorb CO faster than H_2, which is enhanced on small iron particles. Consequently, iron is able to produce unsaturated hydrocarbons better than any other metal. However, iron also deactivates more easily due to surface segregation of graphitic layers.

Analogous to very small nickel particles, the growth of graphite layers on very small (iron) particles is enormously reduced [19, 20]. Filamentous carbon is only observed with metal particles of a size exceeding about 8 nm [21, 22]. Highly dispersed catalysts thus can be expected to exhibit a better stability towards surface-segregation of graphitic layers and carbon fibril growth.

The required high dispersion should be stabilised by the support. Stabilisation could be achieved by a suitable metal-support interaction, which only partially involves the active iron particles and does not deactivate the active species. Furthermore, the support of choice should not interact with the employed promoter so as to diminish its promoting effect. The support of choice in this thesis is zirconia (ZrO_2). Zirconia is not known to pronouncedly interact with alkali metals, while it has been suggested that zirconia interacts with iron [23-26]. However, only catalytic systems with bimodal distributions of sizes of iron particles have been described. In literature, it is also suggested that ZrO_2 changes the catalytic properties of the iron particles. However, the catalytic properties have not been extensively studied. Moreover, the Fischer-Tropsch synthesis was only performed at atmospheric pressure [26]. To achieve iron particles of a uniform small size evenly distributed over a zirconia support, we will employ low loadings of the support with iron. Potassium oxide was chosen to promote the active metal, since it has been reported to raise the production of olefins.

1.7 Scope of this thesis

The scope of this thesis is to design a catalyst which is capable of directly and selectively producing light olefins via the Fischer-Tropsch synthesis. Based on the above considerations, highly dispersed zirconia-supported iron-based catalysts are synthesised. For reasons of comparison the properties of both unpromoted and potassium-promoted catalysts were studied. From the investigations presented in this thesis it will be shown that the catalytic properties do not only depend on the design of the catalyst, but also on the reaction conditions and, possibly more importantly, on the pre-treatment before exposure to the reaction conditions. Especially, the reduction of the supported iron precursor will be considered as well as the possibility of re-oxidation of metallic iron by water at lower temperatures. Thermodynamically a low water vapour pressure is required for the reduction of iron oxide to metallic iron. As the transport of water – strongly adsorbing to the surface of oxidic supports in contrast to hydrogen – out of the pore system of highly porous supports proceeds very slowly, the partial pressure of water cannot be readily decreased within bodies of porous catalytic supports.

It is essential to elaborately investigate the behaviour of the applied catalysts during the pre-treatment procedure prior to the Fischer-Tropsch reaction and the reaction itself.

In order to investigate highly dispersed iron-based catalysts, the preparation of an unpromoted and potassium-promoted zirconia-supported catalyst is described in Chapter 2. In this chapter, it will be demonstrated that the employed calcination temperature is very important for obtaining highly dispersed and monodisperse iron-based catalysts.

Prior to the Fischer-Tropsch reaction the catalyst will generally be reduced in a hydrogen-rich environment. Chapter 3 deals with this reduction behaviour of both the promoted and unpromoted catalysts at ambient as well as at elevated pressure. It is shown that reduction proceeds faster at elevated pressures. Moreover, the presence of a potassium species enhances the reduction of the iron oxide. It is further demonstrated that water plays a prominent role during reduction and that carbon is still present after the preparation step. This chapter will also provide evidence for the existence of a mixed oxide of iron and the zirconia support. This mixed oxide appears to be capable of stabilising small iron particles, although eventual formation of large metallic iron particles cannot be prevented.

Following reduction the catalysts are exposed to Fischer-Tropsch conditions. The nature of the iron species present during this reaction is extensively studied using in situ Mössbauer spectroscopy. In chapter 5 the results of the in situ measurements both at 1 and 9.5 bar are presented. Subsequently, Chapter 6 deals with the activity and selectivity of both promoted and unpromoted catalysts. In this chapter the activity and selectivity are compared in a nanoflow reactor (containing about 40 mg of catalyst). The catalytic behaviour of the potassium-rich catalyst was more extensively investigated at a larger scale (microflow reactor).

In chapter 3 it is assessed that an intimate interaction of the active iron metal with the support exists. This interaction seems to be desirable due to its ability to stabilise small metallic iron particles. This stabilisation may be improved by increasing the amount of the mixed oxide, which can be established by a treatment in H_2/H_2O atmosphere. The influence of such a treatment is described in chapter 4.

In a final chapter 7, the results presented in the above chapters are summarised and some concluding remarks are given.

1.8 References

[1] F. Fischer and H. Tropsch, *Brennstoff-Chem.* **4** (1923) 276.

[2] F. Fischer and H. Tropsch, *Brennstoff-Chem.* **7** (1926) 97.
[3] F. Fischer and H. Tropsch, *Brennstoff-Chem.* **11** (1930) 489.
[4] I. Kroschwitz,; M. Howe-Grant, *Kirk-Othmer Encyclopedia of Chemical Technology*, Wiley & Sons, New York, 4th ed., 1996.
[5] H. Schulz, *Appl.Cat. A:General* **186** (1999) 3.
[6] S.T. Sie, M.M.G. Senden H.M.H. van Wechum, *Catal.Today* **8** (1991), 371.
[7] B. Eisenberg, R.A. Fiato, C.H. Mauldin, G.R. Ray and R.L. Soled, *Stud.Surf.Sci.Catal.* **119** (1998) 943.
[8] R.L. Espinoza, A.P. Steynberg, B. Jager and A.C. Vosloo, *Appl.Catal. A:General* **186** (1999), 13.
[9] A.P. Steynberg, R.L. Espinoza, B. Jager and A.C. Vosloo, *Appl.Catal. A:General,* **186** (1999) 41.
[10] R.B. Anderson, *'The Fischer-Tropsch Synthesis'*,Academic Press, Inc. Orlando, 1984.
[11] R. Snel, *Catal.Rev.-Sci.Eng.* **29(4)** (1987) 361.
[12] M.E. Dry, in *'Catalysis Science and Technology'*, eds. J.R. Anderson and M. Boudart, Vol. 1, Springer Verlag, 1981, Chapter 4.
[13] R.A. Friedel and R.B. Anderson, *J.Am.Chem.Soc.* **72** (1950) 2307.
[14] G.V. Schulz, *Z.Phys.Chem.* **B30** (1935) 379; G.V. Schulz, *Z.Phys.Chem.* **B32** (1936), 27.
[15] P.J. Flory, *J.Am.Chem.Soc.* **58** (1936) 1877.
[16] G.P. van der Laan and A.A.C.M. Beenackers, *Catal.Rev.-Sci.Eng.* **41(3-4)** (1999) 255.
[17] M. Janardanarao, *Ind.Eng.Chem.Res.* **29** (1990) 1735.
[18] V. Ponec, in *'Metal Support and Metal-Additive Effects in Catalysis'*, eds. B.Imelik et al., Elsevier Sci.Publ.Comp., Amsterdam, 1982, 63.
[19] F. van Looij, PhD. thesis, Utrecht University, 1994.
[20] V. Ponec, *Adv.Catal.* **32** (1983) 149.
[21] W. Teunissen, Ph.D. thesis, Utrecht University, 2000.
[22] P.H. de Bokx, A.J.H.M. Kock, E. Boellaard, E. Klop and J.W. Geus, *J.Catal.* **96** (1985) 468.
[23] L.A. Boot, A.J. van Dillen, J.W. Geus and F.R. van Buren, *J.Catal.* **163** (1996) 186.
[24] E. Guglielminotti, *J.Phys.Chem.* **98** (1994) 4884.
[25] E. Guglielminotti, *J.Phys.Chem.* **98** (1994) 9033.
[26] K. Chen, Y. Fan, Z. Hu and Q.Yan, *Catal.Lett.* **36** (1996) 130.
[27] J. van de Loosdrecht, , Ph.D. thesis, Utrecht University, 1995.

2

Synthesis of Highly Dispersed Zirconia-Supported Iron-Based Catalysts

Abstract

In this chapter, zirconia-supported iron-based catalysts were prepared using the incipient wetness impregnation technique. The choice of the precursor, in this case a chelating citrate, and the final distribution of the precursor on the zirconia support depends on the applied calcination temperature. Several techniques reveal that both an unpromoted and a potassium-promoted catalyst can be prepared, of which the iron(III) oxide exhibits a high dispersion and is, moreover, monodisperse.

2.1 Introduction

The preparation method used in this study is the incipient wetness impregnation technique. Very crucial and complex in this procedure is the drying procedure, which mainly determines the final distribution of the precursor within the bodies of the support. Several aspects of the drying step have been described in detail elsewhere [1, 2]. Despite the fact that it is difficult to obtain a (macroscopically) homogeneous distribution of the precursor throughout pre-shaped support bodies, earlier studies have shown that establishment of such a distribution is indeed viable [1, 3, 4].

An important parameter is the tendency of the precursor to crystallize. If the precursor crystallizes readily, small particles of the precursor are immediately (before drying) created at the external edge of the support bodies. During drying, micropores are created by early precursor deposition at the edge of the support body. This drives the solution to these pores due to capillary forces. Consequently, the dissolved precursor is forced to preferably deposit at the external edge. If the precursor is very soluble, it will only crystallize when most of the precursor solution is evaporated. During the drying process, the solvent is mainly evaporated at the external edge of the catalyst body, whereat the increasing precursor concentration eventually results in crystallization. In both cases described above, the drying step leads to an egg-shell distribution of the precursor [1].

In the above examples the crystallisation process is assumed to be only dependent on the precursor concentration. Additionally, the viscosity of the (drying) precursor solution is another important property. A viscosity which increases during the drying step leads to immobilisation of the precursor. Terörde [5] has demonstrated that addition of hydroxy ethyl cellulose (H.E.C.) to the precursor solution improves the macroscopic distribution and, furthermore, can change the crystallization properties of an easily crystallizing salt. Another possibility to raise the viscosity of the solution of the precursor during drying is the use of an organic chelating salt as a precursor. Van de Brink [1] unambiguously showed that good macroscopic distributions and high (microscopic) dispersions could be obtained using such chelating precursors, such as, ammonium iron(III) citrate. Terörde [5] studied the viscosity during drying of an iron(III) nitrate and of an ammonium iron(III) citrate solution. The latter chelating salt exhibits a steep increase in viscosity during drying, whereas the viscosity of the simple salt remains constant. Immobilisation of the chelating salt during drying thus may lead to a homogeneously distributed, highly disperse catalytic system.

While Terörde and Van de Brink mainly investigated silica supports, Chen and coworkers [6] employed zirconia supports. These authors prepared their catalyst by impregnation of a solution of a ferric nitrate precursor. Based on results obtained from Mössbauer spectroscopy and X-ray diffraction, they concluded that the particle size distribution of the iron phase was bimodal containing particles larger than 12 nm beside smaller particles. Taking into account that the nitrate precursor is highly soluble and is not immobilised during drying (no viscosity increase during drying [5]), the formation of such relatively large particles are not surprising. As mentioned above, a better dispersion can be obtained when an organic chelating precursor is used. Boot [4, 9] studied potassium-promoted and unpromoted zirconia-supported iron catalysts using ammonium iron(III) citrate as a precursor. For both the promoted and the unpromoted catalyst he obtained good macroscopic distributions. On a microscopic scale, however, several techniques showed that a bimodal distribution of sizes of iron oxide particles resulted. Mössbauer spectroscopy indicated the presence of relatively large particles which even exceeded 12 nm.

As discussed previously [11], small iron particles are liable to directly and selectivity produce light olefins via the Fischer-Tropsch synthesis. Such very small iron particles are furthermore advantageous, since they are not liable to be encapsulated within graphitic layers or to grow carbon nanofibers that disintegrate the catalyst bodies. The objective of this study is to prepare a catalytic system having a very high dispersion of the active iron phase. In order to assess whether small iron particles are present on the zirconia support, several analysing techniques are employed. We will demonstrate that a lower calcination temperature is beneficial for preparing a highly dispersed and monodisperse catalyst system.

2.2 Experimental

2.2.1 Catalyst preparation

The catalyst was prepared by means of incipient wetness impregnation. The pre-shaped support material used was zirconia (Norton XZ16075). The zirconia extrudates possessed a pore volume of 0.28 ml/g and a specific surface area of 49 m^2/g. Ammonium iron(III) citrate (Merck, 28% Fe) was employed as precursor to obtain a calculated iron loading of 2.5 wt%. The potassium-promoted catalyst was prepared by co-impregnation of ammonium iron(III) citrate and

potassium carbonate; an atomic ratio Fe/K of 1 was applied. For Mössbauer measurements, a citrate complex enriched with the ^{57}Fe isotope was prepared in order to shorten the long measuring times. After impregnation the loaded support was dried at 350 K within flowing air, and subsequently calcined at 723 K for 2 hours (heating rates were 5 K/min). The thus calcined catalysts are referred to as freshly prepared catalysts.

2.2.2 Characterisation

2.2.2.1 X-ray diffraction (XRD)

X-ray diffraction measurements were performed on an Enraf Nonius PDS120 X-ray Powder Diffractometry System. Co $K_{\alpha 1,2}$ radiation having a wavelength of 1.78897 Å was used. The samples were crushed very finely prior to the measurements.

2.2.2.2 Transmission electron microscopy (TEM)

Samples were ground in a mortar and dispersed in ethanol via ultrasonic vibration. This suspension was brought onto a holey carbon film, which was supported by a copper grid. Transmission electron microscopy was performed using a Philips CM 30 T electron microscope operated at 300 kV with a LaB_6 filament as the electron source.

2.2.2.3 Mössbauer absorption spectroscopy (MAS)

Mössbauer measurements were carried out in a constant acceleration mode using a ^{57}Co in Rh source. Isomer shifts are reported relative to the NBS standard sodium nitroprusside ($Na_2Fe(CN)_5NO.2H_2O$). Magnetic hyperfine fields were calibrated with the 515 kOe field of α-Fe_2O_3 at room temperature. The Mössbauer parameters were determined by fitting the spectra with subspectra consisting of Lorentzian-shaped lines using a non-linear iterative minimization routine. The accuracy for the isomer shift (I.S.) is ±0.03 mm/s, for the electric quadrupole splitting (Q.S.) ±0.05 mm/s, and for the spectral contribution (S.C.) 5%.

The measurements were performed at ambient pressure using an in situ Mössbauer reactor described in more detail in [10]. The freshly prepared

unpromoted and potassium-promoted catalysts were measured at various temperatures, *viz.*, 4, 77 and 300 K.

2.2.2.4 Thermogravimetry

To assess the amount of carbon that was left behind from the citrate precursor after the calcination, samples of the Fe/ZrO_2 and the $Fe/K/ZrO_2$ catalyst were heated in a PerkinElmer thermobalance from room temperature to 1123 K. A flow of carefully dried air was passed through the thermobalance. The gas flow out of the thermobalance was analyzed with a mass-spectrometer (Fisons).

2.3 Results and discussion

2.3.1 Transmission electron microscopy and x-ray diffraction of Fe/ZrO_2

For comparison both pure and loaded (but unpromoted) zirconia were investigated. The pure ZrO_2 is very crystalline as is demonstrated by the long-range ordering of the lattices (Figure 2.1 clearly shows fringes indicating the atomic layers). Note that all ZrO_2 particles exhibit smooth surfaces.

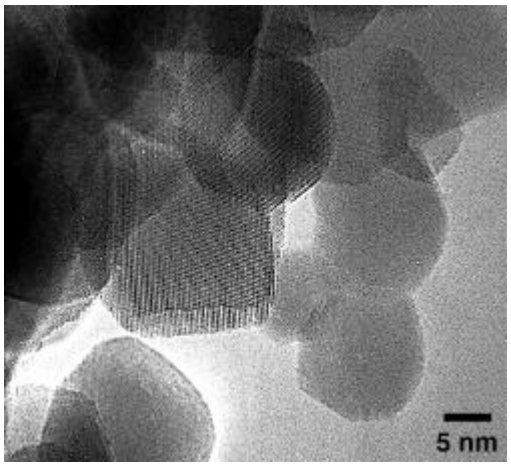

Figure 2.1 TEM image of pure ZrO_2.

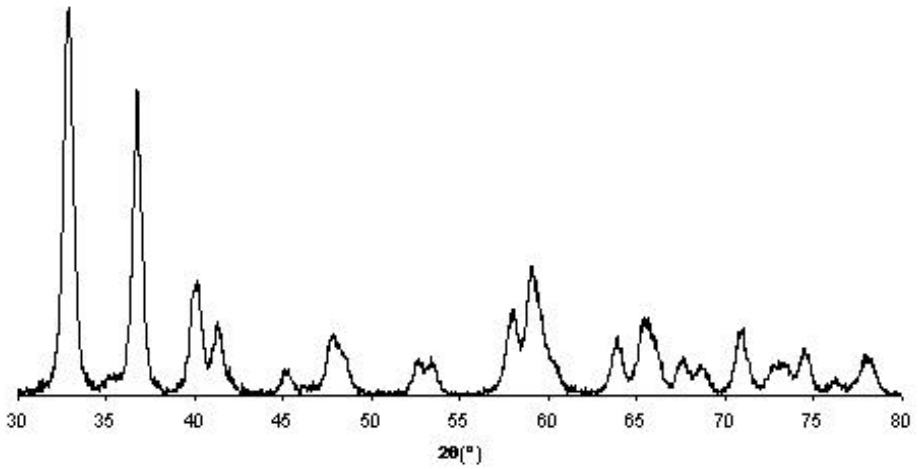

Figure 2.2 X-ray diffraction pattern of freshly prepared 2.5 wt% Fe/ZrO_2.

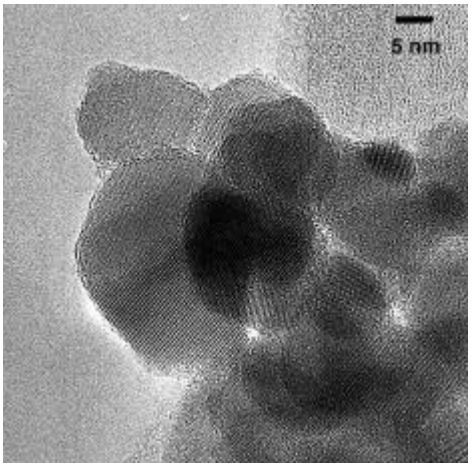

Figure 2.3 TEM image of freshly prepared 2.5 wt% Fe/ZrO_2..

X-ray diffraction shows the ordering of the zirconia to be purely monoclinic [7]; the diffraction profile of the freshly prepared Fe/ZrO_2 catalyst – as represented in Figure 2.2 – demonstrates the crystallinity of the zirconia support. The X-ray diffraction patterns of the loaded support after calcination indicate no

sign of a long-range ordered iron oxide. The iron oxide species is therefore present as either relatively small (beyond the detection limit, which is below approximately 3 nm) particles or it is amorphous.

Figure 2.3 shows a transmission electron micrograph of the calcined zirconia support loaded with iron oxide. Also in this figure the lattice fringes of the support are clearly visible. The surface of the zirconia crystallites exhibits a very thin amorphous layer of approximately 1 nm in contrast to the images of the pure support. Energy-dispersive analysis of the emitted X-rays (EDX) shows that the thin layer contains iron. Studying the specimen of the calcined iron-loaded zirconia at a large number of different spots did not reveal the presence of larger crystalline iron oxide particles. The absence of crystalline iron oxide agrees with the X-ray diffraction results, which do not show any sign of large crystalline iron oxide. It can therefore be concluded that the iron oxide is present in the catalyst within a thin amorphous layer on the crystallites of the zirconia support.

However, when the iron oxide loading is used to calculate the thickness of the amorphous layer, a different value results. For convenience, the density of crystalline α-Fe_2O_3 (ρ = 5.24 g/cm^3) was taken for the density of the iron containing layer. A value of approximately 0.15 nm results for the thickness of this layer. Even after adjusting for an amorphous iron oxide compound, the experimental thickness cannot be reproduced.

The amorphous layer being thicker than can be accounted for by the iron oxide loading may be due to an inhomogeneous distribution of the iron oxide over the crystallites of the zirconia support or to the iron oxide layer incompletely covering the zirconia crystallites. An inhomogeneous distribution of the iron oxide over the zirconia can be ruled out. Investigation of randomly taken samples at low magnification in either the light microscope or the scanning electron microscope did not reveal any inhomogeneity. The presence of flat patches of a thickness of about 1 nm not completely covering the zirconia crystallites of the support is more difficult to exclude based on the images taken in the transmission electron microscope. The amorphous layer is most evident at spots in the specimen where the surface of zirconia crystallites is oriented essentially parallel to the electron beam. Superposition of flat patches of amorphous iron oxide in the image may suggest the presence of a continuous amorphous layer.

In the next chapter, it is proposed that during the thermal pre-treatment at 723 K the carbon of the citrate is incompletely removed during calcination. The thermal pre-treatment therefore leads to a presumably porous layer of intimately

mixed iron oxide and carbon of a uniform thickness on the zirconia support. The carbon remaining after the thermal pre-treatment effectively prevents formation of crystalline iron oxide particles sufficiently large to show up in X-ray diffraction patterns or displaying diffraction contrast in transmission electron micrographs.

2.3.2 Mössbauer absorption spectroscopy

2.3.2.1 Fe/ZrO_2

Figure 2.4 shows Mössbauer spectra of the unpromoted zirconia-supported iron oxide catalyst at different temperatures. All measured spectra reveal a doublet.

The Mössbauer parameters derived from spectra measured at 300, 77 and 4.2 K are presented in Table 2.1. The doublet can be assigned to high spin Fe^{3+}. The absence of a hyperfine splitting at low temperatures points to the presence of either a superparamagnetic or a paramagnetic iron oxide. If a superparamagnetic phase is present, the dispersion of the iron oxide must be high.

Table 2.1 Mössbauer parameters of fresh 2.5 wt% Fe/ZrO_2 at different temperatures.

T (K)	I.S. (mm/s)	Q.S. (mm/s)	Γ (mm/s)	S.C. (%)	Compound
300	0.60	0.99	0.57	100	Fe^{3+}
77	0.72	1.00	0.57	100	Fe^{3+}
4.2	0.73	1.04	0.81	100	Fe^{3+}

The assumption of a high dispersion of the iron oxide is justified by the size of the quadrupole splitting. Since this splitting depends on the electric field gradient, it is a measure for the (a)symmetry of the environment of the iron ions. Van der Kraan [8] concluded that the quadrupole splitting for iron ions present in the surface of α-Fe_2O_3 is higher than for iron ions present in the interior of the oxide, *viz.*, 0.92 ± 0.04 mm/s and 0.52 mm/s, respectively. We observed a value of 0.99 mm/s, which closely resembles the quadrupole splitting of surface ions. Hence, the iron phase in our catalyst exhibits a large fraction of surface ions. These observations are in perfect agreement with the TEM results, which reveal a very thin amorphous layer of intimately mixed small iron oxide particles and carbon.

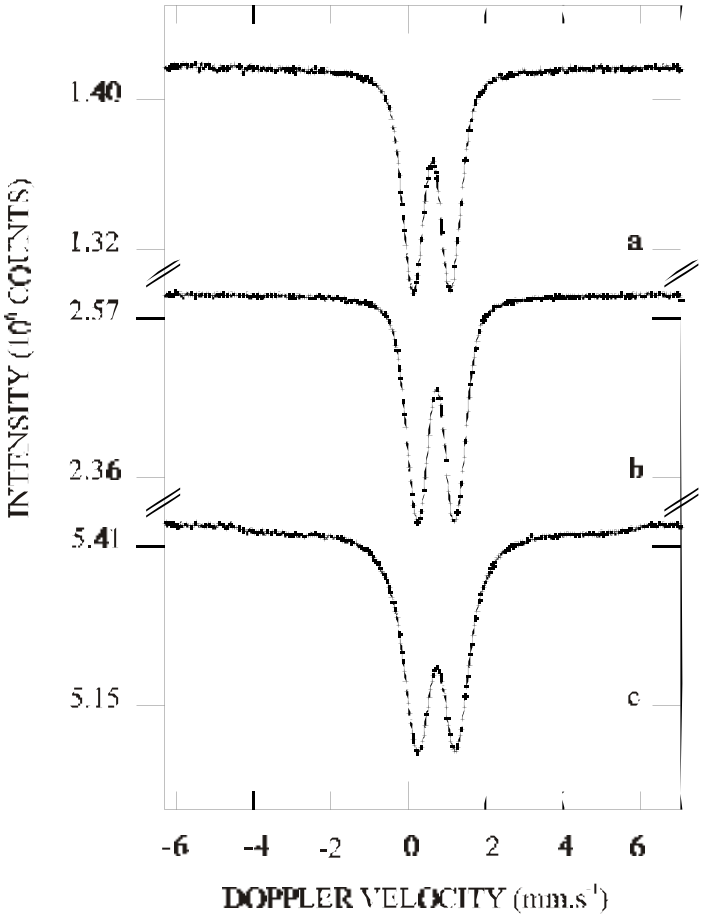

Figure 2.4 *Mössbauer spectra measured at (a) 300, (b) 77 and (c) 4.2 K of freshly prepared zirconia-supported iron oxide containing 2.5 wt% Fe/ZrO_2.*

2.3.2.2 Fe/K/ZrO_2

Table 2.2 and Figure 2.5 represent the Mössbauer parameters and spectra, respectively, of the potassium-promoted catalyst.

Analogous to the doublet shown by the unpromoted catalyst the doublet present in Figure 2.5 can be assigned to high spin Fe^{3+}. Moreover, the absence of a

distinct sextuplet points to a homogeneous and highly disperse distribution of the iron oxide over the zirconia support.

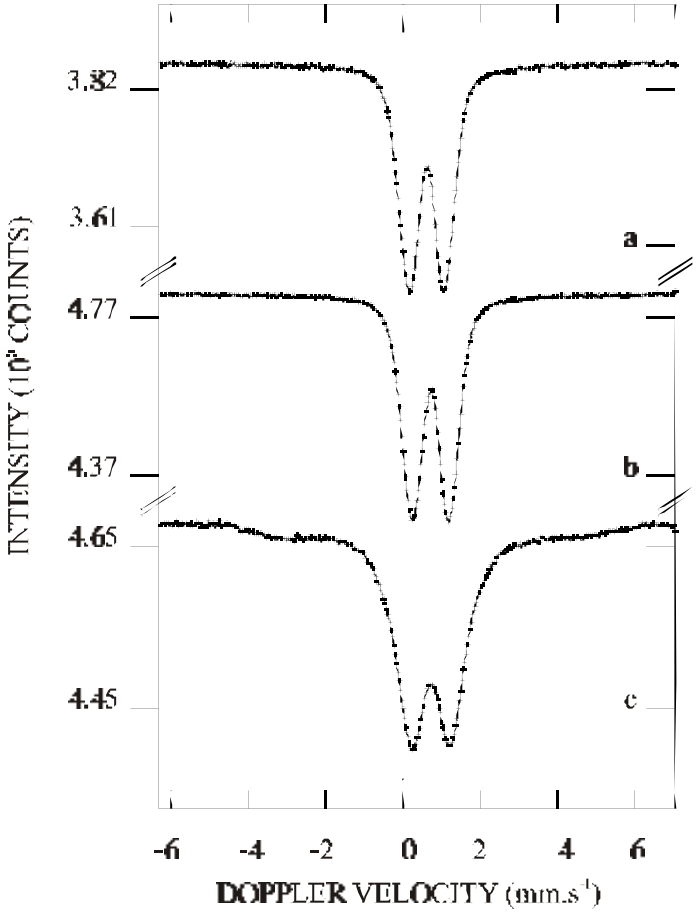

Figure 2.5 *Mössbauer spectra measured at (a) 300, (b) 77 and (c) 4.2 K of freshly prepared zirconia-supported iron oxide containing 2.5 wt% Fe/K/ZrO_2.*

Table 2.2 *Mössbauer parameters of fresh 2.5 wt% Fe/K/ZrO_2 at different temperatures.*

T (K)	I.S. (mm/s)	Q.S. (mm/s)	Γ (mm/s)	S.C. (%)	Compound
300	0.61	0.93	0.57	100	Fe^{3+}
77	0.71	0.97	0.57	100	Fe^{3+}
4.2	0.72	1.05	0.91	100	Fe^{3+}

Comparison of the parameters found for the promoted and unpromoted catalyst leads to the conclusion that the parameters are not significantly different. Hence, the value of the quadrupole splitting, *viz*., 0.93 mm/s, indicates a high contribution of surface ions and thus a very high dispersion. The Mössbauer results thus point to extremely small iron(III) oxide particles present together with carbon as a thin continuous layer on the surface of the zirconia crystallites with both the unpromoted and the potassium-promoted catalyst.

2.3.3 Thermogravimetry

During heating the weight of the Fe/ZrO_2 catalyst dropped by 1.13% up to a temperature of about 473 K due to the release of water as was evident from the results of the mass-spectrometer. The mass-spectrometer indicated that subsequently the weight decreased due to the reaction of carbon to carbon dioxide. The rate of weight loss due to the combustion of carbon was maximum at about 673 K, while the mass-spectrometer displayed a maximum signal of mass 44 due to carbon dioxide. The weight loss from 473 to 1123 K was 0.64 %, which corresponds to the carbon content of the catalyst. With the loading of 2.5 wt.% iron the atomic ratio of iron and carbon of the freshly calcined Fe/ZrO_2 catalyst is Fe/C = 4.5/5.3.

The $Fe/K/ZrO_2$ catalyst lost 0.98 % of its weight due to release of water during heating to a temperature of 473 K. At more elevated temperatures the mass spectrometer indicated the evolution of carbon dioxide (mass 44). The maximum rate of release of carbon dioxide was exhibited at about 573 K. The weight loss of the $Fe/K/ZrO_2$ catalyst due to the combustion of carbon was significantly higher than that of the Fe/ZrO_2 catalyst, *viz*., 2.09 %. The atomic ratio Fe/C of this catalyst is 4.5/17.4.

2.4 Further discussion

With the incipient wetness impregnation technique it is possible to obtain a zirconia-supported iron oxide catalyst of a high dispersion as is shown with transmission electron microscopy and Mössbauer absorption spectroscopy. In the following, our catalyst synthesis is compared to other synthesis described in literature. In particular, the applied calcination temperature is discussed.

After the drying step a very thin amorphous layer of the citrate precursor has been deposited on the support. This is due to the high increase in viscosity upon drying leaving a (flat) gel-like structure behind on the surface of the elementary crystallites of the support [5]. To maintain the thin layer containing iron oxide and carbon the temperature during calcination appears to be essential. Boot [4, 9] calcined up to a temperature of 1023 K. Mössbauer spectroscopy of this calcined catalyst showed a hyperfine splitting even at room temperature, which unambiguously indicates the presence of iron oxide particles larger than 12 nm. TEM and XRD confirmed the presence of larger iron oxide particles in the catalysts investigated by Boot for both the unpromoted and the potassium-promoted zirconia-supported iron oxides, which had a higher loading with iron oxide.

Van de Brink [1] used the impregnation method to deposit ammonium iron(III) citrate on a silica support (OX50, Degussa Germany, specific surface area 50 m^2 per gram). The catalyst was calcined at a significantly lower temperature, *viz*. 770 K. A sextuplet was revealed only at a temperature of 77 K indicating the presence of a (small) fraction of particles larger than 4 nm. In this study a calcination temperature of 723 K was used. It is shown that even at temperatures as low as 4 K hyperfine splitting is still absent. This leads to the conclusion that the iron oxide in the presently investigated catalyst is highly disperse and, moreover, monodisperse.

Furthermore, it appears that the calcination step determines the final microscopic distribution of the Fe^{3+} species formed. As Boot has shown using TEM [4], large clusters of iron oxide were present in his catalysts in contact with a thin layer. At more elevated temperatures the carbon separating the minute iron oxide particles is removed by oxidation. In this manner, contact between the remaining iron oxide particles will be established. Where locally a sufficiently extended contact area between a number of small iron oxide particles arises during calcination, some large iron oxide crystallites result. Therefore, thermally induced migration leading to sintering of the active species is very likely to occur at high temperatures.

2.5 Conclusions

A very thin amorphous layer containing iron oxide and carbon can be deposited on a zirconia support using the incipient wetness impregnation technique with ammonium iron(III) citrate. TEM, XRD and Mössbauer spectroscopy results reveal the presence of monodisperse iron(III) oxide. A low calcination temperature

(723 K) prevents complete oxidation to carbon dioxide and carbon monoxide. In contrast, a higher calcination temperature leads to more intimate contact between the remaining iron oxide particles and, hence, causes sintering to some larger iron oxide particles.

2.6 References

[1] P.J. van de Brink, A. Scholten, A. van Wageningen, M.D.A. Lamers, A.J. van Dillen and J.W. Geus, in *Stud.Surf.Sci.Catal.* **63** (1991) 527.

[2] L.M. Knijff, Ph.D. Thesis, Utrecht University, 1991, Chapter 2.

[3] A.M. Boon, Ph.D. Thesis, Utrecht University, 1990, Chapter 2.

[4] L.A. Boot, A.J. van Dillen, J.W. Geus and F.R. van Buren, *J.Catal.* **163** (1996) 186.

[5] R.J.A.M. Terörde, Ph.D. Thesis, Utrecht University, 1996, Chapter 2.

[6] K. Chen, Y. Fan, Z. Hu and Q.Yan, *Catal.Lett*. **36** (1996) 130.

[7] International Centre for Diffraction Data, JCPDS nr. 37-1484.

[8] A.M. van der Kraan, *Phys.Stat.Sol(A)* **18** (1973) 215.

[9] L.A. Boot, A.J. van Dillen, J.W. Geus, A.M. van der Kraan, A.A. van der Horst and F.R. van Buren, *Appl..Cat.* **147** (1996) 389.

[10] A.M. van der Kraan, J.W. Niemantsverdriet, '*Industrial Applications of the Mössbauer Effect'*, G.J. Long, J.G. Stevens (eds), Plenum, New York, 1986, 609.

3

Reduction Behaviour of Fe/ZrO_2 and $Fe/K/ZrO_2$ Catalysts

Abstract

In this chapter the reduction behaviour of two iron-based catalysts are investigated *viz.* an unpromoted and potassium-promoted zirconia-supported iron-based catalysts. The initial dispersion of both catalysts is very high. To establish reduction the nature of the iron species under hydrogen atmosphere, experiments were performed both at ambient pressure and at elevated pressure *i.e.* 1.8 and 9.5 bar.

It is demonstrated for both catalysts that in the preparation procedure carbon is not completely removed, whereby the potassium-rich catalyst contains the largest amount of the carbon species. During reduction at ambient pressure this carbide reacts with metallic iron to give cementite (θ-Fe_3C), whereas at elevated pressure this iron carbide was not encoutered.

Furthermore, the iron oxide is reduced more profoundly at elevated pressure. It is further shown that the potassium-rich catalyst reduces more easily both at ambient and elevated pressure.

Upon formation of divalent iron, this iron species reacts with the support to give a stable mixed oxide. This species is suggested to be a prerequisite in maintaining a high dispersion of metallic iron. Based on the analyses presented here, a reduction model is proposed.

3.1 Introduction

In the previous chapter, highly dispersed Fe/ZrO_2 and $Fe/K/ZrO_2$ were prepared. Before exposure to the Fischer-Tropsch synthesis, these catalysts are reduced. The aim of this study is to elucidate the reduction behaviour of unpromoted (Fe/ZrO_2) and potassium-promoted ($Fe/K/ZrO_2$) zirconia-supported iron catalysts at ambient and at elevated hydrogen pressures.

The reduction of bulk hematite (α-Fe_2O_3) proceeds via magnetite (Fe_3O_4) and woestite (FeO) to metallic iron [1, 2]. However, the formation of FeO is not observed, because woestite is metastable below 843 K [1, 2, 3] at which temperature disproportionation into Fe_3O_4 and Fe proceeds.

With supported iron catalysts the purely divalent state of iron can be stabilised well below the critical temperature by interaction with the support due to formation of mixed oxides [2, 4-16]. For iron catalysts supported on Al_2O_3 and SiO_2 the formation of ferrous aluminates and silicates has been reported [2, 4-8]. Wielers *et al.* [5] observed the formation of a silicate layer during reduction of trivalent iron indicating that, as soon as divalent iron is formed, iron migrates into the support. Also with TiO_2 and MgO supports mixed oxides are mentioned to account for the intimate contact between the precursor metal oxide and the support resulting in a lower reducibility of the iron oxide [9-11].

A lower reducibility was also found on zirconia-supported iron catalysts with temperature-programmed reduction (TPR). A high extent of reduction was observed to call for reduction temperatures far above 773 K [12-16]. Boot *et al.* [12, 13] attributes the TPR-profile to either the presence of iron oxide particles of various sizes exhibiting different resistances towards reduction and/or stabilizing interactions between metal oxide and support. Guglielminotti [14, 15] reports on the presence of an oxide-oxide interaction, which is responsible for the retarded reduction and formation of large metallic iron (Fe^0) particles. Chen *et al.* [16], who studied the reduction of a zirconia-supported iron oxide catalyst containing 7 wt% Fe_2O_3, also concluded that an interaction of iron oxide with the zirconia support exists. The authors observed that reduction of the iron species proceeds in three steps. They suggest that the reduction of ZrO_2 and the subsequent formation of a mixed spinel, $(Zr_yFe_{3-y})O_4$, account for the first step. In the second step this mixed oxide is transformed into $(ZrO_2)(FeO)_2$ and Fe_2O_3. Reduction to metallic iron proceeds in the last step. However, the species formed in each of these steps appears to be merely assumed and not experimentally proven.

In this chapter, it will be shown that water plays an essential role in the reduction of the zirconia-supported iron oxide catalysts. Furthermore, it is argued that a mixed oxide of iron and the ZrO_2-support is possibly present. Finally, it will be demonstrated that upon formation of metallic iron the dispersion of the iron species will drop rapidly. Our experimental results indicate beyond doubt that the freshly calcined catalysts still contain an appreciable amount of carbon remaining from the impregnated citrate precursor. The potassium oxide promoter appears to affect strongly the mobility of carbon. Since the technical Fischer-Tropsch reaction is generally executed at higher pressures, the reduction of the iron species in the unpromoted and promoted catalyst has also been studied at hydrogen pressures of 1.8 and 9.5 bar. First the results obtained at ambient pressure for the promoted and unpromoted catalyst will be presented and subsequently the data measured at elevated pressures.

3.2 Experimental

3.2.1 Catalyst preparation

For details of the preparation of Fe/ZrO_2 and $Fe/K/ZrO_2$ the reader is referred to chapter 2.

3.2.2 Characterisation techniques

3.2.2.1 Mössbauer absorption spectroscopy (MAS)

The experiments at ambient hydrogen pressure (1 bar) were executed using an in-situ Mössbauer reactor described in more details in [17]. To perform the in-situ measurements at elevated pressures up to 10 bar a modified reactor with Be-windows and an outer vessel of stainless steel was used. The catalysts were reduced in a hydrogen atmosphere at temperatures from 300 K up to 823 K and were in-situ measured at the reduction temperature. In some cases the reduced catalyst is also subsequently measured at room temperature without intermediate exposure to atmospheric air.

Mössbauer measurements were carried out in a constant acceleration mode using a ^{57}Co in Rh source. Isomer shifts are reported relative to the NBS standard sodium nitroprusside ($Na_2Fe(CN)_5NO.2H_2O$). Magnetic hyperfine fields (H_{eff})

were calibrated with the 515 kOe field of α-Fe_2O_3 at room temperature. The Mössbauer parameters were determined by fitting the spectra with subspectra consisting of Lorentzian-shaped lines using non-linear iterative minimisation routine. The accuracy for the isomer shift (I.S.) is ±0.03 mm/s, for the electric quadrupole splitting (Q.S.) ±0.05 mm/s and for the spectral contribution (S.C.) 5%.

3.2.2.2 Thermomagnetic analysis (TMA)

The catalysts (about 150 mg) were pretreated in a quartz flow reactor of a diameter of 10 mm operated at atmospheric pressure. High-field magnetic measurements were performed using a modification of the Weiss-extraction method [18]. With this technique it is possible to monitor the magnetisation of the iron phase under reaction conditions. Figure 3.1 shows a schematic representation of the apparatus. Experiments were carried out at a magnetic field strength of 7 kOe.

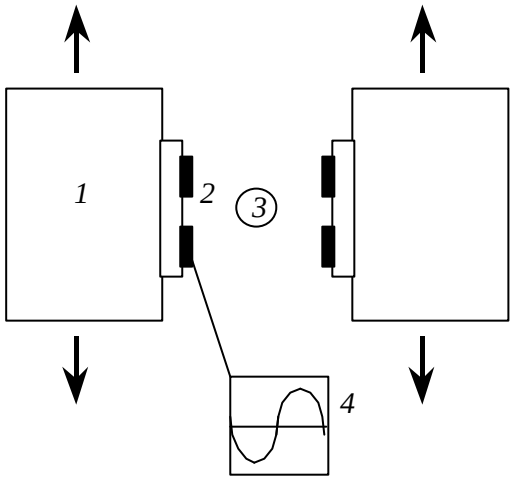

Figure 3.1 *Schematic representation of equipment for magnetic measurements. Horizontal cross-section: 1: moving electromagnet; 2: Helmholz sensing coils; 3: reactor and catalyst; 4: integrator.*

All samples were treated in a 50 ml/min 10% H_2/He (v/v) gas flow at temperatures from 298 K up to a temperature of 823 K. The temperature was raised in steps of 10 K and the magnetisation was determined at every temperature.

Subsequently the magnetisation was measured at temperatures decreasing in steps of 10 K to room temperature. The magnetisation was normalised taking into account the total mass of iron in the measured sample.

3.2.2.3 Temperature-Programmed Reduction (TPR)

The temperature-programmed reduction experiments were performed in a downstream plug-flow reactor at atmospheric pressure. The catalyst was reduced in a 5 % H_2/Ar (v/v) flow of 20 ml/min, while the temperature was increased from room temperature to 1373 K at a linear heating rate of 10 K/min. The water formed was frozen in a cold (aceton-carbon dioxide) trap. The hydrogen consumption was monitored using a hot wire detector.

3.3 Results at ambient pressure

3.3.1 Mössbauer absorption spectroscopy

3.3.1.1 Unpromoted Fe/ZrO_2

Chapter 2 of this thesis discussed that the freshly calcined catalyst contains exclusively trivalent iron. In this section *in situ* Mössbauer measurements during reduction treatments at different temperatures and a hydrogen pressure of 1 bar are described. Furthermore, measurements taken after subsequent cooling to 300 K are dealt with.

Table 3.1 *Mössbauer parameters of 2.5 wt% Fe/ZrO_2 calculated from measurements during reduction at 573 K and subsequent measurements at room temperature.*

T(K)	I.S. (mm/s)	Q.S. (mm/s)	Γ (mm/s)	S.C. (%)	Compound
573	0.75	0.62	0.51	27	Fe^{2+}
	0.99	1.50	0.58	73	Fe^{2+}
300	1.23	2.67	0.28	7	Fe^{2+}
	1.26	1.96	0.35	10	Fe^{2+}
	0.60	0.99	0.58	83	Fe^{3+}

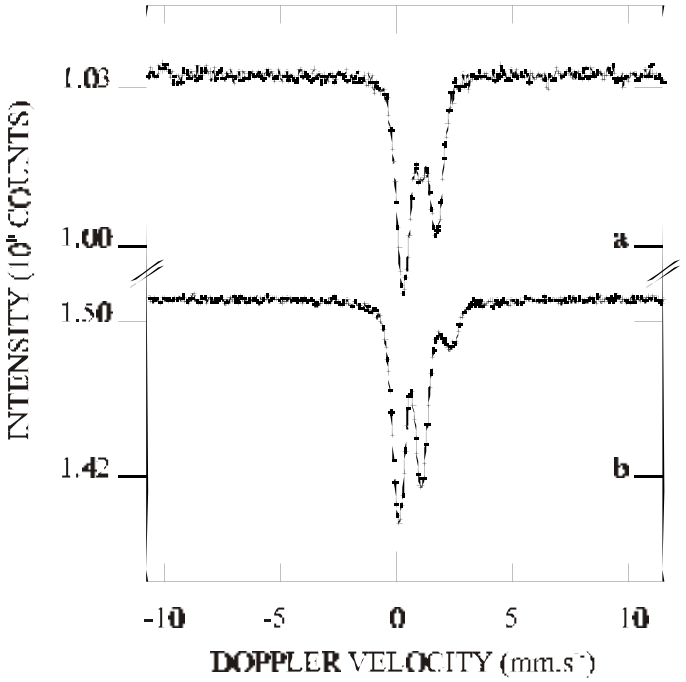

Figure 3.2 *Mössbauer spectra of 2.5 wt% Fe/ZrO_2 measured during reduction at 573 K (a), and subsequently at 300 K (b).*

As can be seen in Table 3.1 and Figure 3.2, reduction at 573 K results in the appearance of two spectral components, which can be assigned to divalent iron species. Obviously, the trivalent iron species has been completely reduced to divalent iron compounds. Both divalent iron species are different in nature considering the different isomer shift and quadrupole splitting. The spectral contributions at 573 K have been calculated from spectra measured during the 22 hours of reducing the sample at 573 K.

After the *in situ* measurement at 573 K the sample was cooled to room temperature in a hydrogen atmosphere, after which a spectrum is subsequently measured. At 300 K the spectral contributions significantly change. A large amount of Fe^{3+} is observed (83 %), whereas at 573 K all trivalent iron had been reduced to Fe^{2+}. During cooling and at room temperature re-oxidation of Fe^{2+} occurs apparently even in a hydrogen atmosphere. It must be noted that the re-oxidation

process takes place both in static and flowing hydrogen, hence excluding the possibility of oxygen leakage.

During reduction at 623 K three spectral contributions are observed in the spectrum. Two contributions can be attributed to divalent iron species. The third spectral component with I.S.= 0.26 mm/s and Q.S.=0.48 mm/s can be attributed to θ–Fe_3C (cementite) above its magnetic ordering temperature of 485 K [19]. This assignment is confirmed by the measurements at 300 K. At room temperature also a magnetically split component (H_{eff}= 205 kOe) is observed. Although the spectral contribution is rather small, a sextuplet contribution with a hyperfine field of 205 kOe is clearly present. This spectral component also points to θ–Fe_3C and gives rise to the deduced third spectral component in the measured spectrum during the reduction treatment at 623 K (a doublet at this temperature). The carbon is very likely a remainder of the organic citrate complex, which upon decomposition leaves carbon behind. The reaction to cementite unambiguously indicates the presence of carbon remaining by decomposition of the citrate precursor in the catalyst which is calcined at 723 K. The atomic ratio of iron-to-carbon in the Fe/ZrO_2 catalyst is 4.5/5.3 [47]. The amount of carbon present within the catalyst is, hence, more than sufficient for complete reaction of the iron in the catalyst to cementite. Apparently a substantial fraction of the carbon is hydrogenated to methane or does not contact the iron particles.

Table 3.2 Mössbauer parameters of 2.5 wt% Fe/ZrO_2 during reduction at 623 K and subsequent measurements at room temperature.

T(K)	I.S. (mm/s)	Q.S. (mm/s)	H_{eff} (kOe)	Γ (mm/s)	S.C. (%)	Compound
623	0.26	0.48		0.23	7	Fe_3C
	0.96	1.42		0.52	58	Fe^{2+}
	0.80	0.75		0.54	35	Fe^{2+}
300	0.47		205	0.29	3	Fe_3C
(0-9hr)	1.31	2.29		0.44	39	Fe^{2+}
	1.25	1.68		0.59	48	Fe^{2+}
	0.58	0.90		0.53	10	Fe^{3+}
300	0.47		205	0.24	3	Fe_3C
(0-20hr)	1.31	2.41		0.39	22	Fe^{2+}
	1.27	1.84		0.57	40	Fe^{2+}
	0.58	0.91		0.59	35	Fe^{3+}

In Table 3.2 the Mössbauer parameters calculated from spectra measured during reduction at 623 K and spectra measured subsequently at room temperature are presented. The corresponding spectra are shown in Figure 3.3.

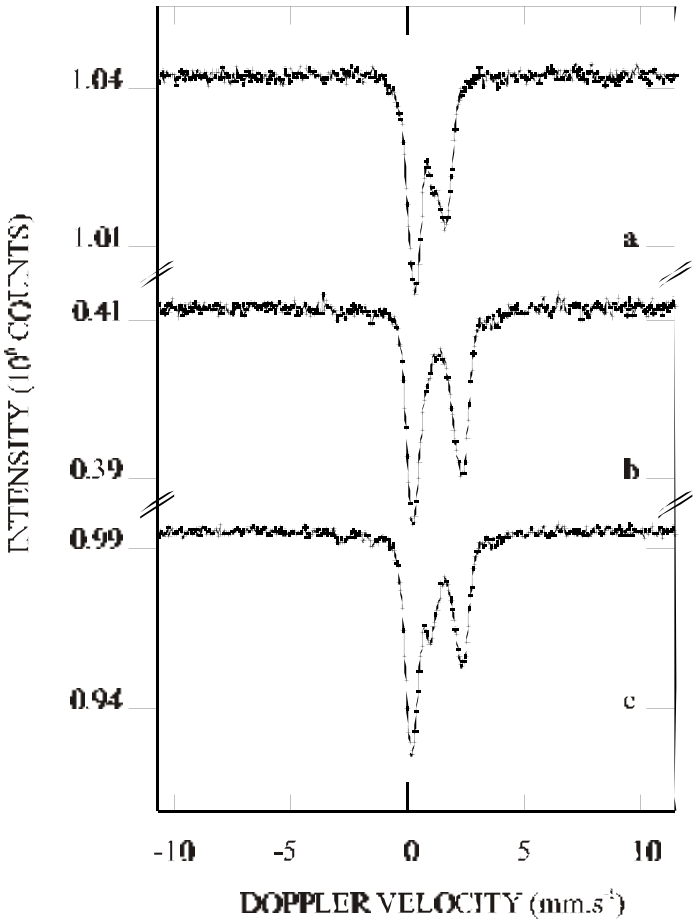

Figure 3.3 *Mössbauer spectra of 2.5 wt% Fe/ZrO_2 measured during reduction at 623 K (a), and measured subsequently at 300 K, of which (b) is measured during the first 9 hours and (c) is measured during the total period of 20 hours.*

The above results indicate that with the catalyst reduced at 623 K re-oxidation by water vapour proceeds during or after decreasing the temperature to room temperature, as was observed after reduction at 573 K. To assess whether the

re-oxidation continues at room temperature, the spectral parameters are computed from measurements taken during the first 9 hours after cooling down and after a more prolonged period of time at room temperature. Comparing the spectral contributions obtained after the first 9 hours and after the total period of 20 hours, it follows that the re-oxidation continues at room temperature. The measurements during the first 9 hours will therefore give a more realistic picture of the final state after reduction at 623 K than the data measured after keeping the reduced catalyst for a longer period of time at room temperature. After reduction at 573 K and cooling to room temperature and keeping the catalyst at room temperature no less than 83 % of the spectrum can be attributed to Fe^{3+}. The Fe^{2+} species resulting after reduction at 623 K, on the other hand, lead to spectral contributions of Fe^{3+} of only 10 % during measurement for 9 hours and of 35 % during measurement for 20 hours.

Table 3.3 *Mössbauer parameters of 2.5 wt% Fe/ZrO_2 calculated from spectra during the reduction at 673 K and spectra subsequently at 300 K.*

T(K)	I.S. (mm/s)	Q.S. (mm/s)	H_{eff} (kOe)	Γ (mm/s)	S.C. (%)	Compound
673	0.02	0.00	293	0.23	6	Fe^0
	0.22	0.46		0.33	19	Fe_3C
	0.97	1.23		0.55	49	Fe^{2+}
	0.68	0.88		0.53	26	Fe^{2+}
300	0.27	0.00	330	0.26	10	Fe^0
(0-8hr)	0.47		204	0.39	14	Fe_3C
	1.31	2.38		0.35	16	Fe^{2+}
	1.26	1.78		0.60	50	Fe^{2+}
	0.58	0.90		0.72	10	Fe^{3+}
300	0.26	0.00	331	0.27	10	Fe^0
(0-26hr)	0.47		205	0.38	14	Fe_3C
	1.24	2.54		0.30	6	Fe^{2+}
	1.21	1.95		0.55	20	Fe^{2+}
	0.61	0.94		0.62	50	Fe^{3+}

Γ is the line width.

During the reduction treatment at the still more elevated temperature of 673 K (Table 3.3 and Figure 3.4) a magnetically split spectral component with H_{eff}= 293 kOe is observed. This contribution is due to the appearance of metallic iron (Fe^0) in the catalyst sample. Next to this metallic contribution the spectrum exhibits the two earlier observed doublets of Fe^{2+} and the doublet ascribed to θ-Fe_3C. Generally the isomer shift (I.S) depends on the temperature and drops at rising temperatures, as is exhibited by the isomer shifts of the Fe^{2+} species. At 300 K the doublet attributed to θ-Fe_3C changes into the sextuplet with H_{eff}= 205 kOe.

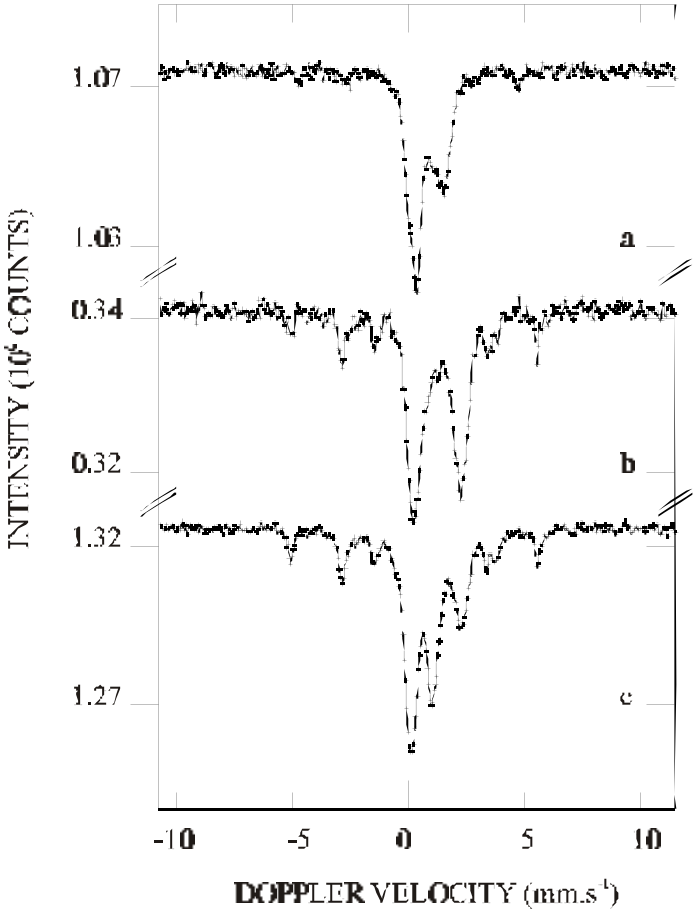

Figure 3.4 *Mössbauer spectra of 2.5 wt% Fe/ZrO_2 measured during 22 hours of reduction at 673 K (a), and subsequently at 300 K, of which (b) is measured during the first 8 hours and (c) is measured during the total period of 26 hours.*

During cooling to and at 300 K re-oxidation of the Fe^{2+} species resulting from the reduction at 673 K does again proceed. By comparing the two spectra measured at 300 K, it follows that only the ferrous species are converted to trivalent iron and that the ferromagnetic phases do not change. Whereas a measurement during the first 8 hours at room temperature leads to a spectral contribution of Fe^{3+} of 10 % as after reduction at 623 K, keeping the reduced catalyst for 26 hours at room temperature results in a spectral contribution of Fe^{3+} of at least than 50 %. It might be that more water due to the reduction to metallic iron is present within the support bodies, which is slowly released at room temperature is causing the more extensive oxidation of the Fe^{2+} species.

The iron carbide phase is known to be very stable [20]. Severe oxidation of the iron carbide by water at lower temperatures is therefore not to be expected. Since the Mössbauer spectra do not indicate the iron carbide particles to be extremely small, oxidation of the surface of the iron carbide will not be apparent from the Mössbauer spectra. However, the fact that the Mössbauer spectra indicate that water vapour oxidizes the iron(II) species to an appreciable extent and not the metallic iron particles, is more difficult to explain.

Molecular oxygen oxidises iron to a thickness of about 1.5 nm, but the extent of interaction of iron with water vapour has not been established accurately. Since water is observed to be much less reactive than molecular oxygen in the oxidation of iron [21], it is possible that the interaction with water vapour remains limited and leads to a coverage of about a monolayer of oxygen atoms and release of molecular hydrogen. If the reaction of water vapour with an iron surface covered by a monolayer of oxygen atoms does not proceed, the experimental results can be smoothly explained. The reaction of a bare iron surface with water vapour will be rapid, and reaction beyond the monolayer of oxygen atoms does not occur. The contribution of metallic iron to the spectra calculated from measurements performed after keeping the sample for different periods of time at room temperature will therefore not differ. The contribution of metallic iron to spectra measured at 673 K and room temperature are difficult to compare. Consequently, a decrease in the contribution of metallic iron during cooling down to room temperature is difficult to assess from the measurements.

Alternatively it may be that the thermal treatment in hydrogen did not remove the last monolayer of adsorbed oxygen from the iron surface. Vink *et al.* [22, 23] have demonstrated that the reduction of oxidised iron single crystals is plane-specific. Exposure of iron surfaces to molecular oxygen leads to oxidation of the iron surface to a depth of about 1.5 nm. Thermal treatment in hydrogen leads to a rapid removal of the subsurface oxygen. However, reduction of an oxidised

Fe(100) single crystal surface does not proceed completely; approximately one monolayer of oxygen remains at the surface. The oxygen taken up by the most closely packed Fe(110) surface, on the other hand, can be readily and completely removed by reaction with hydrogen at elevated temperatures. When the reactivity of the surface of small iron particles is analogous to that of the more open iron surface, the removal of the last monolayer of oxygen may not proceed. When water vapour does not react with an iron surface being covered by a monolayer of oxygen atoms, a drop in the contribution of metallic iron to the Mössbauer spectra will not be apparent. However, Vink *et al.* employed a maximum hydrogen pressure of $2x10^{-2}$ Torr at temperatures from 473 to 643 K. It is likely that a higher hydrogen pressure will be effective in removal of the last monolayer of oxygen atoms.

A final possibility is that a significant fraction of the surface of the metallic iron particles is covered by iron carbide. The carbon taken up from the surface of the zirconia support may remain at the surface of metallic iron particles, while the iron particles grow due to the ongoing reduction. The iron carbide thus protects the metallic iron from interaction with water vapour.

Raising the reduction temperature to 723 K leads to spectra displaying the same four spectral contributions as after reduction at 673 K. Figure 3.5 represents the spectra measured during and after reduction at 723 K. The contributions (see Table 3.4) to the spectra can be assigned to Fe^0, Fe_3C, and the two different Fe^{2+} species.

The spectral contribution of Fe_3C does not significantly change as compared to the contribution found after the previous reduction step at 673 K. The fact that the contribution of Fe_3C does not increase, further agrees with a limited amount of carbon left behind by the decomposed citrate precursor.

The higher reduction temperature of 723 K increases, on the other hand, the contribution of metallic iron to the spectra to about 30%. The slightly higher effective field, 208 kOe as compared to 204 and 205 kOe indicates the presence of slightly larger iron particles, as is to be expected. Keeping the sample for a prolonged period of time at room temperature affects neither the contribution of Fe_3C nor that of metallic iron. As observed earlier after reduction at lower temperatures, the Fe^{2+} species are slowly oxidised at room temperature. Now reoxidation seems to proceed less extensively than after reduction at 673 K, presumably due to desorption of water vapour from the surface of the support leading to a lower water partial pressure.

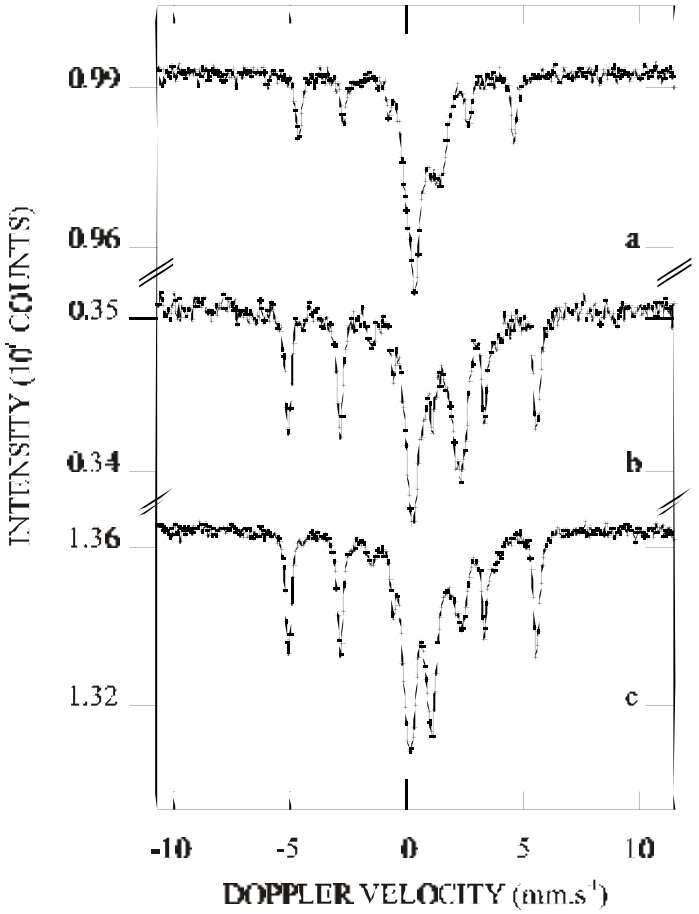

Figure 3.5 Mössbauer spectra of 2.5 wt% Fe/ZrO_2 measured during reduction at 723 K (a), and subsequently at 300 K, of which (b) is measured during the first 6 hours and (c) is measured during the total period of 26 hours.

Table 3.4 *Mössbauer parameters of 2.5 wt% Fe/ZrO_2 calculated from spectra measured during and after reduction at 723K and from spectra measured subsequently at room temperature.*

T(K)	I.S. (mm/s)	Q.S. (mm/s)	H_{eff} (kOe)	Γ (mm/s)	S.C. (%)	Compound
723	-0.02	0.00	288	0.27	27	Fe^0
	0.19	0.45		0.38	19	Fe_3C
	0.92	1.21		0.51	28	Fe^{2+}
	0.72	0.81		0.57	26	Fe^{2+}
300	0.26	0.00	332	0.28	34	Fe^0
(0-6h)	0.47		210	0.35	10	Fe_3C
	1.34	2.31		0.38	13	Fe^{2+}
	1.25	1.76		0.63	35	Fe^{2+}
	0.58	0.90		0.71	8	Fe^{3+}
300	0.26	0.00	331	0.27	31	Fe^0
(0-26hr)	0.47		208	0.40	11	Fe_3C
	1.28	2.03		0.67	21	Fe^{2+}
	0.67	1.34		0.50	6	Fe^{2+}
	0.58	0.90		0.57	31	Fe^{3+}

Γ is the line width.

3.3.1.2 Potassium-promoted $Fe/K/ZrO_2$

The behavior of $Fe/K/ZrO_2$ during reduction is also followed *in situ* with Mössbauer spectroscopy. Since the measurements on the Fe/ZrO_2 catalyst have well established the re-oxidation of exclusively the Fe^{2+} species produced during the reduction, we will only present the spectra measured at the applied reduction temperature. Figure 3.6 shows a compilation of the spectra measured during the reduction at 573, 623, and 653 K. In Table 3.5 the Mössbauer parameters calculated from the spectra are given. Figure 3.6 also shows the Mössbauer spectrum measured at 473 K, while Table 3.5 contains the parameters calculated from spectra measured at 300, 373 and 473 K.

Table 3.5 *Mössbauer parameters of 2.5 wt% $Fe/K/ZrO_2$ calculated from spectra measured during the reduction in H_2 at different temperatures.*

T(K)	I.S. (mm/s)	Q.S. (mm/s)	H_{eff} (kOe)	Γ (mm/s)	S.C. (%)	Compound
300	0.60	1.17		0.45	50	Fe^{3+}
(0-20h)	0.61	0.71		0.41	50	Fe^{3+}
373	0.55	1.30		0.45	47	Fe^{3+}
(0-19h)	0.55	0.79		0.42	53	Fe^{3+}
473	0.48	1.37		0.48	51	Fe^{3+}
(0-22h)	0.48	0.83		0.42	49	Fe^{3+}
573	0.75	0.71		0.61	30	Fe^{2+}
(0-23h)	0.98	1.47		0.61	66	Fe^{2+}
	0.21	0.55		0.30	4	Fe_xC
623	0.77	0.72		0.53	28	Fe^{2+}
(0-26h)	0.93	1.38		0.58	61	Fe^{2+}
	0.24	0.44		0.34	11	Fe_xC
623	0.00		295	0.34	1	Fe^{0}
(26-50h)	0.82	0.68		0.54	24	Fe^{2+}
	0.93	1.39		0.57	54	Fe^{2+}
	0.22	0.42		0.35	21	Fe_xC
653	0.00		295	0.29	3	Fe^{0}
(1-20h)	0.83	0.71		0.54	21	Fe^{2+}
	0.92	1.35		0.56	45	Fe^{2+}
	0.20	0.43		0.36	31	Fe_xC
653	0.03		296	0.29	4	Fe^{0}
(20-44h)	0.84	0.68		0.50	18	Fe^{2+}
	0.92	1.35		0.55	42	Fe^{2+}
	0.20	0.43		0.36	36	Fe_xC

Table 3.5 Continued.

T(K)	I.S. (mm/s)	Q.S. (mm/s)	H_{eff} (kOe)	Γ (mm/s)	S.C. (%)	Compound
653	0.02		297	0.27	4	Fe^0
(44-71h)	0.85	0.67		0.47	15	Fe^{2+}
	0.92	1.34		0.56	41	Fe^{2+}
	0.20	0.44		0.37	40	Fe_xC
653	0.02		298	0.27	6	Fe^0
(71-94h)	0.86	0.67		0.46	14	Fe^{2+}
	0.92	1.35		0.56	40	Fe^{2+}
	0.20	0.44		0.36	40	Fe_xC

Reduction at 373 K and 473 K does not affect the spectrum as compared to the initial spectrum at 300 K. The parameters calculated from the spectra point to the presence of exactly the same two Fe^{3+} species as observed in Fe/ZrO_2.

During the reduction at 573 K three spectral contributions appear which are different from the Fe^{3+} doublets. These contributions can be assigned to two different divalent iron species (having isomer shifts of 0.98 and 0.75 mm/s) and an iron carbide (having an isomer shift of 0.21 mm/s). Most likely this iron carbide is θ-Fe_3C as is analogously seen for the unpromoted Fe/ZrO_2. As mentioned previously, in order to avoid re-oxidation of the reduced catalyst, the catalyst is not cooled to room temperature. It is therefore not possible to verify the formation of θ-Fe_3C from its value of H_{eff}.

Raising the reduction temperature to 623 K initially does not result in different spectral contributions. Measuring the catalyst, however, during a second 24 hours leads to the appearance of a relatively low amount (1%) of metallic iron (Fe^0). During reduction at 653 K the spectral contribution of this Fe^0 increases only slightly and does not exceed 6 %.

The Mössbauer spectra indicate that the spectral contribution of the iron carbide increases with the reduction temperature up to a value of 40 % at 653 K. This amount is twice as large as in the case of the unpromoted Fe/ZrO_2, which agrees with the higher carbon content of the $Fe/K/ZrO_2$ catalyst containing 2.09 wt.% carbon, while the Fe/ZrO_2 catalyst contains only 0.64 wt.% carbon [47]. Analogous to the unpromoted catalyst the carbon needed to form the carbide must

originate from the citrate precursor. The presence of the potassium carbonate leads to more carbon remaining on the surface of the support after calcination at 723 K.

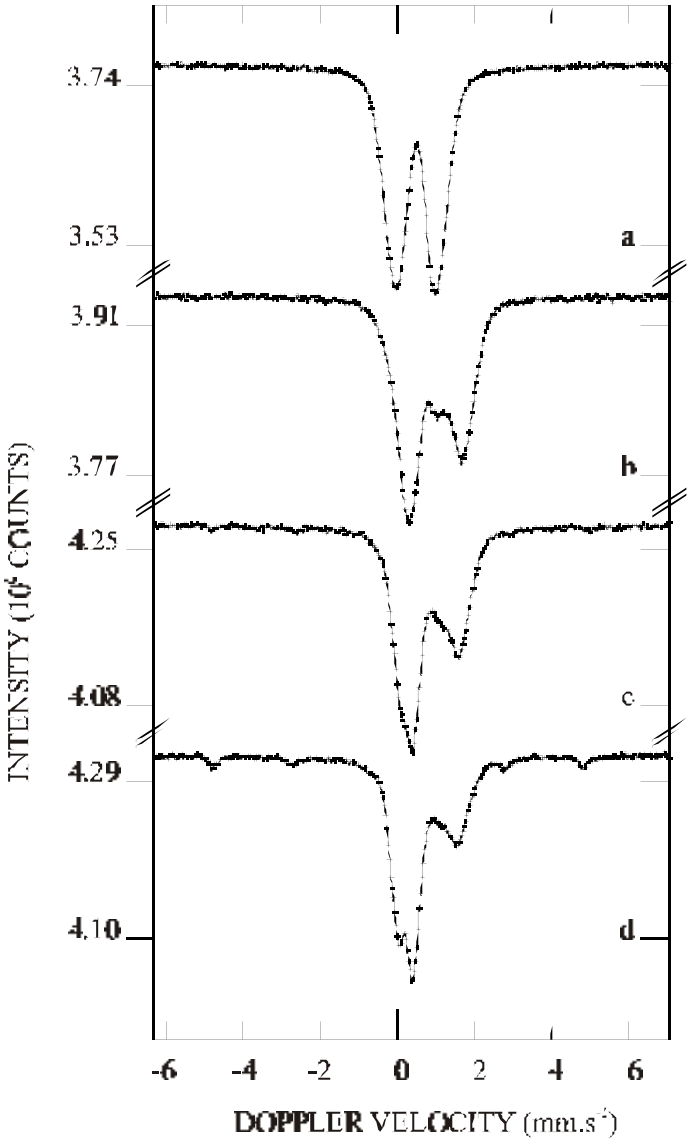

Figure 3.6 *Mössbauer spectra measured during reduction of $Fe/K/ZrO_2$ at ambient hydrogen pressure and at (a) 473 K, (b) 573 K, (c) 623 K, and (d) 673 K.*

The low fraction of metallic iron formed during reduction seems to be related to the relatively large amount of carbon present after calcination. It is very likely that as soon as metallic iron is formed, it will take up carbon from the carbon deposits instantly forming an iron carbide. The Mössabuer spectra are obtained by summation of a large number of subsequently measured spectra. The low spectral contribution of Fe^0 is due to an initial Fe^0 fraction that is only averaged out (resulting in a low spectral contribution) when the Fe^0 sextuplet exists for a short period of time. The rate of carburisation must therefore be high. These results indicate that the iron species are initially to a large extent reduced to metallic iron.

Throughout the reduction two contributions related to divalent iron species are present. Upon reduction both species diminish, but still remain present in relatively large amounts.

3.3.2 Thermomagnetic Analysis

Figure 3.7 represents a thermomagnetic profile wherein the reduction in flowing hydrogen of the zirconia-supported iron-based catalyst (Fe/ZrO_2) is monitored.

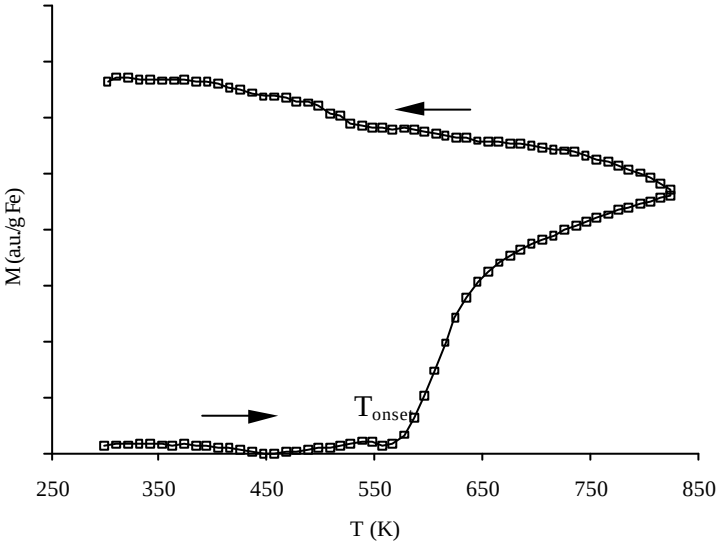

Figure 3.7 Thermomagnetic profile of 2.5 wt% Fe/ZrO_2

With a vibrating sample magnetic measuring technique (VSM) it was established that any ferromagnetism is absent in the fresh calcined catalyst. This agrees well with the results obtained using Mössbauer spectroscopy [24]. Consequently, the measured thermomagnetic profile of the fresh catalyst can be corrected for the observed offset exhibited by the measuring device.

As is shown in Figure 3.7 an increase in magnetisation is observed at about 568 K. The temperature at which an increase in magnetism is seen is referred to as the onset temperature T_{onset}. Above 568 K two regions showing two different slopes are encountered indicating dissimilar reduction rates. The increase in magnetisation cannot be explained by the formation of the observed θ-Fe_3C, since a ferromagnetic contribution at temperatures above its Curie temperature of 485 K [19] will not be observed. Consequently, the magnetisation increase can only be caused by the formation of the ferromagnetic Fe^0 species as is confirmed by the Mössbauer spectroscopy results. With Mössbauer spectroscopy two Fe^{2+} species have been observed during reduction at low temperatures. These species can be ascribed to a surface species Fe_I and a species Fe_{II} which is part of a mixed oxide with the support. It is very likely that during the reduction treatment first the surface species Fe_I will be reduced to Fe^0. In a subsequent step reduction of species Fe_{II} will proceed at a much lower rate as the support possibly stabilizes this iron containing mixed oxide species. In this latter step the 'mixed' Fe^{2+} first migrates to the surface (becoming Fe_I) and, subsequently, is converted to metallic iron Fe^0. The inflection point at which both reduction regimes meet can provide an indication of the amount of Fe_I and, complementary, the amount of Fe_{II}, since reduction to Fe^{2+} proceeds completely prior to the formation metallic iron as shown by the Mössbauer spectra.

The fact that the reduction leads to metallic iron (Fe^0) is also justified by the ferromagnetic profile measured at decreasing temperatures. Extrapolation of this branch of the magnetisation curve to high temperatures shows that the Curie temperature of the involved species is well above the maximum applied reduction temperature (853 K). Since only α-Fe has a sufficiently elevated Curie temperature, *viz.* T_C is 1043 K [19], reduction to metallic iron is apparent.

Figure 3.7 shows that upon cooling an additional increase in magnetisation is exhibited at about 250 °C. The corresponding Curie temperature is estimated to be about 490 K from the inflection point of the curve measured at decreasing temperature [18]. According to the literature [19] two different carbides may be compatible with the above Curie temperature, *viz.*, θ-Fe_3C and χ-Fe_5C_2 having Curie temperatures of 485 K and 530 K, respectively. However, Mössbauer results unambiguously show that the carbide formed during reduction is cementite (θ-

Fe_3C). Consequently, it can be concluded that θ-Fe_3C is present within the reduced catalyst Fe/ZrO_2.

Additionally, from the observed TMA profile, it is possible to calculate the (molar) contribution of the carbide species. The magnetisation observed at room temperature is a superposition of the magnetisation of cementite and zerovalent iron. The magnetic contribution of the iron carbide is determined as indicated in Figure 3.8.

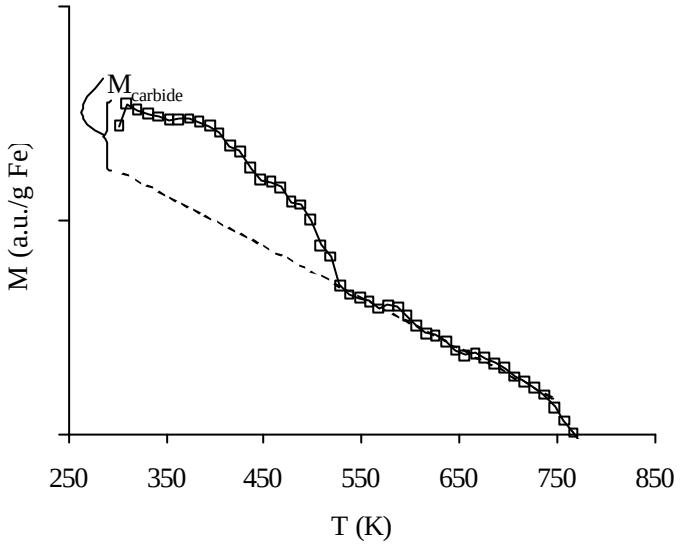

Figure 3.8 *Determination of the magnetic contribution of θ-Fe_3C in the TMA-profile. This Figure is a magnification of part of Figure 3.7.*

In the thermomagnetic experiment, the magnetisation is only provided in arbitrary units. However, the ratio of the magnetisation due to Fe^0 and to the iron carbide is a direct measure for their contributions in the catalyst, and can be used to determine the fraction of θ-Fe_3C. This ratio is calculated to be (0.4/6.4=) 0.06. For determination of the molar contribution of the carbide, the lower saturation magnetisation for the carbide must be taken into account. The relative saturation magnetisation (*i.e.* the ratio of the saturation magnetisation of metallic iron and the carbide) is estimated to be the ratio of the hyperfine splittings of Fe^0 (331 kOe) and θ-Fe_3C (208 kOe) observed with Mössbauer spectroscopy [25]. The thus calculated value for the amount of cementite becomes 10 % of the zerovalent iron present in

the catalyst. Assuming that the reduction is complete (100 %) this value of 10 % is in full agreement with the Mössbauer results.

3.3.3 Temperature-programmed reduction (TPR)

The TPR-profile is represented in Figure 3.9. Two regions can be distinguished, which are divided by a low hydrogen consumption at about 823 K. The degree of reduction is calculated to be 100 % after the completion of the second region, which leads to complete reduction of the iron in the catalyst.

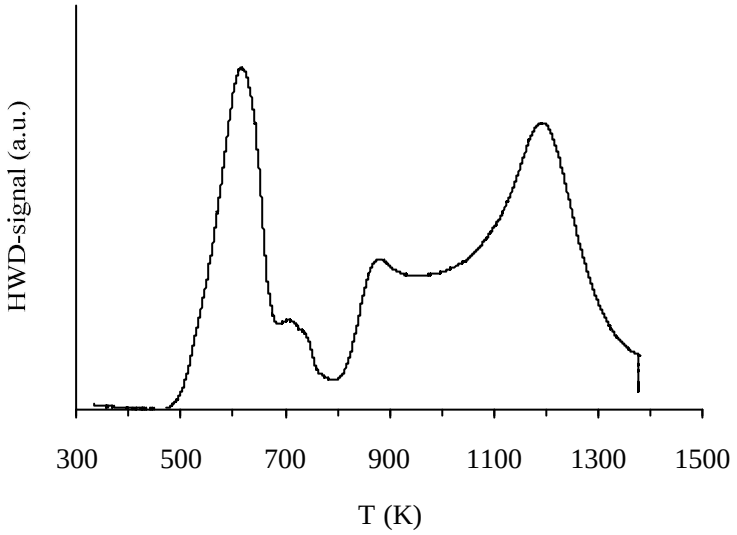

Figure 3.9 TPR profile of 2.5wt% Fe/ZrO_2.

The first region contains a (relatively) large peak and a small shoulder. The degree of reduction was roughly estimated to be around 33% after the first region, indicating the reduction from Fe^{3+} to Fe^{2+}. The ratio of the hydrogen consumption upon reduction of Fe_2O_3 to Fe_3O_4 and the hydrogen consumption upon further reduction to FeO is 1:2. The measured profile, however, shows that the area of the shoulder is much smaller than that of the first peak. Accordingly, it follows that the reduction does not proceed via a magnetite phase, which result is in agreement with those obtained by Mössbauer spectroscopy.

The second region can be assigned to the reduction of Fe^{2+} to Fe^{0}. This region consists of two maxima, both probably related to two different Fe^{2+} species reacting to Fe^{0}.

3.3.4 Discussion

The Mössbauer measurements have demonstrated that re-oxidation of the Fe^{2+} species present in the catalyst after reduction at elevated temperatures proceeds in hydrogen at ambient pressure at 300 K. A high water concentration within the support bodies causes the oxidation to be thermodynamically feasible [1]. The results show that transport of H_2O out of the pores of the support is very slow. Such a high residence time cannot be explained by diffusion alone, since water diffuses out of the pores within seconds [26]. Adsorption of water onto the pore walls or onto the iron surface is more likely to account for the slow transport. Agron et al. [27] have shown that monoclinic zirconia is capable of reacting with water to give two OH-groups at the support surface, or water can be physically adsorbed to a great extent. This was also observed on loaded zirconia [28]. Analogous to alumina [29], it is very likely that on zirconia two chemisorbed hydroxyl groups recombine to give water. This means that both chemisorbed and physisorbed H_2O may contribute to the slow removal of water out of the pores and, consequently, the re-oxidation of Fe^{2+}.

The slow transport of water out of the pores of the support can also explain the differences in extent of reduction obtained with the different techniques employed. In the TPR experiments a lower extent of reduction is found as compared to the MAS and TMA results. With MAS and TMA, this is demonstrated by the presence of metallic iron at reduction temperatures well below 773 K. The reduction to metallic iron is controlled by the ratio of water and hydrogen partial pressures, p_{H2O}/p_{H2}, and, in particular, the ratio present locally within the support bodies. This ratio determines the thermodynamic equilibrium between metallic iron and either Fe^{2+} or magnetite species. When the water partial pressure increases the equilibrium is shifted to the oxidised iron species [1]. Wimmers et al. [30] provided experimental confirmation showing that when water is added to the gas stream, especially the second reduction step is significantly delayed (exceeding 100 K). In TPR experiments presented here the applied heating rate is much higher as compared to the other techniques. The higher water production per unit time combined with a relatively low rate of water removal leads to a strongly delayed reduction.

From the experiments described above it must be clear that the (local) partial pressure of water plays an important role in reduction experiments. The volume of the catalyst being investigated, the gas flow through the catalyst bed and the rate at which the temperature is raised are affecting the transport of water out of the porous catalyst bodies. The local partial pressure of water in the catalyst bodies determines the rate and the extent of reduction of the iron species within the catalyst. Differences in the water vapour pressure during the reduction can lead to misinterpretations of the iron species present during the initial stage of, *e.g.* the Fischer-Tropsch reaction.

The Mössbauer experiments have shown that cooling of a reduced iron catalyst can result in re-oxidation of iron species. Slow re-oxidation at room temperature of the Fe^{2+} species formed during reduction at low temperature has been demonstrated beyond doubt.

The absence of the two hyperfine splittings of magnetite and the observed TPR-profile leads to the conclusion that Fe_3O_4 is an intermediate during the reduction to metallic iron or iron carbide. The absence of magnetite during reduction points to the formation of a ferrous species due to an intimate interaction with the support [2, 4-16].

With zirconia-supported iron catalysts a metal oxide-support interaction was suggested to account for the low reducibility [12-16]. Chen *et al.* [16] studied the reduction of a 7 wt% Fe_2O_3/ZrO_2 catalyst and claimed the presence of two mixed oxides, *viz.*, an initially formed spinel, $(Zr_yFe_{3-y})O_4$, which subsequent transforms into $(ZrO_2)(FeO)_2$. Both oxides would appear in different reduction steps. Our experiments exclude the presence of two different mixed oxides. The Mössbauer measurements reveal the presence of a high spin Fe^{2+} with a quadrupole splitting (1.2 to 1.5 mm/s) significantly higher than for bulk FeO (about 0.55 mm/s). Ghigna et al. [31] studied the incorporation of iron into a cubic ZrO_2 using Mössbauer spectroscopy, Fe K edge X-ray absorption spectroscopy and XANES. They found that iron enters the ZrO_2 lattice mainly as Fe^{2+} into two different sites, *viz.*, interstitial sites and substitutionally into defect sites. The quadrupole splitting at room temperature are reported to be for both sites as 2.41 ± 0.07 and 2.04 ± 0.03 (without assigning both contributions). These quadrupole splittings are much higher than the quadrupole splittings observed in this study for the Fe^{2+} species present in our catalysts. Our reduced catalysts exhibits a spectral component with an isomer shift of 0.7 to 0.8 mm/s and a quadrupole splitting of 0.6 to 0.8 mm/s, and a component with an isomer shift of 0.9 to 1.0 mm/s and a quadrupole splitting of 1.2 to 1.5 mm/s. The experimental data suggest that the component of the higher isomer shift and quadrupole splitting is more difficult to reduce than the other

component attributed to Fe^{2+} species. The doublet having the isomer shift of about 1.02 mm/s and the quadrupole splitting of about 1.41 mm/s is attributed to a mixed iron-zirconium oxide and the other Fe^{2+} contribution (isomer shift about 0.78 mm/s and quadrupole splitting about 0.73 mm/s) to a surface species. The mixed oxide is more difficult to reduce than the surface species.

The quadrupole splitting of the trivalent iron species formed upon re-oxidation of the divalent species is not significantly different from that of the fresh calcined catalyst, which indicates that the number of surface ions does not change upon reduction to Fe^{2+} and subsequent re-oxidation [32]. As to be expected, reduction to an iron oxide of a lower valency does not significantly affect its dispersion. The absence of a sextuplet at 300 K, which is indicative for the formation of larger hematite clusters (> 7 nm), also points to reduction to Fe^{2+} without a loss of dispersion.

The reduction of zirconia-supported iron catalysts proceeds roughly in two steps. The first step is the reduction to divalent iron. As mentioned above the dispersion of the iron(II) phase does not change significantly. The second step is reduction to metallic iron, which does affect the dispersion. The observed sextuplet at 300 K after reduction at 673 and 723 K points to the presence of large metallic iron particles. Ruckenstein and coworkers [33, 34] claim that a zerovalent metal phase exhibits a higher interfacial free energy than the oxidic phase. The lower wettability of the oxidic support by metallic iron thus causes coalescence of Fe^0 resulting in the formation of large(r) particles. The sintering of metallic nickel particles was found to proceed faster on a continuous $NiAl_2O_4$ layer [35]. It is not likely that the low loading of the support of our catalysts is sufficient to maintain a continuous layer of iron(II) oxide either or not penetrated into the zirconia surface with the catalyst thus reduced that a significant fraction of metallic iron is present. Some coalescence of the metallic iron particles is therefore to be expected as indicated by the Mössbauer spectra.

3.4 Results at elevated hydrogen pressures

3.4.1 Mössbauer absorption spectroscopy

3.4.1.1 Unpromoted Fe/ZrO_2

The reduction behavior of the freshly prepared Fe/ZrO_2 catalyst was additionally studied at elevated pressures of 1.8 bar and 9.5 bar, and at different temperatures. Some of the measured spectra are given in Figure 3.10.

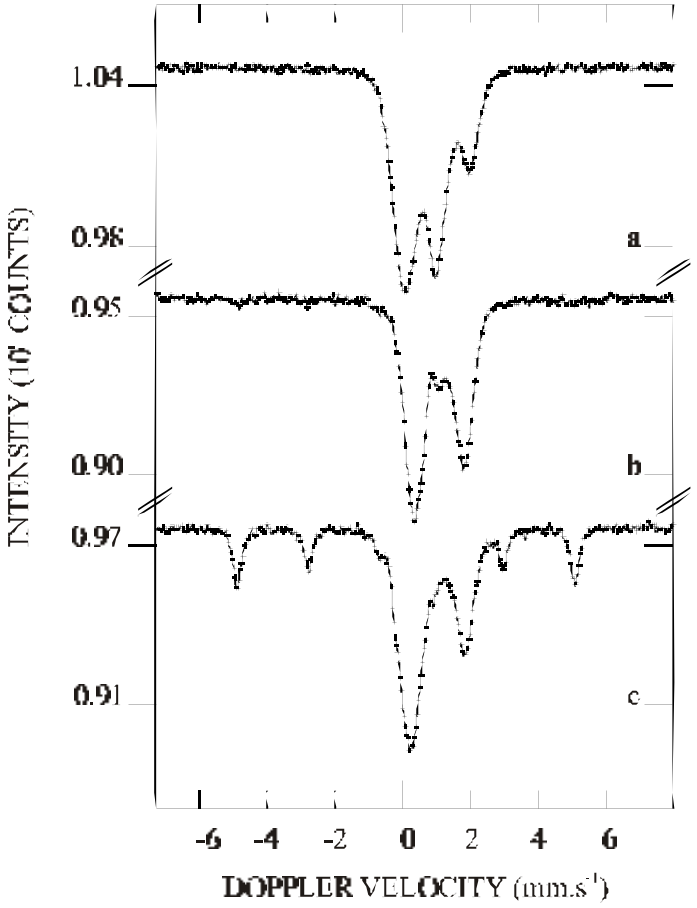

Figure 3.10 Reduction of Fe/ZrO_2 at (a) 473K, 1.8 bar; (b) 573K, 1.8 bar; (c) 623 K, 9.5 bar.

Table 3.6 *Mössbauer parameters of 2.5 wt% Fe/ZrO_2 calculated from spectra measured during reduction in H_2 at different temperatures at 1.8 and 9.5 bars.*

T(K)	p(bar)	I.S. (mm/s)	Q.S. (mm/s)	H_{eff} (kOe)	Γ (mm/s)	S.C. (%)	Compound
373	1.8	0.54	0.84		0.42	50	Fe^{3+}
(0-22h)		0.54	1.33		0.48	50	Fe^{3+}
473	1.8	0.48	0.88		0.49	46	Fe^{3+}
(0-22h)		0.48	1.42		0.44	21	Fe^{3+}
		1.15	1.62		0.56	33	Fe^{2+}
573	1.8	0.13			0.31	8	Fe^{0}
(0-19h)		0.70	0.86		0.37	13	Fe^{2+}
		1.12	1.37		0.56	79	Fe^{2+}
623	1.8	0.07	0.00	302	0.27	12	Fe^{0}
(0-23h)		0.09			0.49	18	Fe^{0}
		0.69	0.87		0.41	12	Fe^{2+}
		1.08	1.32		0.54	58	Fe^{2+}
623	1.8	0.05	0.00	302	0.27	20	Fe^{0}
(23-49h)		0.06			0.55	25	Fe^{0}
		0.67	0.84		0.29	6	Fe^{2+}
		1.08	1.33		0.55	49	Fe^{2+}
623	9.5	0.09	0.00	308	0.27	22	Fe^{0}
(0-21h)		0.06			0.53	26	Fe^{0}
		0.75	0.95		0.41	5	Fe^{2+}
		1.11	1.44		0.53	47	Fe^{2+}
673	9.5	0.05	0.00	301	0.28	28	Fe^{0}
(0-20h)		0.02			0.57	30	Fe^{0}
		0.68	0.84		0.29	4	Fe^{2+}
		1.07	1.38		0.52	38	Fe^{2+}

Γ is the line width.

The Mössbauer parameters derived from the spectra are tabulated in Table 3.6. Already during the reduction at 473 K (at 1.8 bars) trivalent iron is partially reduced to divalent iron. At 573 K all Fe^{3+} is reduced to Fe^{2+} and a small amount (8%) of metallic iron (Fe^0). The metallic iron (Fe^0) thus produced is present as such small particles that it behaves superparamagnetically at the measuring temperature of 573 K (no H_{eff}, only a single line is observed). Metallic iron in the normal ferromagnetic state is firstly observed at 623 K together with an increased amount of superparamagnetic Fe^0. Raising the pressure from 1.8 bar to 9.5 bar at 623 K does not change the spectral composition. However, the hyperfine field is observed to increase significantly; this increase is very likely caused by the compression of the metallic iron particles at the elevated pressure. Subsequent raising of the reduction temperature from 623 K to 673 K at 9.5 bar brings about an additional increase in the extent of reduction.

Whereas at ambient hydrogen pressure reduction at 573 K only leads to the presence of Fe^{2+}, reduction at 623 K leads to θ-Fe_3C, and reduction at 673 K is required to produce metallic iron, a higher hydrogen pressure leads already at 573 K to metallic iron. The reduction of the Fe^{3+} in the unpromoted Fe/ZrO_2 catalyst proceeds thus more easily at 1.8 bar as compared to reduction at 1 bar. The effect of the hydrogen pressure indicates that the extent of reduction after a long period of time is mainly determined by thermodynamics. Additionally, another very remarkable difference in the behavior during reduction at 1 bar and 1.8 bar is observed. The formation of iron carbide (θ-Fe_3C) during the reduction at 1 bar, as soon as the oxidic iron species becomes reduced to metallic iron, is totally absent during the reduction at 1.8 bar. Hence, it can be concluded that at the higher hydrogen pressure, the carbon present on the surface of the catalyst particles remaining from the citrate complex is hydrogenated. It is possible that the carbon first reacts to the iron carbide and is subsequently hydrogenated by hydrogen dissociated on the surface of the carbide or by dissociated hydrogen upon generated by metallic iron.

A large fraction of the formed metallic iron particles remains in the superparamagnetic state. Consequently, the iron particles are very small. The anchoring of these small particles on the ZrO_2-support seems to be facilitated by the removal of the carbon from the catalyst.

3.4.1.2 Potassium-promoted $Fe/K/ZrO_2$

Some of the *in situ* measured spectra are represented in Figure 3.11 and the results of the analysis of the spectra are also given in Table 3.7.

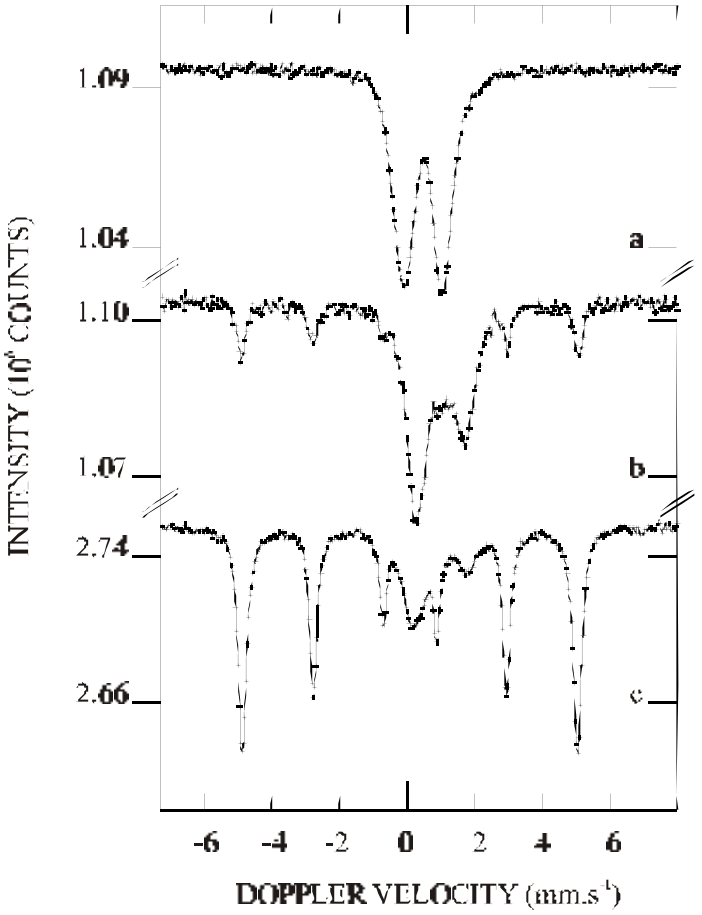

Figure 3.11 Mössbauer spectra measured during reduction of $Fe/K/ZrO_2$ at (a) 473 K, 1.8 bar; (b) 573 K, 1.8 bar, and (c) 623 K, 9.5 bar.

The Mössbauer parameters measured at 300 K and at different hydrogen pressure, *viz.*, 1 and 1.8 bar (not shown here), do not reveal any significant changes. The doublets observed at both pressures can be ascribed to a high-spin trivalent iron species. When the reduction temperature is increased to 473 K, the spectrum can still be fitted with similar Fe^{3+} -doublets indicating that no changes have occurred. At a higher reduction temperature, *viz.*, 573 K, the spectrum

changes substantially. A sextuplet is encountered representing metallic iron (Fe^0) in the normal ferromagnetic state, a single line representing Fe^0 in the superparamagnetic state and two doublets due to divalent iron species. As discussed in the previous section, one doublet having an isomer shift of 1.02 mm/s and quadrupole splitting of 1.41 mm/s relates to a mixed zirconium-iron(II) oxide and the other Fe^{2+} contribution (isomer shift is 0.78 mm/s and quadrupole splitting of 0.73 mm/s) represents a surface species.

By raising the reduction temperature to 623 K the amount of metallic iron in the ferromagnetic state increases enormously to above 70 %, while the amount of superparamagnetic Fe^0 remains constant. In contrast, the spectral contribution of the Fe^{2+} doublet relating to a mixed oxide has decreased, whereas the other Fe^{2+} doublet vanishes completely. When, at this temperature, the pressure is subsequently increased from 1.8 to 9.5 bars, the spectra are not revealing any significant change. This increase of the hydrogen pressure does not seem to bring about marked differences in the extent of reduction of the potassium-promoted $Fe/K/ZrO_2$ catalyst. Increasing the reduction temperature from 623 K to 673 K (while maintaining the pressure at 9.5 bar) neither changes the extent of reduction and the spectral composition significantly.

Table 3.7 *Mössbauer parameters of 2.5 wt% $Fe/K/ZrO_2$ calculated from spectra measured during reduction in H_2 at different temperatures at hydrogen pressures of 1.8 and 9.5 bars.*

T(K)	p(bar)	I.S. (mm/s)	Q.S. (mm/s)	H_{eff} (kOe)	Γ (mm/s)	S.C. (%)	Compound
300	1	0.62	0.71		0.44	54	Fe^{3+}
		0.62	1.16		0.44	46	Fe^{3+}
300	1.8	0.61	0.73		0.44	53	Fe^{3+}
(0-19h)		0.61	1.21		0.44	47	Fe^{3+}
373	1.8	0.54	0.83		0.45	56	Fe^{3+}
(0-21h)		0.54	1.33		0.48	44	Fe^{3+}
473	1.8	0.47	0.91		0.50	47	Fe^{3+}
(0-19h)		0.45	1.42		0.57	53	Fe^{3+}

Table 3.7 Continued.

T(K)	p(bar)	I.S. (mm/s)	Q.S. (mm/s)	H_{eff} (kOe)	Γ (mm/s)	S.C. (%)	Compound
573	1.8	0.080		308	0.27	20	Fe^0
(0-19h)		0.08			0.42	9	Fe^0
		0.78	0.73		0.61	22	Fe^{2+}
		1.02	1.41		0.59	49	Fe^{2+}
623	1.8	0.06	0.00	301	0.28	66	Fe^0
(0-25h)		0.06			0.49	8	Fe^0
		0.69	0.60		0.41	5	Fe^{2+}
		1.00	1.32		0.61	21	Fe^{2+}
623	1.8	0.05		302	0.28	71	Fe^0
(25-48h)		0.05			0.55	9	Fe^0
		0.60	0.60		0.35	4	Fe^{2+}
		1.01	1.32		0.62	16	Fe^{2+}
623	9.5	0.08		305	0.28	73	Fe^0
(0-22h)		0.08			0.65	11	Fe^0
		1.06	1.36		0.60	15	Fe^{2+}
623	9.5	0.08		306	0.28	75	Fe^0
(22-47h)		0.08			0.58	11	Fe^0
		1.08	1.35		0.62	14	Fe^{2+}
673	9.5	0.05		300	0.29	77	Fe^0
(0-21h)		0.05			0.65	11	Fe^0
		1.03	1.30		0.61	12	Fe^{2+}

Γ is the line width

Although the potassium-promoted catalyst $Fe/K/ZrO_2$ contains much more carbon remaining of the applied citrate complex than the unpromoted Fe/ZrO_2 catalyst, no iron carbide formation is observed during the reduction in H_2 at 1.8 bar. As with the Fe/ZrO_2 catalyst the carbon on the surface of the support is hydrogenated either by hydrogen atoms spilt over from neighboring metallic iron particles or after reaction with metallic iron to an iron carbide. However, it appears

that the larger amount of carbon present within the $Fe/K/ZrO_2$ catalyst delays the reduction at 473 K. At this reduction temperature no Fe^{2+} is observed and the formation of the corresponding mixed oxide seems to be necessary to anchor the metallic iron particles to avoid rapid sintering.

Above it was observed that thermal treatment at higher hydrogen pressures leads to removal of the carbon species remaining of the applied citrate complex. As with the reduction of the iron species present in the catalysts, the effect of the pressure points the hydrogen pressure affecting the thermodynamic equilibrium. In the reduction experiments of the unpromoted Fe/ZrO_2 catalyst at ambient hydrogen pressures, it has been found that cementite was even present during reduction for a long period of time both at low and at high temperatures. If the removal of the initial carbon species was dominated by kinetics, θ-Fe_3C would not be observed at all or the amount of the carbide would decrease during reduction for a long period of time. It is therefore concluded that the hydrogenation of the carbon species present after calcination is thermodynamically driven.

3.5 General discussion

First of all, the reduction of the unpromoted Fe/ZrO_2 catalyst will be discussed. It is important to note that the calcination temperature of the support loaded with ammonium iron(III) citrate is not sufficiently high to completely remove the carbon species remaining after decomposition of the chelating citrate [47]. As a result the zirconia support is covered by an amorphous layer containing iron(III) oxide and carbonaceous material.

Reduction at relatively low temperatures and ambient hydrogen pressure leads to formation of two types of iron(II) species. One is identified as a Fe^{2+} which upon formation immediately migrates into the zirconia support to give a mixed oxide. This species is –considering its high quadrupole splitting – well-ordered. the other relates to a surface species which is lowly ordered. This species is liable to be in contact with the said carbon species. It is demonstrated that first the surface species will be reduced which is to be expected taking into account that the mixed oxide is more stable under reducing conditions. Analogous to other mixed oxides *e.g.* silicates, aluminates [2, 4-16] the resistance to reduction increases, hence these oxides are only reduced at higher temperatures. In the case of the zirconia support, the zirconium ion binds the oxygen (which is part of the mixed oxide) more strongly resulting in a lower reducibility. As mentioned, in the proximity of the

surface species carbon is located, which appears to react with metallic iron. In this way, cementite is formed, which is present in relatively large particles (considering the sextuplet at 300 K). This can be explained by the high mobility of iron atoms in metallic iron surfaces, as opposed to the low mobility of iron in carbide lattices. This mobility enables Fe^0 particles to coalesce, after which these Fe^0 particles are readily converted to θ-Fe_3C. This process proceeds relatively fast as only the carbide is observed at low reduction temperatures.

The presence of cementite possibly induces the formation of relatively large iron clusters (demonstrated by a sextuplet). As soon as the maximum observed amount of the carbide species is reached metallic iron is found. Already at small Fe^0 contributions, iron is present as large clusters. It is known that metallic iron is rather mobile, consequently it will travel over oxidic surfaces (to which it is not bound to a great extent) [33, 34]. It further seems plausible that metallic iron preferably remains within the boundary of a mixed oxide island [35]. It is not excluded that these zerovalent iron particles move across the zirconia support or a carbonaceous layer, but these particles eventually end up in contact with an iron-containing underlayer (which acts as a kind of energy well) and cause the zerovalent iron to sinter directly after formation. The carbonaceous material remaining from the citrate was observed to prevent sintering of the iron(III) species during calcination [24], but it (and/or θ-Fe_3C) promotes sintering of the iron particles produced by subsequent reduction.

Performing the reduction at hydrogen pressure at about 1.8 bar removes the carbon by hydrogenation. This hydrogenation reaction is thermodynamically driven and already proceeds at relatively low temperatures (below 573 K). As a consequence, the carbide is not observed and reduction of divalent iron proceeds directly to metallic iron. Together with the (surface) Fe^{2+} species already present, the small metallic iron particles will be anchored by the patches of the mixed iron-zirconium oxide. Subsequent reduction at elevated pressures and higher temperatures leads to more small metallic iron particles. Since mobility and thus coalescence of small iron particles cannot be completely prevented, reduction at a hydrogen pressure of 9.5 bar and 673 K will eventually produce about 30 % of large and about 30 % of superparamagnetic and, hence, small iron particles. The interesting feature of the reduction at more elevated pressure is that, whilst the carbonaceous material prevents sintering of the iron(III) oxide during calcination, the carbon is rapidly removed during the reduction (at low temperatures), its removal bringing about the presence of small Fe^0 particles.

Co-impregnation with potassium carbonate changes the behavior of the zirconia-supported iron catalysts during thermal treatment completely. In our experiments it is clearly shown that the potassium-rich sample reduces more easily both at ambient and elevated pressure compared to the unpromoted catalyst. In literature, it is often encountered that potassium retards the reduction process by impeding the dissociation of hydrogen [36] or by blocking of the pores by potassium compounds limiting H_2 accessibility or preventing water to leave the reduced iron site [12, 13, 37]. In contrast, it is also reported that potassium – when part of the metal lattice – is able to enhance the hydrogen dissociation and, hence, the reduction [38]. The high initial dispersion of the catalysts under study may account for the enhanced reduction as was also observed by Guglielminotti *et al.* [39]. It is empirically established that upon mixing ammonium iron(III) citrate with potassium carbonate, NH_3 and CO_2 evolve, indicating that (at least part of the) potassium is atomically spread in the citrate precursor. Considering this, it is likely that the potassium species is well spread over the oxidic iron surface. Therefore it may accelerate the dissociation of hydrogen on the iron surface, or it is so well spread that this compound does not block any pores (enabling water to be removed and hydrogen to be provided).

In the following, the possible nature of the potassium species present in the catalyst will be discussed. In view of this, the interaction of potassium carbonate during calcination with the iron oxide and the carbonaceous material resulting from the decomposition of the citrate has to be considered. Potassium carbonate reacts at more elevated temperatures (above 1000 K) with iron(III) oxide to potassium ferrite, $KFeO_2$, under release of carbon dioxide [40, 41]. If the α-Fe_2O_3 species is highly dispersed and also in the presence of steam the reaction to $KFeO_2$ occurs already at 723 K [42]. $KFeO_2$ has a characteristic light-green color, but the compound is not stable upon exposure to atmospheric air [43, 44]. The olive green colour was never observed in our experiments. Stobbe [43] observed $KFeO_2$ at calcination temperatures above 923 K for a well-dispersed iron-on-magnesia catalyst. Zirconia-supported iron-based catalysts reveal $KFeO_2$ after calcination at 1023 K [44]. Both Stobbe [43] and Boot [44] prepared their catalyst through incipient wetness impregnation with the same precursors (ammonium iron(III) citrate and potassium carbonate) as applied here. The main difference between their experiments and those described here is the lower calcination temperature, namely 723 K. Apparently, this temperature is too low for the reaction to $KFeO_2$ to occur and, moreover, Mössbauer experiments have not shown any sign of the potassium ferrite. Although the ferrite is not present, Boot has shown using infrared

experiments that K_2CO_3 is present after calcination [44]. Based on the aforementioned it is likely that K_2CO_3 is initially present in the catalyst.

In literature, it is reported that this carbonate may react with hydrogen to potassium hydroxide (KOH) or it may disproportionate to potassium oxide (K_2O) and carbon dioxide [37, 45]. On carbon, KOH and/or K_2O spread out over the carbon surface [46] and in this way impeding the oxidation (of the carbon species) during calcination. Consequently, the carbon content of the catalyst prepared by co-impregnation of potassium carbonate is much more elevated than that of the catalyst prepared by impregnation of ammonium iron citrate only.

3.5.1 Reduction model

Based on the above, a model of the reduction of the iron(III) oxide is proposed. A schematic representation of this reduction model is shown in Figure 3.12. It must be noted that the presence of a potassium species or the presence of an iron carbide are not considered in the presented reduction model. A specific reduction temperature cannot be mentioned in the model as this temperature heavily depends on the amount of water present (or produced).

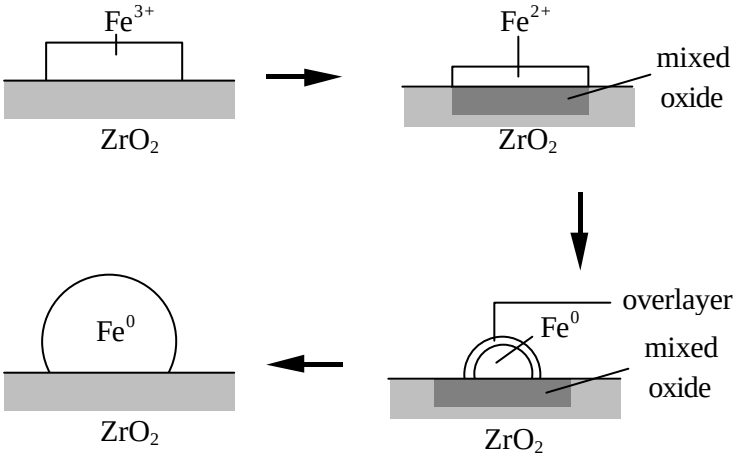

Figure 3.12 Schematic model for the reduction of 2.5 wt% Fe/ZrO_2. The sequence of reduction is indicated by the arrows.

The initial state of the iron phase is characterised by a very thin (superparamagnetic) amorphous layer in which iron is exclusively in the trivalent

state [47]. Upon reduction Fe^{3+} is converted to two Fe^{2+} species, one of which is related to a mixed oxide, the other to a surface species.
Further reduction to metallic iron proceeds in two steps. The first step is the transformation of an easier reducible divalent iron species which is probably a surface species into metallic iron. In the second step the mixed oxide is reduced. At ambient pressure (when θ-Fe_3C is present), large agglomerates of iron are formed as soon as metallic iron is formed, which results in loss of dispersion. In contrast, at elevated pressure next to these large Fe^0 clusters, superparamagnetic Fe^0 is encountered. This latter species very likely interacts with the underlying mixed oxide. The larger iron clusters are possibly covered by either an oxidic overlayer or a carbidic overlayer which prevents the iron to be oxidised by water at room temperature.

3.6 Conclusions

From the results presented in this chapter it is deduced that the reduction of the initially present iron species proceeds according to the steps shown in the Figure below.

In this Figure Fe_I and Fe_{II} denote surface and mixed oxide divalent iron species, respectively. Both species are directly formed upon reduction of Fe^{3+}, whereby this trivalent component is almost completely converted to Fe^{2+} before metallic iron is formed. The mixed oxide species is stabilised by the support and is reduced at higher temperatures compared to the surface Fe^{2+} species.

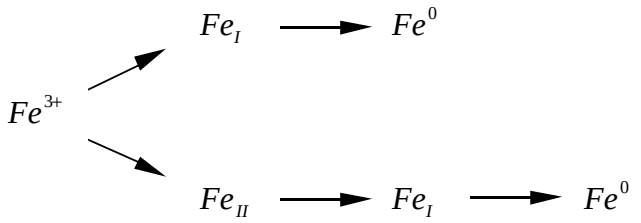

Figure 3.13 Reduction of highly dispersed trivalent iron.

Reduction at 1 bar reveals cementite for both potassium-promoted and unpromoted catalysts. This θ-carbide is formed immediately after zerovalent iron is present, which formation is a consequence of the presence of a carbon species remaining in both catalysts after decomposition of the organic chelate precursor.

The amount of carbon is larger in the potassium-promoted catalyst. At elevated pressure this carbide is not encountered due to its removal at temperatures below 573 K. The absence of carbon enables the formation of a superparamagnetic Fe^0 species. Next to this species, large Fe^0 clusters are observed. In contrast, reduction at 1 bar only reveals the larger metallic iron species.

The above reduction process is found to proceed faster on the potassium-rich catalyst and, moreover, proceeds faster at elevated pressures.

It is further shown that water (formed during reduction) can hardly be removed due to adsorption on the pore walls of the support. This water gives rise to re-oxidation when the reaction temperature is decreased to 300 K. Remarkable is the observation that only Fe^{2+} is oxidised to Fe^{3+} and not Fe^0, which is explained by an oxidic or a carbidic protecting layer. In view of these considerations, it should be borne in mind that high local water concentrations may lead to misinterpretations of the iron species present in the initial stage in *e.g.* the Fischer-Tropsch reaction.

3.7 References

[1] A.J.H.M. Kock, H.M. Fortuin and J.W. Geus, *J.Catal.* **96** (1985) 261.

[2] X. Gao, J. Shen. Y. Hsia and Y. Chen, *J.Chem.Soc.Faraday Trans.* **89(7)** (1993) 1079.

[3] Gmelins Handbuch der Anorganische Chemie, 59: Eisen, Teil A-Ableihung II, Verlag Chemie, Berlin, Germany, 1692.

[4] M.V. Cagnoli, S.G. Marchetti, N.G. Gallegos, A.M. Alvarez, R.C. Mercader and A.A. Yeramian, *J.Catal.* **123** (1989), 21.

[5] A.F.H. Wielers, A.H.J.M. Kock, C.E.C.A. Hop, J.W. Geus and A.M. van der Kraan, *J.Catal.* **117** (1989) 1.

[6] Y-Y. Huang and J.R. Anderson, *J.Catal.* **40** (1975) 143.

[7] M.C. Hobson Jr and H.M. Gager, *J. Colloid Interface Sci.* **34(3)** (1970) 357.

[8] S. Yuen, Y. Chen, J.E.Kubsh, J.A. Dumesic, N. Topsøe and H. Topsøe, *J.Phys.Chem.* **86** (1982) 3022.

[9] B.J. Tatarchuk and J.A. Dumesic, *J.Catal.* **70** (1981) 335.

[10] S.J. Tauster, S.C. Fung, R.T.K. Baker and J.A. Horsley, *Science* **211**, 4487 (1981) 1121.

[11] D.E. Stobbe, F.R. van Buren, A.W. Stobbe-Kreemers, A.J. van Dillen and J.W. Geus, *J.Chem.Soc.Faraday.Trans.* **87(10)** (1991) 1631.

[12] L.A. Boot, A.J. van Dillen, J.W. zGeus and F.R. van Buren, *J.Catal.* **163** (1996), 186.

[13] L.A. Boot, A.J. van Dillen, J.W. Geus, A.M. van der Kraan, A.A. van der Horst and F.R. van Buren, *Appl..Cat.* **147** (1996) 389.

[14] E. Guglielminotti, *J.Phys.Chem.* **98** (1994) 4884.

[15] E. Guglielminotti, *J.Phys.Chem.* **98** (1994) 9033.

[16] K. Chen, Y. Fan, Z. Hu and Q.Yan, *Catal.Lett.* **36** (1996) 130.

[17] A.M. van der Kraan, J.W. Niemantsverdriet, *'Industrial Applications of the Mössbauer Effect'*, G.J. Long, J.G. Stevens (eds), Plenum, New York, 1986, 609.

[18] P.W. Selwood, *'Chemisorption and Magnetization'*, Academic Press, New York, 1975.

[19] J. van de Loosdrecht, Ph.D Thesis, Utrecht University, 1995, Chapter 2.

[20] Thermodynamic calculations with "HSC Chemistry", Version 3.02, Outukumpu Research oy, Pori, Finland.

[21] S.J. Roosendaal, Thesis, Utrecht University, Utrecht, 1999, Chapter 6.

[22] T.J. Vink, J.M. der Kinderen, O.L.J. Gijzeman and J.W. Geus, *Appl.Surf.Sci.* **26** (1986) 357.

[23] T.J. Vink, S.J.M. Sas, O.L.J. Gijzeman and J.W. Geus, *J.Vac.Sci.Technol.* **A5** (1987) 1028.

[24] Chapter 2 of this thesis.

[25] J.W. Niemantsverdriet, *'Spectroscopy in Catalysis'*, Weinheim, VCH, 1993, Chapter 5

[26] J.H. de Boer, 'The dynamical Character of adsorption', Clarendon Press, Oxford, 1953.

[27] P.A. Agron, E.L. Fuller, Jr. and H.F. Holmes, *J.Colloid Interface Sci.* **52** (1975) 553.

[28] L.A. Boot, PhD Thesis, Utrecht University, 1994, Chapter 7.

[29] H. Knözinger and P. Ratnasamy, *Catal.Rev.-Sci.Eng*. **17** (1978) 31.

[30] O.J. Wimmers, P. Arnoldy and J.A. Moulijn, *J.Phys.Chem.* **90** (1986) 1331.

[31] P.Ghigna, G. Spinolo, U. Anselmi-Tamburini, F. Maglia, M. Dapiaggi, G. Spina and L. Cianchi, *J.Am.Chem.Soc.* **121** (1999), 301.

[32] A.M. van der Kraan, *Phys.Stat.Sol.(a)* **18** (1973) 215.

[33] I. Sushumna and E. Ruckenstein, *J.Catal.* **94** 1985), 239.

[34] E. Ruckenstein and X.D. Hu, *J.Catal.* **100** (1986) 1.

[35] P.H. Bolt, Ph.D. Thesis, Utrecht University, 1994, Chapter 7.
[36] C-K. Kuei, J-F. Lee and M-D. Lee, *Chem.Eng.Comm.* **101** (1991) 77.
[37] Jan van de Loosdrecht, Ph.D. Thesis, Utrecht University, 1995, Chapter 7.
[38] J.J. Mortenson, B. Hammer, and J.K. Norskov, *Phys.Rev.Lett.* (80) (1998) 4333.
[39] E. Guglielminotti, F. Boccuzzi, F. Pinna and G. Strukul, *J.Catal.* **167** (1997), 153.
[40] N.V. Dvoretskii, E.G. Stepanov, T.N. Sudzilovskaya, G.R. Kotel'nikov and V.V. Yun, *Kin.Catal.* **17** (1976), 654.
[41] J. Subrt, J. Vins, I.S. Shaplygin and A.A. Zakharov, *Thermochim. Acta* **93** (1985), 489.
[42] L.M. Plyasova, M.M. Andrushkevich, G.R. Kotel'nikov, R.A. Buyanov, G.A. Khramova and S.F. Bednov, *Kin.Catal* **17** (1976) 1116.
[43] D.E. Stobbe, PhD Thesis, Universiteit Utrecht, 1990, Chapter 7.
[44] L.A. Boot, PhD Thesis, Universiteit Utrecht, 1994, Chapter 4.
[45] D.J. Dwyer, *'Physics and Chemistry of Alkali Metal Adsorption'*, Elsevier, New York, 1989, 307.
[46] A. Cerfontain, Ph.D thesis, University of Amsterdam, 1986, Chapter 3.
[47] Chapter 2 of this thesis.

4

The Effect of H_2/H_2O Pre-treatment on the Reduction Behaviour of Fe/ZrO_2

Abstract

In this chapter the effect of pre-treatment in H_2/H_2O atmosphere of a zirconia-supported iron-based catalyst is studied.

It is found that such a treatment results in a slightly lower reducibility which is due to a larger amount of iron interacting with the zirconia support via stabilising a mixed oxide. Divalent iron is easily removed out of the mixed oxide by oxidation at room temperature.

The catalyst under study contains carbon before treatment in H_2/H_2O. It is observed, that at relatively low temperature and at ambient pressure the initially present carbon is removed.

4.1 Introduction

A highly dispersed Fe/ZrO_2 was prepared and its reduction behaviour was studied in chapter 3. It was found that a mixed oxide of iron with the ZrO_2 support is able to stabilise (small) metallic iron particles.

In literature, several possibilities are suggested for preventing metal particles from sintering. One possibility is the addition of a textural promoter, e.g., alumina with iron catalysts for the ammonia synthesis [1] and magnesium oxide with nickel-on-α-alumina catalysts [2]. Enhancing the interaction of the active species with the support is another possibility. Many authors have mentioned an interaction between iron species and the support resulting in a lower reducibility of the iron compound [3-8]. On alumina- and silica-supported catalysts the interaction is attributed to the presence of ferrous aluminates and silicates, respectively. Wielers observed the formation of a silicate layer during reduction indicating that as soon as divalent iron is formed, iron migrates into the support [5]. Also titania and magnesia carriers mixed oxides are reported to account for the intimate contact between metal and support [9,10]. Guglielminotti used FTIR to demonstrate an interaction between an iron precursor and a zirconia support after calcination at 623 K [11]. His study furthermore revealed a lower reducibility of the iron phase interacting strongly with the zirconia support.

For a nickel-on-alumina model system Bolt has shown that the resistance against sintering is improved in the presence of an interfacial layer of $NiAl_2O_4$. In order to increase the sintering resistance a discontinuous layer of the aluminate appeared to be even more favorable [12]. Furthermore, it was shown that addition of steam results in a higher rate of spinel formation due to hydroxylation of the surface, which enhances diffusion of the metal ion [13].

Summarizing, with silica- and alumina-supported catalysts an interaction between the iron precursor and the support is generally established through reduction of Fe^{3+} to Fe^{2+}, which subsequently migrates into the support forming a new compound. The migration is a relatively slow (diffusion-controlled) process, which proceeds more rapidly at higher temperatures and/or by treatment with steam. In addition, thermodynamics predicts that in a gaseous environment of a H_2/H_2O ratio of 1, reduction to metallic iron is impossible below 1000°C [14]. Based on the previously mentioned arguments, pre-treatment with H_2 and H_2O should enhance the metal-support interaction. The improved interaction will change the reduction behaviour of the iron precursor.

This chapter deals with an investigation of the effect of thermal pre-treatment in a H_2/H_2O flow on the reducibility of the zirconia-supported iron-based

catalyst. Using Mössbauer spectroscopy (MAS) and thermomagnetic analysis (TMA) structure-property relation are studied. Moreover, with Mössbauer spectroscopy the changes induced by the pre-treatment were monitored *in situ* prior to reduction. The results are particularly relevant for the production of iron catalysts on a large scale. With large volumes of catalyst to be reduced, it is inevitable that some sections of the catalyst bed will be exposed at elevated temperatures to a flow containing steam that is produced by the reduction of other sections of the catalyst bed. When exposure to steam during the reduction leads to a lower reducibility of the iron species within the catalyst, scaling up of the reduction treatment has to be performed cautiously.

4.2 Experimental

4.2.1 Catalyst preparation

For details of the preparation of Fe/ZrO_2 and $Fe/K/ZrO_2$ the reader is referred to chapter 2.

4.2.2 Characterisation techniques

4.2.2.1 Mössbauer Absorption Spectroscopy (MAS)

Mössbauer measurements were carried out in a constant acceleration mode using a ^{57}Co in Rh source. Isomer shifts are reported relative to the NBS standard sodium nitroprusside ($Na_2Fe(CN)_5NO.2H_2O$). Magnetic hyperfine fields were calibrated with the 515 kOe field of α-Fe_2O_3 at room temperature. The Mössbauer parameters were determined by fitting the spectra with subspectra consisting of Lorentzian-shaped lines using non-linear iterative minimisation routine. The accuracy for the isomer shift (I.S.) is ±0.03 mm/s, for the electric quadrupole splitting (Q.S.) ±0.05 mm/s and for the spectral contribution (S.C.) 5%.

Approximately 60 mg of the catalyst was mounted into an *in situ* Mössbauer reactor described in more details in [15]. This catalyst sample is pre-treated in a flow of Ar(90 ml/min)/H_2(3 ml/min) passed through a water column kept at room temperature leading to a H_2/H_2O of 1 (mol/mol). Pre-treatments are performed at 573 K, 623 K, and 673 K during approximately 24 hours. The sample is measured during a pre-treatment, as well as at room temperature after each pre-treatment step.

Subsequent to the described pre-treatment, the catalyst was measured during exposure to H_2 at 573, 623, 673, and 773 K.

4.2.2.2 Thermomagnetic Analysis (TMA)

The catalysts – approximately 150 mg of Fe/ZrO_2 of a grain size from 150 to 500 µm – were pre-treated in a quartz flow reactor of a diameter of 10 mm at atmospheric pressure. The gas feed contained 10 vol% H_2, 10 vol% H_2O and balance He at a total flow rate of 100 ml/min. The catalysts were exposed to this gas flow at 673 K for 0, 2, and 24 hours. Other conditions were 2 hours within the above gas flow at 573 and 773 K. Following this pre-treatment the samples were analysed using thermomagnetic analysis as described in the following.

High-field magnetic measurements were performed using a modification of the Weiss-extraction method [16, 17]. With this technique (thermomagnetic analysis or TMA), it is possible to monitor the magnetisation of the iron phase under reaction conditions. Experiments were carried out with a magnetic field strength of 7 kOe.

All samples were measured in a 50 ml/min 10% H_2/He gas flow from 298 K up to a temperature of 823 K. The temperature was raised in steps of 10 K and the magnetisation was determined at every temperature. Subsequently, the magnetisation was measured at temperatures decreasing in steps of 10 K to room temperature. The magnetisation was normalised taking into account the total mass of iron in the measured sample.

4.3 Results

4.3.1 Mössbauer Absorption Spectroscopy (MAS)

In this section the changes of the iron species during (*in situ*) pre-treatment in the H_2/H_2O atmosphere are first described. Subsequently, reduction of the pre-treated catalyst as studied with Mössbauer spectroscopy is discussed.

4.3.1.1 *In situ* H_2/H_2O pre-treatment

The zirconia-supported iron-based catalyst was exposed to the gas flow containing H_2 and H_2O at different temperatures. Figure 4.1 represents the Mössbauer spectra measured during the H_2/H_2O pre-treatments. The Mössbauer

parameters derived from these spectra are given in Table 4.1.

Table 4.1 *Mössbauer parameters of 2.5 wt% Fe/ZrO_2 calculated from spectra recorded during pre-treatment in H_2/H_2O (1/1 vol/vol) at different temperatures.*

T(K)	I.S. (mm/s)	Q.S. (mm/s)	Γ (mm/s)	S.C. (%)	Compound
300	0.61	0.71	0.39	49	Fe^{3+}
	0.60	1.18	0.44	51	Fe^{3+}
573	0.46	0.75	0.48	33	Fe^{3+}
(0-21h)	0.44	1.23	0.49	25	Fe^{3+}
	1.07	1.46	0.60	42	Fe^{2+}
623	0.46	0.88	0.58	32	Fe^{3+}
(0-23h)	1.03	1.17	0.50	39	Fe^{2+}
	1.07	1.66	0.44	29	Fe^{2+}
673	0.49	0.91	0.67	37	Fe^{3+}
(2-21h)	1.01	1.50	0.42	32	Fe^{2+}
	0.98	1.05	0.42	31	Fe^{2+}
300	0.60	0.72	0.39	40	Fe^{3+}
(0-19h)	0.61	1.16	0.48	60	Fe^{3+}

Γ is the line width.

As presented in Chapter 2 of this thesis the spectrum of the fresh Fe/ZrO_2 catalyst consists of a doublet exclusively assigned to high-spin Fe^{3+} (see Figure 4.1a). The spectrum is analysed with two high-spin Fe^{3+} contributions, with equal I.S.-values, but different Q.S.-values. Following Van der Kraan [18], these different Q.S.-values can be attributed to iron ions surrounded by other ions within small iron oxide particles (Q.S.= 0.71 mm/s) and iron ions situated at the surface of such particles (Q.S.= 1.18 mm/s).

Due to the pre-treatment in H_2/H_2O at 573 K, the spectral shape is changed (see Figure 4.1b). The Fe^{3+} in the catalyst is partly reduced to Fe^{2+}. The spectrum is

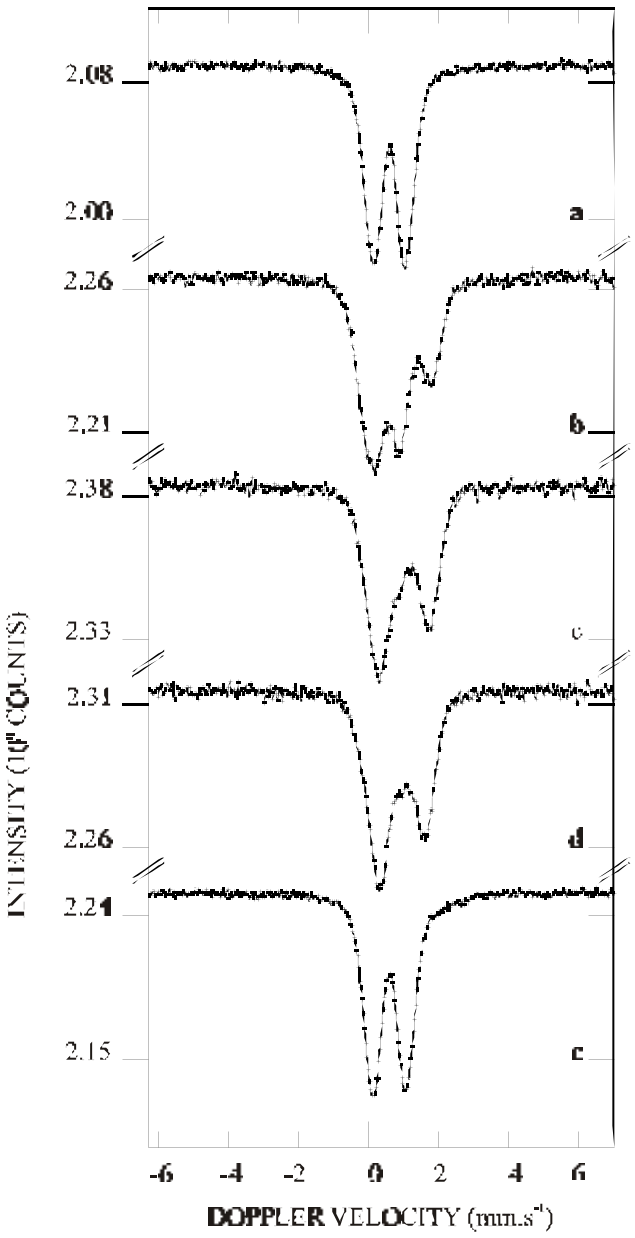

Figure 4.1 *Mössbauer spectra of 2.5 wt% Fe/ZrO_2: (a) freshly prepared catalyst at 300 K, and during pre-treatment in H_2/H_2O at (b) 573 K; (c) 673 K; (d) 773 K and subsequently at (e) 300 K.*

analysed with two Fe^{3+} contributions and one Fe^{2+} contribution which has been ascribed to a mixed oxide with ZrO_2 forming at the iron-support interface[16].

Following pre-treatment at 573 K, the catalyst was cooled to 300 K and several measurements were subsequently performed at room temperature (not shown in Figure 4.1 and Table 4.1). From these measurements it followed that at 300 K the divalent iron species is almost completely re-oxidised by water released from the zirconia support. It turned out that this oxidation process initially proceeds slowly, but after approximately 20 hours rather rapidly. After about 65 hours, the Fe^{2+} responsible for the mixed oxide is still present (with a spectral contribution of 19%).

Increasing the temperature of the pre-treatment to 623 K causes an increase in the total spectral contributions of the Fe^{2+} species as compared to the results at 573 K. A further increase of the pre-treatment temperature to 673 K (see Figure 4.1d) has hardly any influence on the calculated spectral composition. As opposed to reduction in pure hydrogen [16], these experiments do not reveal any metallic iron. This is easily understood from thermodynamics: the applied relative partial pressure $P_{H2}/P_{H2O}= 1$ (during the pre-treatment) prevents reduction to metallic iron. Figure 4.1e clearly shows that after cooling the catalyst to 300 K almost complete re-oxidation to trivalent iron proceeds.

For silica-supported iron oxide Wielers [5] observed that after reduction to Fe^{2+} a silicate layer was formed. The divalent iron species can be extracted out of this silicate layer by oxidation at high temperatures (during evacuation) to form hematite (α-Fe_2O_3). In our experiments oxidation occurs already at ambient temperature, whereby the Fe^{2+} is almost completely extracted from the mixed oxide. The calculated parameters of the spectrum of the fresh catalyst and of the re-oxidised catalyst are similar (after a pre-treatment at 673 K, see Table 4.1 and Figure 4.1d). It can thus be concluded that the dispersion has not changed significantly during the pre-treatment. The reduction-re-oxidation process is fully reversible.

4.3.1.2 Subsequent reduction

After the pre-treatment in H_2/H_2O at 673 K, the catalyst is reduced for approximately 24 hours in H_2 at 573 K, 623 K, and 673 K. Figure 4.2 shows the Mössbauer spectra measured during the reduction treatments. The Mössbauer parameters calculated from the spectra recorded during the reduction experiments are represented in Table 4.2.

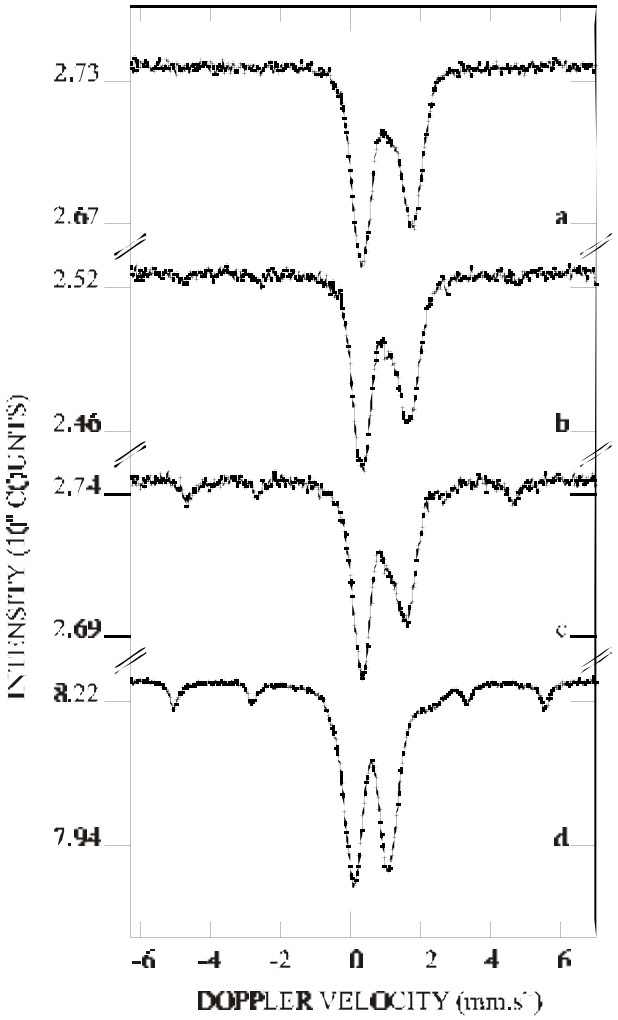

Figure 4.2 *Mössbauer spectra of a pre-treated (H_2/H_2O, 673 K) 2.5 wt% Fe/ZrO_2 catalyst recorded during subsequent reduction in H_2 at (a) 573 K; (b) 623 K; (c) 673 K and subsequently cooled to and measured at (d) 300 K.*

It turns out that the spectral contributions during the reduction at 573 K (see Figure 4.2a) and 623 K (see Figure 4.2b) are similar. Two Fe^{2+} species are found which exhibit the same parameters as the Fe^{2+} species found during pre-treatment, *viz*., a mixed oxide (with a high quadrupole splitting) and a surface

species (with a low quadrupole splitting), as represented by the proposed reduction model [16]. In addition, a rather small amount of a singlet is observed. The singlet can be ascribed to superparamagnetic $Fe^{0.}$

Table 4.2 *Mössbauer parameters of pre-treated (H_2/H_2O, 673 K) 2.5 wt% Fe/ZrO_2 calculated from spectra recorded during reduction in H_2 at different temperatures.*

T(K)	I.S. (mm/s)	Q.S. (mm/s)	H_{eff} (Oe)	Γ (mm/s)	S.C. (%)	Compound
573	0.00			0.29	4	Fe^0
(0-24h)	1.00	1.05		0.60	45	Fe^{2+}
	1.08	1.58		0.46	51	Fe^{2+}
623	0.03			0.28	5	Fe^0
(0-23h)	0.94	0.97		0.59	47	Fe^{2+}
	1.05	1.47		0.46	48	Fe^{2+}
673	0.02		290	0.36	13	Fe^0
(0-24h)	0.03			0.33	5	Fe^0
	0.83	0.81		0.50	28	Fe^{2+}
	0.99	1.32		0.50	54	Fe^{2+}
300	0.27		331	0.31	13	Fe^0
(24-96h)	0.60	0.79		0.43	38	Fe^{3+}
	0.61	1.28		0.50	39	Fe^{3+}
	1.21	2.17		0.71	10	Fe^{2+}
773	-0.04		275	0.27	42	Fe^0
(0-24h)	0.00			0.43	3	Fe^0
	0.71	0.73		0.48	30	Fe^{2+}
	0.94	1.16		0.45	25	Fe^{2+}

Γ is the line width.

Reduction at 673 K (see Figure 4.2c) leads to a sextuplet attributed to metallic iron (13% spectral contribution), a singlet ascribed to superparamagnetic Fe^0 (5% spectral contribution) and the two divalent iron species of which the mixed oxide is most abundant. Subsequent cooling to 300 K (see Figure 4.2d) again shows re-oxidation of the divalent iron species; only a small amount of the mixed

oxide remains present. The superparamagnetic iron is completely oxidised. Only the spectral contribution of the sextuplet of Fe^0 does not seem to change.

The catalyst is further reduced at 773 K. During this reduction treatment the amount of metallic Fe^0 rises to a spectral contribution of about 45% (see Table *4*.2). By cooling the catalyst to room temperature, it is found that also after this reduction treatment re-oxidation of the catalyst only affects the divalent iron species and the small spectral contribution of the superparamagnetic Fe^0. Subsequent exposure to air did not change the spectrum.

Although during the reduction of the H_2/H_2O pre-treated catalyst metallic Fe^0 is formed (see Table *4*.2 and Figure *4*.2), the formation of iron-carbides as described in Chapter 3 of this thesis is not observed. Most likely the carbon species remaining in the catalyst after decomposition of the citrate precursor in the calcination step is removed by the pre-treatment in H_2/H_2O. This is explained by the catalytic effect of iron oxide on the reaction of steam with carbon to hydrogen and carbon monoxide.

4.3.2 Thermomagnetic Analysis

As an example the thermomagnetic profile of the Fe/ZrO_2, as presented in Figure 3.7 [16], comprises several characteristics, *viz*., (i) an onset temperature T_{onset}, at which an increase in magnetisation is observed, (ii) a first reduction range M_I following T_{onset} ended by an inflection point, (iii) the temperature $T_{inflection}$ marking the inflection point, (iv) a second reduction range M_{II} following the inflection point up to the maximum reduction temperature, and (v) a final magnetisation M_{final} at room temperature (following cooling from the maximum temperature). These characteristics are indicated in the Figure 4.3 below.

In this section thermomagnetic analysis will be employed to investigate the reduction of zirconia-supported iron catalysts that are pre-treated in a H_2/H_2O flow. In these experiments the temperature at which the pre-treatment is carried out is varied. The object is to assess whether the pre-treatment changes the reduction behaviour of the iron species in the catalyst. A change in reducibility can be easily established by not only considering the final magnetisation, but also T_{onset}, the relative size of M_I and the temperature $T_{inflection}$.

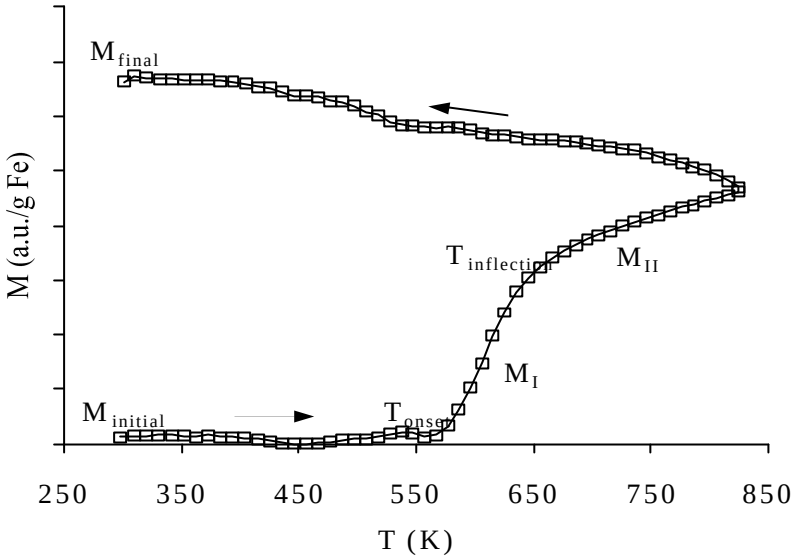

Figure 4.3 *Characteristic features of a TMA-profile of Fe/ZrO_2 (this Figure is similar to Figure 3.7 [16].*

4.3.2.1 The influence of temperature

The effect of the temperature of the pre-treatment is studied by pre-treating the catalyst for 2 hours at 673 and at 773 K. Figure 4.4 presents the resulting TMA-profiles. It is clearly shown that the profiles of the pre-treated catalyst show the same characteristics as the profile of the fresh catalyst. However, it is also evident that details of the profiles differ significantly. Some aspects of the measured profiles are tabulated in Table 4.3.

Table 4.3 *Thermomagnetic analysis of the freshly prepared catalyst and the catalyst pre-treated for 2 hours at 673 and 773 K.*

Conditions	M_{final} (a.u.[a])	Red. degree (%)	T_{onset} (K)	M_I (a.u.[a])
Fresh	6.4	100	570	2.9
673 K	4.4	65	590	2.5
773 K	4.0	61	590	1.5

[a] value is normalised per gram Fe^0.

The data of Table 4.3 show that both the pre-treated catalysts exhibit a smaller final magnetisation, M_{final}, as compared to that of the fresh catalyst. Based on the discussion in chapter 3, the extent of reduction can be calculated. Table 4.3

includes the thus calculated extents of reduction. The calculated extents of reduction suggest that reduction to metallic iron is more limited after pre-treatment at higher temperature.

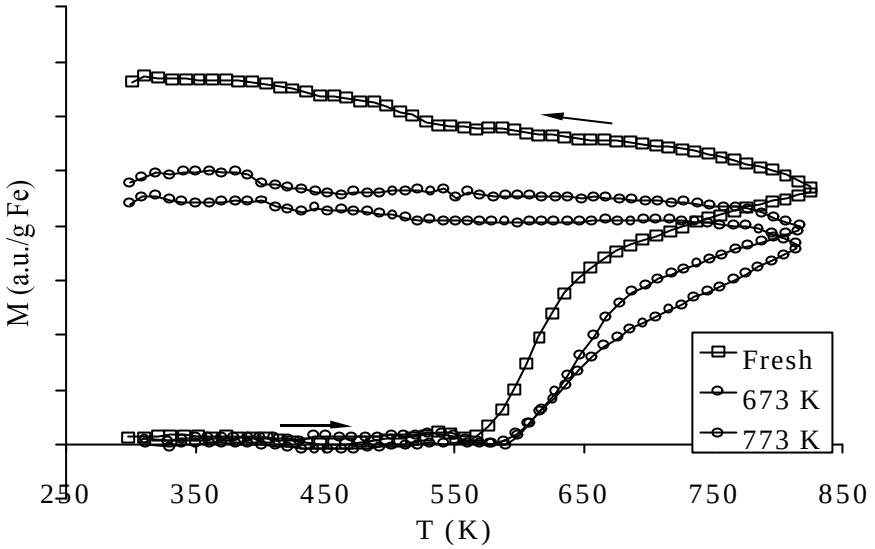

Figure 4.4 *TMA-profiles of freshly prepared Fe/ZrO_2 and pre-treated catalyst in a H_2/H_2O flow for 2 hours at 673 K and 773 K.*

The onset temperature also shows that the reducibility of the catalyst decreases after pre-treatment in hydrogen-water. The onset temperature found from the thermomagnetic profile indicates the start of the reduction to ferromagnetic iron. Consequently, the observed increase in T_{onset} reveals that the iron in the pre-treated catalyst is less reducible.

The increase in magnetisation during the first range of the reduction, M_I, furthermore, reflects the lower reducibility. M_I is defined as the first reduction range, which predominantly involves the reduction of Fe^{2+} situated at the surface. The difference between the final magnetisation and the magnetisation at the end of the first reduction range, M_I, indicates the amount of iron present in the mixed oxide with zirconium. A relatively small increase in magnetisation during M_I points to a large amount of Fe^{2+} to be present as the mixed oxide. Table 4.3 demonstrates that the increase in magnetisation during M_I drops upon pre-treatment at higher temperature. The decrease of the slope of the profile of the magnetisation-versus-temperature plot in the M_I range reveals the lower reducibility for the

catalyst sample pre-treated for 773 K.

These results unambiguously show that the catalyst becomes less reducible after pre-treatment in hydrogen-steam. It is also apparent that pre-treatment at 773 K affects the reducibility most profoundly. The decrease in M_4 points to a larger amount of the mixed oxide species in the catalyst after pre-treatment at 773 K.

4.4 Discussion

4.4.1 Carbon

Both thermomagnetic analysis and Mössbauer spectroscopy unambiguously show that carbon is present in the freshly calcined catalyst (after decomposition of the citrate precursor in the calcination step). During reduction the carbon species reacts to θ-Fe_3C [16]. During the pre-treatment in the hydrogen-steam flow no carbide of iron is observed using Mössbauer spectroscopy. Moreover, a carbide is absent during the subsequent reduction experiments. It is very likely that the pre-treatment in H_2/H_2O has removed the carbon species. Also the thermomagnetic analysis (TMA) points to removal of the carbon, since a carbide (which is characterised by its Curie temperature) is not observed.

The removal of the carbon species is better illustrated by the following experiment. The catalyst is pre-treated at 573 K. Subsequently, the catalyst is reduced in hydrogen, and the reduction is monitored using TMA. Figure *4*.6 shows the resulting TMA profile together with the profile of the freshly calcined catalyst for reasons of comparison.

From Figure *4*.6, it can be deduced that the final magnetisation is similar for both catalysts. The cooling curve of the pre-treated catalyst sample does not show any sign of an iron carbide. This indicates that the carbon initially present has been removed by the pre-treatment in the hydrogen-steam flow already at 573 K.

The final magnetisation, M_{final}, measured after reduction at the maximum temperatures, of the freshly calcined catalyst and the catalyst pre-treated in a hydrogen-steam flow is equal. The fact that the magnetisation does not differ indicates that the extent of reduction of the pre-treated catalyst sample is lower than that of the freshly calcined catalyst sample, since the latter contains cementite, which has a lower magnetic magnetisation than metallic iron. The lower extent of reduction is confirmed by the higher T_{onset} (590 K).

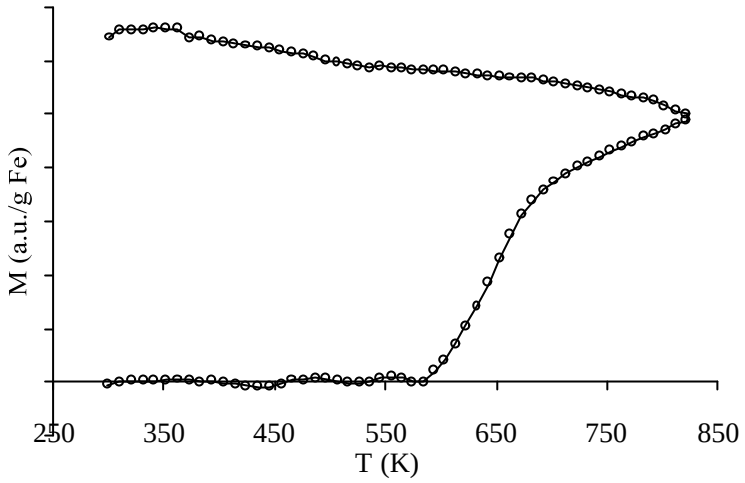

Figure 4.6 *TMA profiles of freshly prepared Fe/ZrO_2 pre-treated in a H_2/H_2O flow for 2 hours at 573 K.*

The effect of the pre-treatment in the hydrogen-steam flow on the reducibility can be due to the formation of more mixed oxide and/or the absence of carbon. Comparison of the TMA profiles of the catalyst samples pre-treated at 673 K and at 773 K shows a clear reduction of the reducibility with the catalyst sample pre-treated at a higher temperature. Since the pre-treatment at either temperature removes the carbon, the difference in reducibility must be due to the formation of the mixed oxide.

6.4.2 Reducibility

Our goal was to assess whether pre-treatment in a hydrogen-steam flow has an effect on the reduction of Fe/ZrO_2. This effect – an expected lower reducibility after pre-treatment – is determined by comparison of the reduction behavior of a pre-treated and a freshly calcined catalyst. With Mössbauer spectroscopy, the reducibility can be evaluated from the spectral contributions found at 673 K. The pre-treated catalyst reveals 18 % metallic iron, while the fresh catalyst shows 6 % Fe^0 and 19 % θ-Fe_3C; both Fe^0 and iron carbide are formed through reduction of Fe^{2+} to zerovalent iron. These results indicate that the pre-treated catalyst is reduced to only a slightly lower extent.

The pre-treatment in the hydrogen-steam flow brings about the lower reducibility as also observed in the TMA experiments. Several characteristics of the TMA profile, such as, the final magnetisation, M_{final}, and the intermediately measured magnetisation, M_i, reveal that the pre-treated catalyst is less reducible. These experiments further show that at higher pre-treatment temperatures (673 K versus 773 K) the reducibility drops more.

4.5 Conclusions

In situ experiments in which the Fe/ZrO_2 catalyst was pre-treated in a H_2/H_2O flow have revealed that the final extent of reduction is lower than after reduction in pure H_2, which is easily explained from thermodynamics. Pre-treatment of Fe/ZrO_2 in a H_2/H_2O flow results only in a slightly lower reducibility. The lower reducibility can be attributed to the formation of a larger amount of a mixed oxide of iron and the ZrO_2 support.

It has been further established that more mixed oxide results with pre-treatment at higher temperatures. However, Fe^{2+} is relatively easily extracted out of the mixed oxide by re-oxidation which proceeds already at room temperature.

4.6 References

[1] G.C. Bond, '*Heterogeneous Catalysis: Principles and Applications*', Clarendon Press, Oxford, 1987.
[2] L.M. Knijff, Ph.D. Thesis, Utrecht University, 1991, Chapter 6.
[3] X. Gao, J. Shen. Y. Hsia and Y. Chen, *J.Chem.Soc.Faraday Trans.* **89(7)** (1993) 1079.
[4] M.V. Cagnoli, S.G. Marchetti, N.G. Gallegos, A.M. Alvarez, R.C. Mercader and A.A. Yeramian, *J.Catal.* **123** (1989) 21.
[5] A.F.H. Wielers, A.H.J.M. Kock, C.E.C.A. Hop, J.W. Geus and A.M. van der Kraan, *J.Catal.* **117** (1989) 1.
[6] Y-Y. Huang and J.R. Anderson, *J.Catal.* **40** (1975) 143.
[7] M.C. Hobson Jr and H.M. Gager, *J. Colloid Interface Sci.* **34(3)** (1970) 357.
[8] S. Yuen, Y. Chen, J.E.Kubsh, J.A. Dumesic, N. Topsøe and H. Topsøe, *J.Phys.Chem.* **86** (1982) 3022.
[9] B.J. Tatarchuk and J.A. Dumesic, *J.Catal.* **70** (1981) 335.
[10] D.E. Stobbe, Ph.D. Thesis, Utrecht University, 1990, Chapter 4.

[11] E. Guglielminotti, E. Giamello, F. Pinna, G. Strukul, S. Martinengo and L. Zanderighi, *J.Catal.* **146** (1994) 422.
[12] P.H. Bolt, Ph.D. Thesis, Utrecht University, 1994, Chapter 7.
[13] P.H. Bolt, Ph.D. Thesis, Utrecht University, 1994, Chapter 6.
[14] A.J.H.M. Kock, Ph.D. Thesis, Utrecht University, 1985, Chapter 6.
[15] P.W. Selwood, *'Chemisorption and Magnetization'*, Academic Press, New York, 1975.
[16] Chapter 3 of this thesis.
[17] Chapter 2 of this thesis.
[18] A.M. van der Kraan, *Phys.Stat.Sol(A)* **18** (1973) 215.

5

The Fischer-Tropsch Synthesis: an *in situ* Mössbauer Spectroscopy Study

Abstract

In this chapter the composition of unpromoted Fe/ZrO_2 and promoted $Fe/K/ZrO_2$ during Fischer-Tropsch synthesis are investigated using *in situ* Mössbauer spectroscopy. Measurements were performed at ambient and elevated pressure.

During reaction conditions, two carbides ε'-$Fe_{2.2}C$ and χ-Fe_5C_2 are encountered together with an oxidic iron species. The latter species, a mixed oxide of iron with the ZrO_2 support, stabilises the carbide species. Furthermore, it is found that the carbon present in the carbide is more difficukt to remove on the unpromoted catalyst.

It is further observed that the ε'-carbide can be decarburized to χ-carbide and oxidized by water (which is formed during the Fischer-Tropsch reaction) to divalent iron. Both these transformations are reversible.

5.1 Introduction

Highly dispersed unpromoted Fe/ZrO_2 and potassium-promoted $Fe/K/ZrO_2$ were prepared for their (presumed) ability to directly and selectively produce light olefins. Since before the actual exposure to Fischer-Tropsch reaction the applied catalyst is generally reduced. In chapter 3, the reduction behaviour of both mentioned catalysts were elaborately investigated. The next step is (of course) exposure to syngas (H_2/CO gas mixture). This chapter focuses, in particular, on the (chemical) nature of the iron species during reaction.

For many years the chemical transformation during the Fischer-Tropsch synthesis of iron-based catalysts has been studied. It is believed that the final product distribution of the synthesis strongly relates to the chemical composition and structure of the selvedge of the iron species. Many investigators have tried to elucidate the nature of the active sites, which are located at the outer surface – not necessarily the outer monolayer – of the catalytically active metal. In order to get more insight in the iron species present during the Fischer-Tropsch synthesis, in situ analysis are a prerequisite.

The Fischer-Tropsch reaction commences with the dissociation of carbon monoxide leaving carbon and oxygen atoms on or within the surface and the dissociation of H_2. The oxygen is assumed to either react with the metal to an oxide or react with hydrogen to water or with carbon monoxide to carbon dioxide, which in turn can desorb and end up in the product stream. Especially during the initial stage of the Fischer-Tropsch reaction the oxygen atoms react with carbon monoxide to carbon dioxide. Another possible pathway is the incorporation of oxygen into a hydrocarbon chain forming *e.g.* an alcohol or aldehyde. On iron-based catalysts, however, such products are only observed in small quantities relative to the paraffin and/or olefin fractions. When oxygen atoms migrate into reduced iron particles, magnetite (Fe_3O_4) is generally observed [1]. Reaction to magnetite particularly proceeds with fused iron catalysts, which contain large metallic iron particles. Reymond *et al.* [2] have studied the reaction behaviour of reduced and unreduced iron catalysts and found that the unreduced catalyst – comprising mainly iron oxide - was more active and exhibited a higher stability. These authors suggest that magnetite plays an essential role in the Fischer-Tropsch reaction.

The fate of the carbon resulting from the decomposition of carbon monoxide is almost similar to that of oxygen. Niemantsverdriet *et al.* [3] suggest that carbon can end up in either (i) a carbide, or (ii) a hydrocarbon, or (iii) inactive

carbon. The latter two possibilities will first be discussed. The hydrocarbon refers to one of the reaction products, which are formed via recombination of hydrogen and carbon and subsequent polymerisation as explained in Chapter 1 of this thesis [4]. Iron-based catalysts mainly produce olefins and paraffins.

The inactive carbon relates to graphite-like carbon species covering the active sites and leading, eventually, to deactivation. Dwyer and Somorjai [5], studying single crystals of iron, were the first to propose the growth of graphitic carbon layers, which are believed to lead to deactivation also of supported catalysts [6].

Carbon can also migrate into the iron particles resulting in the formation of iron carbides. In literature different carbides are encountered. The most commonly known carbides are ε-Fe_2C, ε'-$Fe_{2.2}C$, χ-Fe_5C_2 and θ-Fe_3C [7], of which the characteristics are shown in Table 5.1. The first iron carbide, ε-Fe_2C, has been suggested to exhibit a hexagonal or approximately hexagonal close-packed (hcp) structure and a Curie temperature of around 653 K. Niemantsverdriet *et al.* [8] demonstrated that the results leading to the assignment of this carbide were misinterpreted and, consequently, ε-Fe_2C has never been observed. ε'-$Fe_{2.2}C$ is characterized by a hexagonal close-packed crystal structure and a Curie temperature of about 723 K. The Hägg carbide (χ-Fe_5C_2) has a long-range ordering that resembles a monoclinic crystal structure. The magnetic ordering of this carbide is absent above a temperature of 530 K. The Curie temperature of the last carbide, θ-Fe_3C (also referred to as cementite), is lower and is observed at 480 K. θ-Fe_3C (cementite) has a orthorhombic structure. The carbides can be arranged in the following order of increasing stability, *viz.*, ε'-$Fe_{2.2}C$ < χ-Fe_5C_2 < θ-Fe_3C, *i.e.*, at higher temperature the carbides should eventually transform into the most stable cementite. [9, 10]. The iron carbides can be classified according to the site occupied by the carbon atoms, which are present either in trigonal prismatic interstices, denoted as 'TP', or in octahedral interstices, referred to as 'O'. The ε'-carbide is an 'O'-carbide, and the χ-carbide and θ-carbide are classified as 'TP'-carbides.

Table 5.1 Different iron carbides, their crystal structures, Curie temperatures and carbon sites.

Carbide type	Trivial name	Crystal structure	T_C (K)	Type
ε'-$Fe_{2.2}C$		hcp	723 ± 10	O
χ-Fe_5C_2	Hägg	monoclinic	530 ± 10	TP
θ-Fe_3C	Cementite	orthorhombic	485 ± 8	TP

The above-mentioned carbides can be identified using Mössbauer

spectroscopy. The isomer shifts and magnetic hyperfine splittings at room temperature of the different iron carbides are tabulated in Table 5.2. It should be noted that the Hägg carbide exhibits three contributions. These sextuplets represent iron atoms having inequivalent crystallographic sites [10].

Table 5.2 *Mössbauer parameters of different iron carbides at 295 K [8].*

Carbide type	I.S. (mm/s)	H_{eff} (kOe)
ε'-$Fe_{2.2}C$	0.50	173
χ-Fe_5C_2 (χ_I)	0.43	189
χ-Fe_5C_2 (χ_{II})	0.51	218
χ-Fe_5C_2 (χ_{III})	0.47	110
θ-Fe_3C	0.45	212

The aim of this study is to provide more insight in the nature of the iron species present under Fischer-Tropsch synthesis conditions. The catalysts under study are an unpromoted and potassium-promoted zirconia-supported iron catalysts, in which the initial dispersion of the iron species is very high. In order to study the nature of the iron species during synthesis, *in situ* Mössbauer spectroscopy is employed. After a period of Fischer-Tropsch synthesis the catalyst is subsequently regenerated by a H_2-treatment and subjected to a second period of Fischer-Tropsch synthesis. The chosen reaction sequence allows comparison of the nature of the iron species before and after the Fischer-Tropsch synthesis and their behavior during the Fischer-Tropsch synthesis.

5.2 Experimental

5.2.1 Catalyst preparation

For details of the preparation of Fe/ZrO_2 and $Fe/K/ZrO_2$ the reader is referred to chapter 2.

5.2.2 Characterization technique: Mössbauer absorption spectroscopy

Mössbauer measurements were carried out in a constant acceleration mode using a ^{57}Co in Rh source. Isomer shifts are reported relative to the NBS standard sodium nitroprusside ($Na_2Fe(CN)_5NO.2H_2O$). Magnetic hyperfine fields (H_{eff})

were calibrated with the 515 kOe field of α-Fe_2O_3 at room temperature. The Mössbauer parameters were determined by fitting the spectra with subspectra consisting of Lorentzian-shaped lines using a non-linear iterative minimisation routine. The accuracy for the isomer shift (I.S.) is ±0.03 mm/s, for the electric quadrupole splitting (Q.S.) ±0.05 mm/s and for the spectral contribution (S.C.) 5%.

The experiments at ambient pressure (1 bar) were performed using an in situ Mössbauer reactor described in more details in [12]. To perform the in situ measurements at elevated pressures up to 10 bar a modified reactor with Be-windows and an outer vessel of stainless steel was used.

5.2.3 Fischer-Tropsch synthesis

The Fischer-Tropsch synthesis was performed at ambient pressure or at 9.5 bar. Firstly, about 60 mg of Fe/ZrO_2 or $Fe/K/ZrO_2$ was reduced in a mixture of 10 % H_2 in argon (vol/vol).

The thus reduced catalyst was cooled to 623 K and at this temperature exposed to the syngas of a H_2/CO ratio of 1. The gas mixture was flushed over the catalyst at a rate of 60 ml/min. After the measurements during the Fischer-Tropsch synthesis, the catalysts were cooled to 300 K.

An (eventual) subsequent regeneration step was performed at temperatures and pressures (indicated in the respective Tables).

Further details of the experiments, in particular reaction pressure and temperature, will be indicated in the text.

5.3 Results at ambient pressure

In this section the results obtained from experiments at 1 bar will be presented. The experiments at 9.5 bar will be dealt with in the subsequent section 5.4.

5.3.1 Unpromoted Fe/ZrO_2

The highly disperse zirconia-supported iron catalyst, Fe/ZrO_2, was reduced in 10% H_2 in argon (vol/vol) at ambient pressure at a temperature of 653 K for 42 hours. Simultaneously a spectrum was measured, which is shown in Figure 5.1a. The corresponding Mössbauer parameters calculated from the spectrum are presented in Table 5.3.

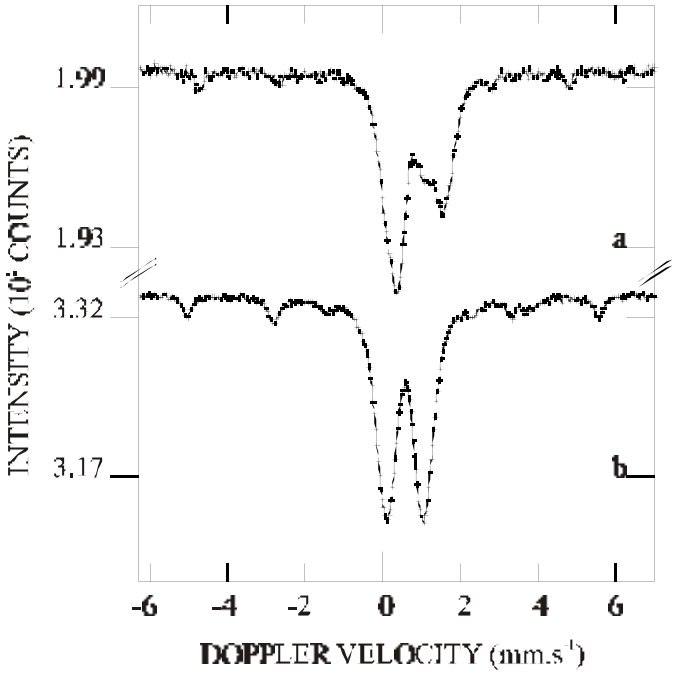

Figure 5.1 *Part I: Mössbauer spectra of 2.5 wt% Fe/ZrO_2: (a) measured during reduction at 653 K (18-42h); (b) after (a) measured at 300 K.*

Table 5.3 *Mössbauer parameters of 2.5 wt% Fe/ZrO_2 calculated from the spectrum recorded during reduction at 653 K.*

T (K)	I.S. (mm/s)	Q.S. (mm/s)	H_{eff} (kOe)	Γ (mm/s)	S.C. (%)	Compound
653	0.05		297	0.22	6	Fe^0
(18-42h)	0.67	0.90		0.45	25	Fe^{2+}
	0.99	1.22		0.53	57	Fe^{2+}
	0.26	0.46		0.29	12	θ-Fe_3C

Γ is the line width.

Table 5.3 shows the presence of four different iron species, *viz.* a zerovalent (metallic), two divalent and a carbidic iron species. This result is in agreement with the reduction result of the reduction at 673 K represented in Table 3.3 [11]. The amount of metallic iron is small as compared to that of the other iron

species.

The contribution with an isomer shift of 0.26 mm/s is assigned to the carbidic species cementite, θ-Fe_3C. Both the isomer shift and the amount, expressed in the spectral contribution, appear to be in agreement with those observed after reduction at 673 K (see Table 3.3). The formation of θ-Fe_3C is additionally proven by cooling the reduced catalyst to room temperature, (see Figure 5.1b). The presence of carbon in the catalyst sample is due to incomplete combustion of the citrate precursor.

The contributions with isomer shifts of 0.67 mm/s and 0.99 mm/s are both classified as Fe^{2+}. These divalent species are most probably related to a mixed oxide with the ZrO_2 (I.S. = 0.99 mm/s) and a surface species (outer shell of Fe-particle (I.S. = 0.67 mm/s) [11].

Subsequent to the above described reduction treatment (including cooling to room temperature), the catalyst was re-treated in 10% H_2 in Ar (vol/vol) during 4 hours at 623 K before the catalyst was exposed to the synthesis gas at 623 K. The Fischer-Tropsch reaction was running for 72 hours, while the composition of the catalyst was monitored by Mössbauer spectroscopic measurements. The Mössbauer parameters calculated from the measured spectra are shown in Table 5.4.

Table 5.4 *Mössbauer parameters of 2.5 wt% Fe/ZrO_2 calculated from spectra recorded during Fischer-Tropsch synthesis at 623 K, 1 bar ($H_2/CO=1$).*

T(K)	I.S. (mm/s)	Q.S. (mm/s)	Γ (mm/s)	S.C. (%)	Compound
623	0.68	0.99	0.45	14	Fe^{2+}
(0-24h)	1.01	1.29	0.55	58	Fe^{2+}
	0.25	0.48	0.34	28	Fe_xC
623	0.66	0.96	0.47	15	Fe^{2+}
(24-48h)	1.01	1.30	0.56	59	Fe^{2+}
	0.25	0.50	0.34	26	Fe_xC
623	0.66	0.99	0.48	14	Fe^{2+}
(48-72h)	1.01	1.30	0.57	59	Fe^{2+}
	0.25	0.50	0.36	27	Fe_xC

Γ is the line width.

As the contribution do not differ significantly in time, it can be concluded that the composition of the catalyst under Fischer-Tropsch synthesis conditions is very stable. From a comparison of the spectra measured during reduction and during the

Fischer-Tropsch synthesis, it follows furthermore that the reduced catalyst very rapidly assumes a stable composition under Fischer-Tropsch synthesis conditions.

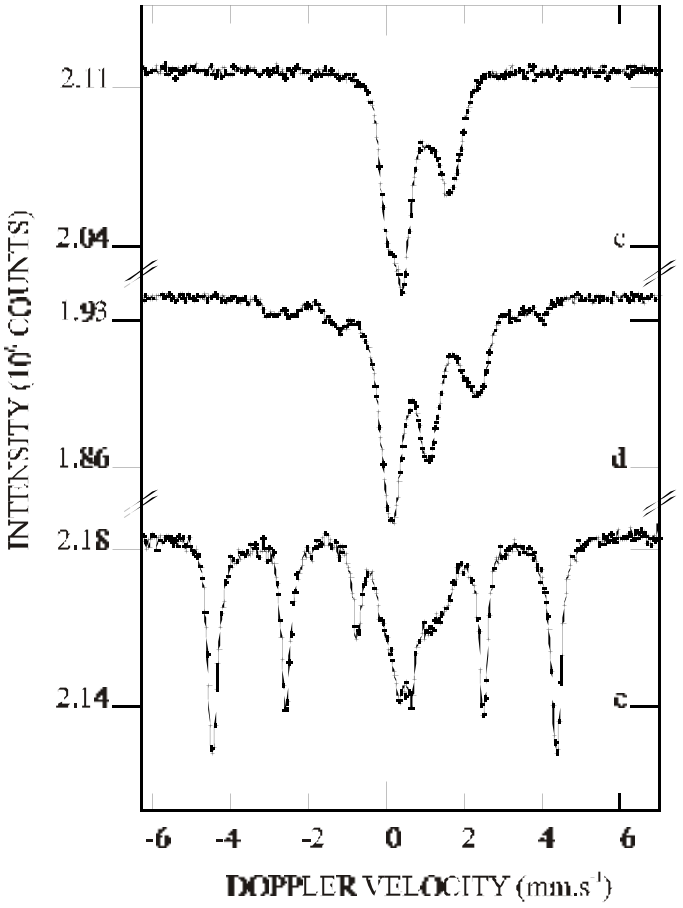

Figure 5.1 *Part II: Mössbauer spectra of 2.5 wt% Fe/ZrO_2: (c) measured during FTS at 623 K, 1 bar (48-72h); (d) after (c) measured at 300 K; (e) measured during regeneration at 773 K (0-27h).*

It can be seen that the contribution of the metallic iron species has completely vanished after exposing the catalyst to the synthesis gas at 623 K. From the increase in spectral contribution of the iron carbide, it follows that upon exposure to the carbon monoxide containing gas the zerovalent iron species very

likely reacts to iron carbide. Additionally, a part of the Fe^{2+} surface species (IS= 0.67 mm/s) is converted into the iron carbide. The contribution of the Fe^{2+} mixed oxide species has not changed significantly. The contribution of the surface Fe^{2+} species drops from 25 to 15 %, whereas the Fe^{2+} relating to the more stable mixed oxide remains unchanged. The rise in the contribution of the iron carbide, from 12 to 27 %, nicely agrees with the loss of metallic iron and of the surface Fe^{2+} species.

In order to determine the type of iron carbide that is formed during the Fischer-Tropsch synthesis, the catalyst sample was cooled to 300 K. Figure 5.1d shows the subsequently measured spectrum. The Fe_xC mentioned in Table 5.4 appears to be mainly χ-Fe_5C_2, the Hägg carbide. Apparently, the most stable carbide, θ-Fe_3C, takes up more carbon and reacts to the Hägg carbide during exposure to the carbon monoxide-hydrogen flow.

Following the Fischer-Tropsch reaction the catalyst is regenerated by exposure to the reducing 10% H_2 in Ar (vol/vol) gas flow at 773 K. The observed spectrum is included in Figure 5.1, while the Mössbauer parameters calculated from this spectrum are represented in Table 5.5.

Table 5.5 Mössbauer parameters of 2.5 wt% Fe/ZrO_2 calculated from spectra recorded during regeneration in H_2 at 773 K.

T(K)	I.S. (mm/s)	Q.S. (mm/s)	H_{eff} (kOe)	Γ (mm/s)	S.C. (%)	Compound
773	-0.03		275	0.30	64	Fe^0
(0-27h)	0.16	0.34		0.35	8	Fe_xC
	0.84	0.88		0.80	28	Fe^{2+}

Γ is the line width.

The spectrum reveals an enormous change as compared to that measured during the Fischer-Tropsch synthesis. The main spectral contribution is now a sextuplet that can be assigned to metallic iron. From this result, it is easily deduced that at this temperature the carbon in the iron carbide has reacted with H_2 leaving zerovalent iron behind. It is interesting that the θ-Fe_3C present in the reduced Fe/ZrO_2 catalyst can withstand thermal treatment in hydrogen of ambient pressure at temperatures exceeding 773 K [11], whereas the large fraction of χ-Fe_5C_2 present after exposure to carbon monoxide and hydrogen smoothly reacts to metallic iron. It must be noted that the metallic iron particles are relatively large as is indicated by the observed sextuplet [13]. The spectral contribution of the sextuplet indicates that also the two divalent iron species are partly reduced to metallic iron. The

quadrupole splitting of the remaining Fe^{2+} species is significantly lower than that of the mixed oxide Fe^{2+} species originally present.

The regenerated catalyst consisting of mainly large metallic iron particles is subsequently exposed again to the synthesis gas at 623 K. A first spectrum was taken during the first 4 minutes on stream. In this spectrum it could be clearly seen that the large contribution of metallic iron has disappeared completely. This result leads to the conclusion that the metallic iron species is carburized very fast, probably within seconds.

The catalyst was further exposed to synthesis gas for 14 hours and, subsequently, cooled to ambient temperature. Figure 5.2 shows the measured spectra. The Mössbauer parameters calculated from these spectra are given in Table 5.6. In the spectrum recorded after 14 hours on stream three spectral contributions can be identified. The contribution with an isomer shift of 0.87 mm/s can be attributed to the divalent iron species that relates to the mixed oxide, which spectral contribution decreased from about 58 to 28 % during the re-reduction treatment at 773 K. Exposure to the carbon monoxide-hydrogen flow brought about a drop of the spectral contribution to 15 %. The highly dispersed and Fe^0-poor catalyst obtained upon the initial reduction and exposure to the carbon monoxide and hydrogen flow exhibited only one contribution of a low isomer shift (χ-Fe_5C_2).

Upon exposure to the carbon monoxide-hydrogen flow, the regenerated catalyst, on the other hand, reveals two separate contributions having relatively low isomer shifts, *viz.*, 0.24 mm/s and 0.29 mm/s, instead of one. These two contributions split into four sextuplets when measured at 300 K. Three of the four sextuplets, *viz*., with isomer shifts of 0.43, 0.47 and 0.51 mm/s and, more specifically, with corresponding hyperfine splittings of 191, 112 and 212 kOe unambiguously point to the presence of Hägg carbide (χ-Fe_5C_2) [8]. The remaining sextuplet with an isomer shift of 0.48 mm/s and a hyperfine splitting of 175 kOe is recognised as the metastable and more carbon-rich ε'-$Fe_{2.2}C$.

At the temperature of the Fischer-Tropsch synthesis (623 K) the Hägg carbide (χ-Fe_5C_2) is above its Curie temperature (530 K) and its magnetic hyperfine splitting will not be displayed. However, the Curie temperatures for ε'-$Fe_{2.2}C$ is 723 K, which is above the synthesis temperature. Nevertheless the magnetic hyperfine splitting is absent and as a consequence a doublet is observed. An explanation can be found in a relatively high dispersion of this iron carbide resulting in a lower Curie temperature [14].

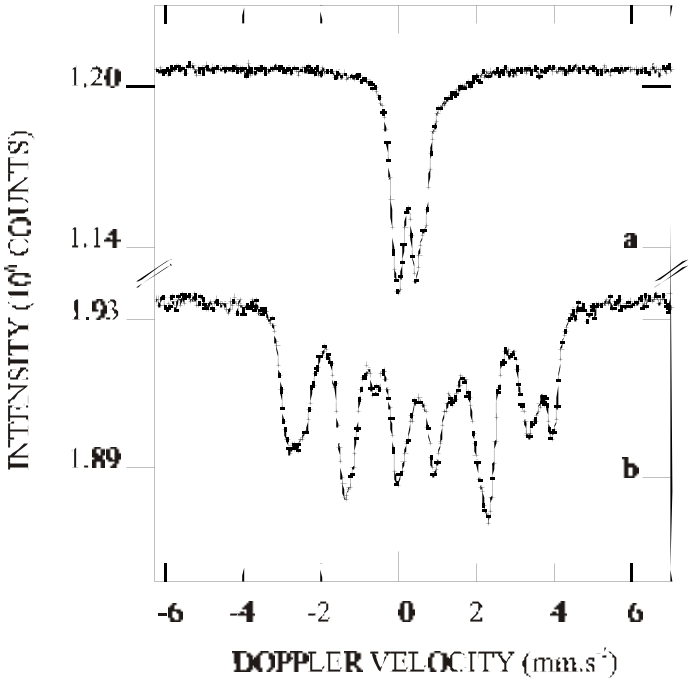

Figure 5.2 *Mössbauer spectra of regenerated 2.5 wt% Fe/ZrO_2: (a) measured during Fischer-Tropsch synthesis at 623 K, 1 bar (0-14h); (b) after (a) measured at 300 K.*

Table 5.6 *Mössbauer parameters of the regenerated 2.5 wt% Fe/ZrO_2 catalyst calculated from spectra measured during Fischer-Tropsch synthesis at 623 K and 1 bar (H_2/CO=1).*

T(K)	I.S. (mm/s)	Q.S. (mm/s)	H_{eff} (kOe)	Γ (mm/s)	S.C. (%)	Compound
623	0.24	0.42		0.31	57	Fe_xC
(0-14 h)	0.29	0.82		0.26	28	Fe_xC
	0.87	0.91		0.90	15	Fe^{2+}
300	0.51	-0.044	212	0.35	28	χ_{II}-Fe_5C_2
(0-22h)	0.43	-0.034	191	0.32	16	χ_{I}-Fe_5C_2
	0.47	-0.057	112	0.30	16	χ_{III}-Fe_5C_2
	0.48	0.012	175	0.40	23	ε'-$Fe_{2.2}C$
	0.49	1.00		0.54	10	Fe^{3+}
	1.13	1.60		0.41	6	Fe^{2+}

Γ is the line width.

Next to the iron carbide contributions two other contributions are present in the spectra measured at 300 K. The first contribution with an isomer shift of 1.13 mm/s can be assigned to divalent iron. Trivalent iron accounts for the second contribution (I.S. is 0.49 mm/s). The sum of the spectral contributions of both Fe^{3+} and Fe^{2+} is equal to that of the divalent contribution calculated from spectra recorded during the Fischer-Tropsch reaction at 623 K. This indicates that, even after performing the Fischer-Tropsch synthesis, only divalent iron reacts to Fe^{3+} at room temperature. The oxidation must be due to the presence of water, since water is a (primary) reaction product. As observed in Chapter 3 of this thesis, the carbidic species remain unaffected by water at ambient temperature.

5.3.2 Potassium-promoted Fe/K/ZrO_2

Following the reduction in a 10% H_2 in Ar (vol/vol) gas flow at 653 K, the catalyst is cooled to 623 K, at which the Fischer-Tropsch synthesis is performed. Figure 5.3 shows the spectra measured during the reduction treatment and subsequent Fischer-Tropsch synthesis. The Mössbauer parameters calculated from these spectra are tabulated in Table 5.7.

Table 5.7 Mössbauer parameters of 2.5 wt% Fe/K/ZrO_2 during reduction at 653 K and during FT synthesis at 623 K and 1 bar (H_2/CO=1).

T(K)	I.S. (mm/s)	Q.S. (mm/s)	H_{eff} (kOe)	Γ (mm/s)	S.C. (%)	Compound
653	0.02		298	0.27	6	Fe^0
(71-94h)	0.86	0.67		0.46	14	Fe^{2+}
	0.92	1.35		0.56	40	Fe^{2+}
	0.20	0.44		0.36	40	Fe_xC
623	0.87	0.89		0.56	18	Fe^{2+}
(0-22h)	0.97	1.44		0.53	37	Fe^{2+}
	0.23	0.45		0.35	39	Fe_xC
	0.29	0.82		0.23	6	Fe_xC
623	089	0.74		0.61	16	Fe^{2+}
(49-70h)	0.96	1.41		0.55	42	Fe^{2+}
	0.22	0.42		0.31	34	Fe_xC
	0.29	0.82		0.23	8	Fe_xC

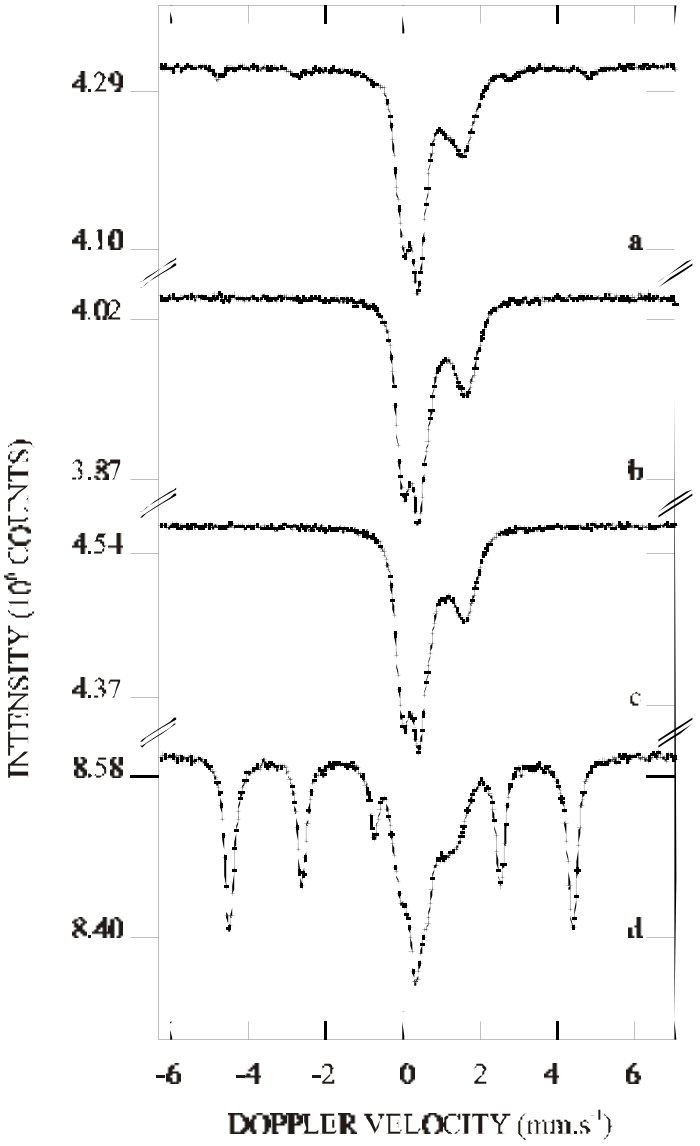

Figure 5.3 *Mössbauer spectra 2.5 wt% Fe/K/ZrO_2: (a) measured during reduction at 653 K and 1 bar (71-94h); (b) measured during Fischer-Tropsch synthesis at 623 K and 1 bar (49-70h); (c) after (b) measured during regeneration at 623 K and 1 bar (24-48h); (d) after (c) measured during regeneration at 773 K and 1 bar (0-48h).*

As has already been reported in Chapter 3 of this thesis, the reduction at 653 K leads to only a small spectral contribution of metallic iron (Fe^0). Also the large spectral contribution of 40 % ascribed to an iron carbide (Fe_xC) that is measured besides the two Fe^{2+} contributions has been described in Chapter 3. One of these last two contributions (Q.S.= 1.35 mm/s) is attributed to a mixed oxide of iron and zirconium and the other one to a surface species [11].

From the Mössbauer data it is obvious that the composition of the catalyst is hardly changing during the Fischer-Tropsch synthesis at 623 K. The spectral contribution of metallic iron (Fe^0) is no longer observed because it is transformed into an iron carbide contribution. The contribution of the iron carbide is split into two iron carbide species. These species are similar to those observed for the unpromoted 2.5 wt% Fe/ZrO_2 catalyst during the Fischer-Tropsch synthesis after regeneration (see Table 5.6). The large amount of θ-Fe_3C present in the freshly reduced $Fe/K/ZrO_2$ catalyst readily reacts to more carbon-rich iron carbides. It is interesting that the unpromoted Fe/ZrO_2 catalyst only exhibits the two iron carbides, χ-Fe_5C_2 and ε'-$Fe_{2.2}C$, after exposing the regenerated catalyst to carbon monoxide-hydrogen, whereas the freshly reduced $Fe/K/ZrO_2$ catalyst exhibits the two iron carbides already upon Fischer-Tropsch synthesis at 623 K (prior to a regeneration step).

Subsequent to exposure to the carbon monoxide-hydrogen gas mixture, H_2 gas is passed over the catalyst in order to investigate whether the carburization process is reversible. The results obtained during this regeneration procedure are shown in Table 5.8.

From the above Table 5.8 it is apparent that the catalyst does not change during regeneration at 623 K; the same contributions as observed during Fischer-Tropsch synthesis are present in similar amounts. Whereas at 723 K the contribution of χ-Fe_5C_2 to the spectra increases at the expense of ε'-$Fe_{2.2}C$ carbide which contains slightly more carbon, only during regeneration in hydrogen at 773 K a large amount of zerovalent iron results. Besides the decrease of the Fe^{2+} species, it is further observed that the amount of carbide also reduces to form metallic iron indicating that carbon is extracted from the carbide during this regeneration step at 773 K. It is interesting that in spite of the shift in the thermodynamic equilibrium between methane and carbon and hydrogen (CH_4 C + 2 H_2) at more elevated temperatures to the carbon and hydrogen side, the iron carbide becomes thus unstable at 773 K that reaction to metallic iron proceeds.

Table 5.8 Mössbauer parameters of Fe/K/ZrO_2 calculated from spectra measured during regeneration at different temperatures following Fischer-Tropsch synthesis at 623 K and 1 bar (H_2/CO=1).

T(K)	I.S. (mm/s)	Q.S. (mm/s)	H_{eff} (kOe)	Γ (mm/s)	S.C. (%)	Compound
623	0.85	0.68		0.59	19	Fe^{2+}
(0-24h)	0.94	1.41		0.54	41	Fe^{2+}
	0.22	0.43		0.31	32	Fe_xC
	0.29	0.82		0.23	8	Fe_xC
623	0.74	0.79		0.54	16	Fe^{2+}
(24-48h)	0.95	1.36		0.57	44	Fe^{2+}
	0.24	0.44		0.30	29	Fe_xC
	0.29	0.82		0.24	11	Fe_xC
723	0.90	0.98		0.71	52	Fe^{2+}
(0-18h)	0.15	0.40		0.35	43	Fe_xC
	0.21	0.82		0.20	5	Fe_xC
773	-0.04		276	0.29	52	Fe^0
(0-48h)	0.75	0.63		0.52	13	Fe^{2+}
	0.87	1.12		0.57	17	Fe^{2+}
	0.12	0.40		0.39	17	Fe_xC

Γ is the line width.

5.4 Results at elevated pressure

5.4.1 Unpromoted Fe/ZrO_2

Following reduction at 673 K as described in chapter 3 of this thesis, the catalyst is exposed to synthesis gas at 9.5 bar of a H_2/CO of 1. The Fischer-Tropsch reaction is performed at 623 K. During the Fischer-Tropsch synthesis Mössbauer spectra are measured. The parameters calculated from these spectra are tabulated in Table 5.9. Figure 5.4 represents Mössbauer spectra of 2.5 wt% Fe/ZrO_2 during various subsequent treatments, such as reduction, Fischer-Tropsch synthesis, and regeneration of the catalyst.

Table 5.9 Mössbauer parameters of 2.5 wt% Fe/ZrO_2 Fischer-Tropsch reaction at 623 K and 9.5 bar (H_2/CO= 1).

T(K)	I.S. (mm/s)	Q.S. (mm/s)	H_{eff} (kOe)	Γ (mm/s)	S.C. (%)	Compound
623	1.10	1.61		0.64	49	Fe^{2+}
(0-6h)	0.28	0.41		0.30	33	Fe_xC
	0.32	0.81		0.28	19	Fe_xC
623	1.10	1.62		0.63	46	Fe^{2+}
(6-23h)	0.27	0.41		0.31	36	Fe_xC
	0.32	0.81		0.26	18	Fe_xC
623	1.10	1.62		0.65	46	Fe^{2+}
(23-32h)	0.27	0.42		0.31	37	Fe_xC
	0.33	0.82		0.24	17	Fe_xC
300	0.56		215	0.44	22	χ_{II}-Fe_5C_2
(1-16h)	0.46		187	0.53	21	χ_{I}-Fe_5C_2
	0.38		114	0.44	8	χ_{III}-Fe_5C_2
	0.66	0.78		0.58	33	Fe^{3+}
	1.22	2.39		0.48	17	Fe^{2+}
300	0.55		215	0.42	18	χ_{II}-Fe_5C_2
(16-136h)	0.46		187	0.46	18	χ_{I}-Fe_5C_2
	0.38		113	0.41	7	χ_{III}-Fe_5C_2
	0.63	0.97		0.62	55	Fe^{3+}
	1.13	2.52		0.20	3	Fe^{2+}
623	1.11	1.63		0.62	50	Fe^{2+}
(1-20h)	0.27	0.42		0.31	34	Fe_xC
	0.32	0.81		0.26	16	Fe_xC
623	1.11	1.64		0.64	50	Fe^{2+}
(20-29h)	0.27	0.42		0.31	34	Fe_xC
	0.32	0.82		0.26	16	Fe_xC
623	1.11	1.63		0.63	50	Fe^{2+}
(29-45h)	0.28	0.41		0.31	33	Fe_xC
	0.32	0.82		0.25	17	Fe_xC

As Figure 5.4a shows, after reduction at 673 K and a hydrogen pressure of 9.5 bar a substantial contribution of metallic iron (58% spectral contribution) was present (see Table 3.7 [11]). Upon exposure to carbon monoxide and hydrogen the metallic iron species disappears very rapidly and reacts to iron carbides.

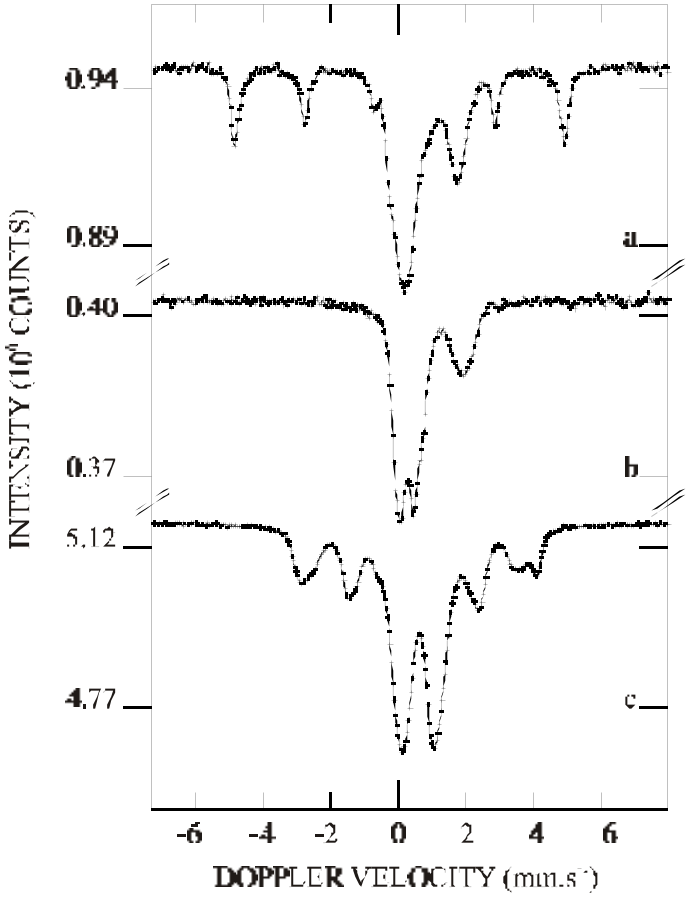

Figure 5.4 *Part I: Mössbauer spectra of 2.5 wt% Fe/ZrO_2: (a) measured during reduction at 673 K and 9.5 bar (0-20h); (b) measured during Fischer-Tropsch synthesis at 623 K and 9.5 bar (23-32h); (c) after (b) measured at 300 K (16-136h)*

Spectra recorded during Fischer-Tropsch synthesis display three spectral contributions (see Figure 5.4b), which can be assigned to two iron carbides and to

divalent iron. Even after prolonged time on stream these carbide species remain present in unchanged amounts. The spectral contribution of the carbides exhibits a level of about 54 %. Of this contribution, an appreciable amount of the ε'-$Fe_{2.2}C$ carbide appears to be present (about 17 %).

After cooling to room temperature, magnetically split sextuplets become clearly visible (see Figure 5.4c). Fitting the spectrum reveals three sextuplets with hyperfine splittings characteristic for the Hägg carbide (χ-Fe_5C_2). It is interesting that the contribution of the ε'-$Fe_{2.2}C$ carbide is not apparent at room temperature, where solely the Hägg carbide is found. The total contribution of the iron carbides at 623 and 300 K is only slightly different, *viz*., 54 and 51 %, respectively.

.

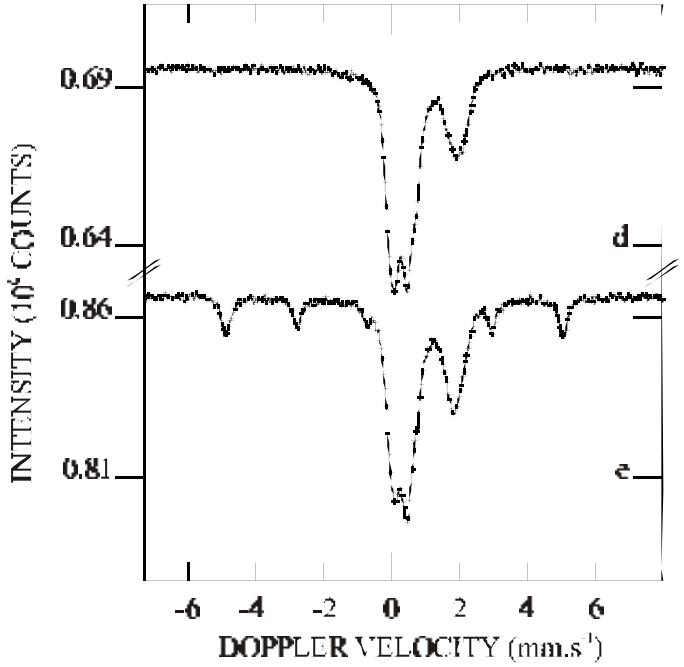

Figure 5.4 *Part II: Mössbauer spectra of 2.5 wt% Fe/ZrO_2: (d) after (c) measured during Fischer-Tropsch synthesis at 623 K and 9.5 bar (29-45h); (e) measured during regeneration at 623 K and 9.5 bar (52-72h).*

A new spectral component is observed at 300 K, which can be assigned to

trivalent iron. This contribution increases with time at 300 K. From these results, it is again clear that re-oxidation (of mainly Fe^{2+}) not only takes place after reduction, but also occurs after performing the Fischer-Tropsch reaction at elevated pressure for a prolonged period of time. Similar to the behavior after reduction, it appears that at room temperature mainly divalent iron is converted to Fe^{3+}, while the iron carbide contribution is less strongly affected. The contribution of the iron carbides drops while keeping the catalyst in hydrogen at room temperature, *viz*., from 51 to 43 %, whereas the contribution of the Fe^{2+} and Fe^{3+} species rises from 50 to 58%. The final contribution of Fe^{2+} to the spectra is only 3 %. As mentioned above, water is one of the main products of the Fischer-Tropsch reaction. It is thus very likely that some water remains in the catalyst and is responsible for the observed re-oxidation. The divalent iron species is only slowly oxidized at room temperature. This slow process may involve either transport of oxygen through a surface layer of Fe^{3+} species or migration of divalent iron ions (from the mixed oxide) to the surface whereat it is oxidized. The divalent iron species may also be located at the interface of the iron carbide particles and the mixed oxide or the support material. The slow oxidation of this interfacial Fe^{2+} species and the more limited attack (of water) on the iron carbide seem to point to the occurrence of oxidation at the interface. It is also contemplated, in combination with the interfacial oxidation, that the carbide particles do not completely cover the mixed oxide layer. Accordingly, oxidation of the bare (uncovered) mixed oxide and the interfacial species proceeds.

When the temperature is increased again to 623 K (see Figure 5.4d), the species present during the first period of Fischer-Tropsch synthesis at elevated pressure re-appear. The results indicate that an intermediate re-oxidation step does not affect the nature of the iron species and the spectral contributions during the Fischer-Tropsch synthesis.

Following the Fischer-Tropsch synthesis, the catalyst is exposed to hydrogen in a regeneration step at 623 K and a hydrogen pressure of 9.5 bar (see Figure 5.4e). The Mössbauer parameters deduced from the measured spectra are shown in Table 5.10.

t is noteworthy that thermal treatment of the freshly calcined catalyst at 623 K in hydrogen of a pressure of 1.8 bar did not lead to iron carbide(s) due to reaction of the metallic iron with the carbon remaining from the decomposition of the citrate [11]. The iron carbides produced by exposure of the reduced catalyst to carbon monoxide and hydrogen at 623 K, on the other hand, are much more stable at 623 K and a hydrogen pressure of 9.5 bar. Thermal treatment at 623 K

nevertheless leads to some metallic iron. This is apparent from a sextuplet appearing in the spectra, which is due to metallic iron. The data of Table 5.10 indicate that a small fraction of the iron carbide looses carbon and reacts to zerovalent iron, whereas the spectral contribution of Fe^{2+} remains constant.

Table 5.10 Mössbauer parameters of 2.5 wt% Fe/ZrO_2 calculated from spectra recorded during regeneration in H_2 at 623 K and 9.5 bar.

T(K)	I.S. (mm/s)	Q.S. (mm/s)	H_{eff} (kOe)	Γ (mm/s)	S.C. (%)	Compound
623	0.08		307	0.26	8	Fe^0
(0-52h)	0.28	0.41		0.30	28	Fe_xC
	0.32	0.81		0.24	12	Fe_xC
	1.10	1.56		0.63	52	Fe^{2+}
623	0.08		307	0.28	17	Fe^0
(52-72h)	0.29	0.43		0.31	25	Fe_xC
	0.33	0.83		0.21	7	Fe_xC
	1.09	1.52		0.61	51	Fe^{2+}

Γ is the line width.

5.4.2 Potassium-promoted Fe/K/ZrO_2

In Figure 5.5 some of the Mössbauer spectra measured on the 2.5 wt% Fe/K/ZrO_2 catalyst are presented. These spectra have been measured during the reduction treatment, the Fischer-Tropsch synthesis at 9.5 bar, and after cooling the catalyst to room temperature. Table 5.11 tabulates the Mössbauer parameters derived from the different spectra recorded under Fischer-Tropsch conditions at 9.5 bar, and subsequently under hydrogen at room temperature first at 9.5 bar and finally at ambient pressure.

When the catalyst is exposed to synthesis gas at 623 K the spectrum changes drastically as compared to the spectrum recorded after reduction. The sextuplet of metallic iron is replaced by doublets with isomer shift of 0.26 mm/s and 0.32 mm/s, which are assigned to iron carbides. The doublet with an isomer shift of 1.10 mm/s is recognised as the divalent iron species which is part of a mixed oxide.

The spectral component observed in Figure 5.5b with a rather small hyperfine splitting (~ 98 kOe) – and which spectral component vanishes as a

function of time on stream (see Figure 5.5c) – is most probably related to ε'-$Fe_{2.2}C$. Only this iron carbide has a Curie temperature above the measuring temperature (see Table 5.1). From the disappearance of the contribution with the small hyperfine field, it can be concluded that some larger iron particles initially react to the ε'-$Fe_{2.2}C$ carbide upon exposure to carbon monoxide-hydrogen and transform subsequently into another iron carbide. The contribution to the spectrum recorded at 623 K displaying an isomer shift of 0.26 mm/s and a quadrupole splitting of 0.42 mm/s is assigned to χ-Fe_5C_2, the Hägg carbide. The contribution of the χ-Fe_5C_2 carbide does not significantly vary during exposure to carbon monoxide and hydrogen for no less than 240 hours.

The spectra measured at 623 K also exhibit a contribution with an isomer shift of 0.32 mm/s and a quadrupole splitting of 0.82 mm/s. Also this contribution does not change significantly during exposure to carbon monoxide-hydrogen. We attribute this contribution to the spectrum measured at 623 K to ε'-$Fe_{2.2}C$ present as particles thus small that the Curie temperature is too low to display a measurable hyperfine splitting at 623 K. At 623 K within the carbon monoxide-hydrogen flow the contribution of the two iron carbides remains at 81 % and that of the Fe^{2+} species at 19 % after 144 hours on stream.

Upon cooling to room temperature and during keeping the catalyst at room temperature, oxidation of the Fe^{2+} species to Fe^{3+} is apparent. The amount of iron carbide in the catalyst drops only slightly (by about 4 %) at room temperature. It is further noteworthy, that during Fischer-Tropsch synthesis at 623 K two carbides are present, *viz.* ε'-$Fe_{2.2}C$ and χ-Fe_5C_2, of which the ε'-carbide vanishes at 300 K. Considering the slight increase of the amount of oxidic iron species, the metastable ε'-$Fe_{2.2}C$ is predominantly converted to Hägg carbide. As shown in Table 5.11 the spectrum does not reveal a significant change when the hydrogen pressure is lowered to 1 atmosphere.

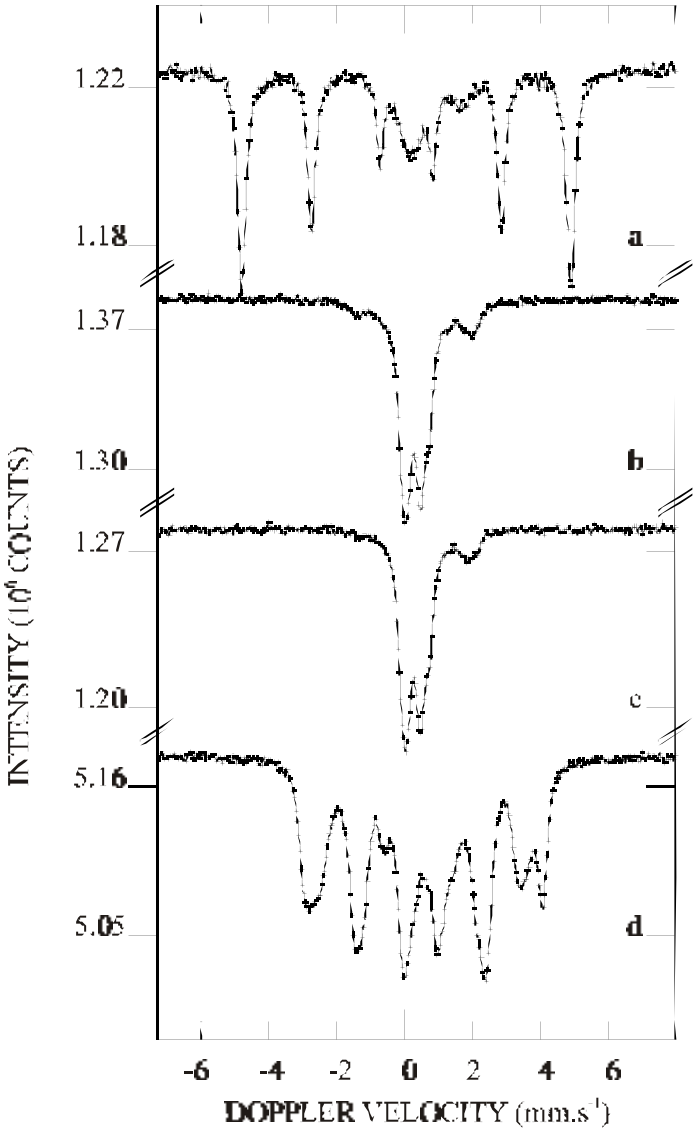

Figure 5.5 *Mössbauer spectra of 2.5 wt% Fe/K/ZrO_2: (a) measured during reduction at 673 K and 9.5 bar (0-21h); (b) measured during Fischer-Tropsch synthesis at 623 K and 9.5 bar (0-25h); (c) measured during Fischer-Tropsch synthesis at 623 K and 9.5 bar (216-240h); (d) after (c) measured at 300 K.*

Table 5.11 *Mössbauer parameters of 2.5 wt% Fe/K/ZrO_2 calculated from spectra recorded during Fischer-Tropsch reaction at 623 K and 9.5* bar *with $H_2/CO=1$, at 300 K under hydrogen of initially 9.5 bar and finally at ambient pressure.*

T(K)	p (bar)	I.S. (mm/s)	Q.S. (mm/s)	H_{eff} (kOe)	Γ (mm/s)	S.C. (%)	Compound
623	9.5	0.24	0.08	98	0.50	12	Fe_xC
(0-25h)		0.26	0.42		0.35	52	Fe_xC
		0.32	0.83		0.27	23	Fe_xC
		1.17	1.72		0.44	13	Fe^{2+}
623	9.5	0.26	0.42		0.33	55	Fe_xC
(48-144h)		0.32	0.83		0.27	24	Fe_xC
		1.10	1.61		0.69	21	Fe^{2+}
623	9.5	0.26	0.41		0.32	54	Fe_xC
(144-168)		0.32	0.82		0.27	27	Fe_xC
		1.10	1.60		0.61	19	Fe^{2+}
623	9.5	0.26	0.41		0.31	54	Fe_xC
(168-192)		0.31	0.81		0.27	27	Fe_xC
		1.10	1.61		0.59	19	Fe^{2+}
623	9.5	0.26	0.42		0.34	58	Fe_xC
(192-216)		0.32	0.82		0.26	23	Fe_xC
		1.11	1.63		0.62	19	Fe^{2+}
623	9.5	0.26	0.41		0.32	55	Fe_xC
(216-240)		0.32	0.82		0.27	25	Fe_xC
		1.09	1.60		0.61	19	Fe^{2+}
300	9.5	0.53	-0.05	215	0.35	27	χ-Fe_5C_2
(0-96h)		0.42	-0.05	184	0.50	36	χ-Fe_5C_2
		0.48	-0.08	111	0.42	15	χ-Fe_5C_2
		0.54	1.02		0.67	16	Fe^{3+}
		1.29	1.91		0.37	6	Fe^{2+}

Table 5.11 Continued.

T(K)	p (bar)	I.S. (mm/s)	Q.S. (mm/s)	H_{eff} (kOe)	Γ (mm/s)	S.C. (%)	Compound
300	1	0.52	-0.05	215	0.34	26	χ-Fe_5C_2
(0-17h)		0.44	-0.03	185	0.49	36	χ-Fe_5C_2
		0.48	-0.08	111	0.31	15	χ-Fe_5C_2
		0.54	1.00		0.53	17	Fe^{3+}
		1.21	1.77		0.46	6	Fe^{2+}

Γ is the line width.

Following the earlier described Fischer-Tropsch synthesis, the catalyst was exposed at 623 K to hydrogen at 1 bar in order to establish the resistance of the iron carbides to hydrogenation. Table 5.12 shows the corresponding Mössbauer parameters.

From Table 5.12 it is immediately clear that the catalyst can be decarburised at 623 K in hydrogen of ambient pressure, but the hydrogenation of the iron carbides does not proceed rapidly. First of all, it is interesting that some additional reduction takes place during exposure of the catalyst to hydrogen of ambient pressure at 623 K.

Table 5.12 Mössbauer parameters of 2.5 wt% Fe/K/ZrO_2 calculated from spectra recorded during a regeneration step in hydrogen at 623 K and ambient pressure.

T(K)	I.S. (mm/s)	Q.S. (mm/s)	H_{eff} (kOe)	Γ (mm/s)	S.C. (%)	Compound
623	0.5	0.00	302	0.29	36	Fe^0
(0-19h)	0.25	0.41		0.33	38	Fe_xC
	0.31	0.85		0.21	11	Fe_xC
	0.99	1.36		0.64	15	Fe^{2+}
623	0.05	0.00	302	0.28	78	Fe^0
(19-115h)	0.26	0.46		0.47	8	Fe_xC
	0.99	1.32		0.69	14	Fe^{2+}
300	0.27	0.00	330	0.28	77	Fe^0
(0-25h)	0.61	1.04		0.95	23	Fe^{3+}

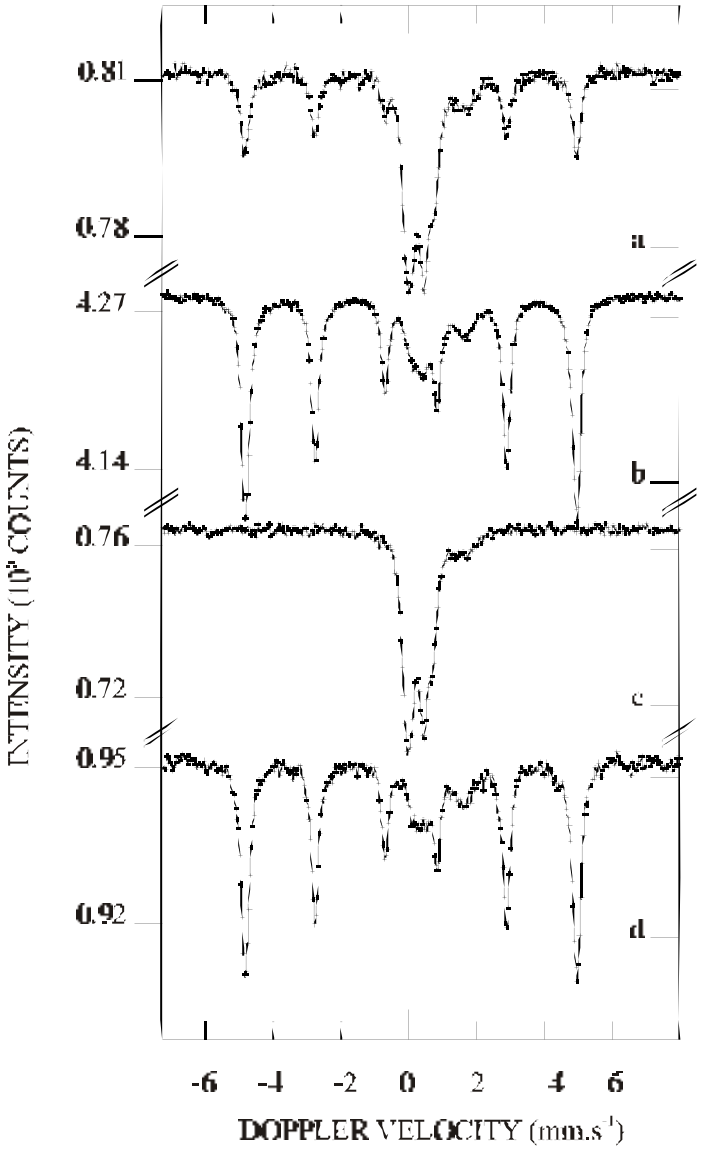

Figure 5.6 *Mössbauer spectra of 2.5 wt% Fe/K/ZrO_2: measured (a) during regeneration at 623 K and 1 bar (0-19h); (b) during regeneration at 623 K and 1 bar (19-115h); (c) during Fischer-Tropsch synthesis after (b) at 623 and 1 bar (26-43h); (d) after (c) during regeneration at 623 K and 1 bar (25-47h).*

After performing the Fischer-Tropsch synthesis at 623 K the contribution of iron carbides was about 81 %, while the contribution of metallic iron and iron carbide after the first 19 hours in hydrogen at 623 K is 85 %, which does not significantly change in 115 hours. The contribution of the Fe^{2+} species also does not change during regeneration. The removal of carbon follows from the large contribution of the Fe^{0} sextuplet and the decrease in the spectral contributions of the carbide. When the catalyst is measured at 300 K, it is clear that metallic iron – characterized by the hyperfine splitting of 330 kOe – is present and that the divalent species reacts to trivalent iron. Simultaneously, the remaining iron carbide is completely oxidized to Fe^{3+} species, which leads to an increase in the oxidized iron species from 14 to 23 % according to the contribution to the spectra. The oxidation is attributed to the oxidation of Fe^{2+} by water.

For comparison reasons, the regenerated catalyst is subsequently exposed to synthesis gas at 1 bar. The parameters deduced from the measured spectra are tabulated in Table 5.13. It follows that the iron species are easily transformed to the same iron carbides and divalent iron species (mixed oxide) as observed at higher pressure (before the regeneration step, see Table 5.11). The contributions of the iron carbides increase from 79 to 84 % during the Fischer-Tropsch synthesis, whereas the contribution of Fe^{2+} drops from 21 to 16 %. Since, prior to cooling the catalyst to room temperature, the contribution of metallic iron and iron carbide was also about 86 %, it can be concluded that the catalyst can be regenerated reversibly and that the pressure does not influence the formation of the carbide and the mixed oxide.

Table 5.13 *Mössbauer parameters of 2.5 wt% Fe/K/ZrO_2 calculated from spectra recorded during Fischer-Tropsch synthesis at 623 K and ambient pressure with $H_2/CO=1$.*

T(K)	I.S. (mm/s)	Q.S. (mm/s)	Γ (mm/s)	S.C. (%)	Compound
623	0.24	0.41	0.33	52	Fe_xC
(0-26h)	0.29	0.83	0.29	27	Fe_xC
	0.98	1.35	0.68	21	Fe^{2+}
623	0.23	0.41	0.32	57	Fe_xC
(26-43h)	0.29	0.82	0.25	27	Fe_xC
	0.96	1.38	0.62	16	Fe^{2+}

Γ is the line width.

Subsequent to the second exposure to carbon monoxide and hydrogen, the catalyst was again exposed to hydrogen at 623 K The Mössbauer parameters derived from spectra recorded during the regeneration in hydrogen at 623 K and hydrogen at ambient pressure are represented in Table 5.14.

Table 5.14 Mössbauer parameters of 2.5 wt% Fe/K/ZrO_2 calculated from spectra recorded during a second regeneration step in hydrogen at 623 K and 1 bar.

T(K)	I.S. (mm/s)	Q.S. (mm/s)	H_{eff} (kOe)	Γ (mm/s)	S.C. (%)	Compound
623	0.06		302	0.28	52	Fe^0
(0-25h)	0.24	0.39		0.32	24	Fe_xC
	0.30	0.80		0.28	11	Fe_xC
	0.99	1.37		0.61	13	Fe^{2+}
623	0.06		302	0.27	80	Fe^0
(25-47h)	0.34	0.41		0.42	5	Fe_xC
	0.95	1.34		0.65	15	Fe^{2+}
300	0.26		331	0.27	73	Fe^0
reox	0.61	0.94		0.80	27	Fe^{3+}

Again, it is apparent that the carbon of the iron carbides can be smoothly hydrogenated, since zerovalent iron is formed at the expense of the iron carbides. When the catalyst is cooled down to room temperature, the Fe^{2+} species is completely oxidized to Fe^{3+}, while also the iron carbide and a fraction of the metallic iron are oxidized to Fe^{3+}.

5.5 Discussion

The results of the present chapter provide information about two items highly important in the Fischer-Tropsch synthesis on supported iron catalysts, *viz*. the extent of reduction of the iron precursor and the formation and stability of the iron carbide species formed by the interaction with carbon monoxide and hydrogen. The extent of reduction of the iron precursor affects the iron surface area and, hence, the activity of the catalyst resulting after reduction, while the amount of the Fe^{2+} species remaining in the catalyst is likely to determine the activity of the

catalyst in the carbon monoxide shift conversion. As dealt with in Chapter 3 the extent of reduction of the unpromoted Fe/ZrO_2 catalyst remains low upon reduction with hydrogen at ambient pressure. Thermal treatment at 723 K in hydrogen at ambient pressure only leads to a contribution of about 46 % of iron carbide (θ-Fe_3C) and metallic iron to the Mössbauer spectra. Raising the hydrogen pressure to 1.8 bar at a reduction temperature of 673 K, the iron carbide is not encountered and the contribution of reduced iron species increases, of which about half of the Fe^0 contribution is due to small superparamagnetic iron particles. Accordingly, a relatively large surface area of the metallic iron can be expected.

The unpromoted catalyst Fe/ZrO_2 employed in the Fischer-Tropsch synthesis at ambient pressure was initially reduced in hydrogen at 653 K. The total contribution of iron carbide (and metallic iron) increases during Fischer-Tropsch synthesis at 623 K relative to prior reduction. Upon exposure to H_2 and CO, the metallic iron completely reacts to iron carbide. The carbon monoxide-hydrogen flow increases the extent of reduction substantially, as is apparent from the rise of the iron carbide contribution to 28 %. The reaction to iron carbide consumes a corresponding fraction of the surface Fe^{2+} species. Performing the Fischer-Tropsch synthesis for a period of 72 hours does not increase the contribution of the iron carbide and the two Fe^{2+} species to the spectra.

Subsequent reduction at 773 K in ambient hydrogen increased the total amount of metallic iron and iron carbide. During this procedure, also Fe^{2+} which is present in the mixed oxide is consumed. Fischer-Tropsch synthesis at 623 K again raises the extent of reduction.

It is found at elevated pressure, that the amount of Fe^0 present after reduction is the same as the amount of carbide during Fischer-Tropsch synthesis. Even after various subsequent treatments, the contribution of iron carbides and metallic iron does not vary. Therefore, it is concluded that exposure to (high-pressure) syngas following reduction at 1.8 and 9.5 bar does not improve the reduction degree.

The promoted $Fe/K/ZrO_2$ catalyst contains much more cementite (θ-Fe_3C) than the Fe/ZrO_2 catalyst. Furthermore, the overall reduction degree at both 1 bar and elevated pressure is higher for the potassium-promoted catalyst. However, the contribution to the spectra of superparamagnetic iron particles is much lower than observed for Fe/ZrO_2. For this reason, the surface area of the metallic iron in $Fe/K/ZrO_2$ is likely to be smaller than that of the unpromoted catalyst, Fe/ZrO_2, reduced under similar conditions.

It is observed that the total amount of iron carbide and metallic iron during

reduction, Fischer-Tropsch synthesis and regeneration (all measured at 623 K) does not change, but is larger than encountered at ambient pressure. Only if the catalyst is regenerated at 773 K the iron species is substantially reduced further. At 9.5 bar the total amount of zerovalent iron was not observed to vary during several treatments including the Fischer-Tropsch synthesis.

The main conclusion is that Fischer-Tropsch synthesis at elevated pressures leads to a relatively low extent of reduction to zerovalent iron with the unpromoted Fe/ZrO_2 catalyst. The extent of reduction of the promoted $Fe/K/ZrO_2$ catalyst is much higher. This discrepancy can be explained by either the presence of the potassium species affecting the reduction properties of the iron oxide or by the amount of water which is (primarily) formed during Fischer-Tropsch synthesis. If the latter is the case, the activity (*i.e.* CO conversion) is higher for the unpromoted Fe/ZrO_2 catalyst, which will be demonstrated in chapter 6.

The types of carbide observed during Fischer-Tropsch synthesis seems to depend on the reduction degree as is discussed above. It is found that for a lowly reduced Fe/ZrO_2 catalyst only Hägg carbide is formed during synthesis at 1 bar. This carbide exhibits an isomer shift of 0.25 mm/s. In other experiments at ambient pressure this carbide is also encountered as well as another carbide (ε'-$Fe_{2.2}C$) having a higher isomer shift of 0.29 mm/s. However, at elevated pressure also two carbides are found but with higher isomer shifts *viz.* about 0.29 and 0.33 mm/s, respectively. This is explained by a pressure effect. A high pressure environment causes the particles to become more dense (atoms are located more closely to each other), which leads to a higher isomer shift. A similar effect is observed previously for the hyperfine splitting of metallic iron, which increases significantly at high(er) pressure [11].

During Fischer-Tropsch synthesis at 1 bar three iron species are observed in the promoted catalyst, which are identified as surface and 'mixed oxide' divalent iron and a carbidic species. These three species (except for a different carbide) were also observed during prior reduction at 653 K at which temperature a small amount of metallic iron was found additionally. Comparing the spectra during reduction and during the Fischer-Tropsch reaction, it appears that the spectral contribution of the metallic Fe^0 vanishes and the total spectral contribution of the two Fe^{2+} species decreases during Fischer-Tropsch synthesis, and, consequently, the total contribution of the carbide is increased. The latter observation points to a further reduction of the catalyst by reduction of Fe^{2+} to Fe^0 and a rapid conversion of the zerovalent iron species into the carbide during the Fischer-Tropsch synthesis. Considering the divalent species, it is obvious that the change in atmosphere (from

H_2 to H_2/CO) causes only a decrease in the amount of less ordered Fe^{2+} at the surface, whereas the Fe^{2+} situated in the ZrO_2 support as a mixed oxide remains unaffected.

The unpromoted catalyst contains cementite after hydrogen reduction, which, in turn, reacts to χ-carbide upon exposure to synthesis gas. The Mössbauer parameters (of the doublets) of both iron carbide species, which are measured above their Curie temperature, are observed to be similar. The reaction to a different iron carbide phase could only be distinguished after cooling the catalyst to room temperature. At this temperature the iron carbide species present during Fischer-Tropsch reaction shows magnetically split (sub)spectra, which are different for θ-Fe_3C (cementite) and χ-Fe_5C_2 (Hägg carbide) (see Table 5.2 and [8]).

At elevated pressures different results are observed. As described previously [11], the amount of Fe^0 is much higher upon reduction at elevated hydrogen pressures than at ambient pressure. The effect of the hydrogen pressure is due to the removal of the carbon originating from the citrate complex at relatively low temperature. As a consequence, no iron carbide is present in the catalyst reduced at elevated hydrogen pressures. After exposure to the carbon monoxide-hydrogen flow at ambient pressure only χ-carbide is observed, whereas reaction at 9.5 bar reveals both ε'- and χ-carbide. The observed difference in carbide presence seems to depend on the extent of reduction of the iron species, i.e. a high reduction degree leads to formation of two (ε' and χ) carbides.

A completely regenerated catalyst having large metallic iron particles (as evident from the presence of the sextuplet in the spectra) was next exposed to carbon monoxide and hydrogen at 1 bar. It was shown that, also at low pressure, reaction to the Hägg carbide proceeds, which indicates that reaction to the carbide does not depend on the pressure and does depend on the size of the iron particles and/or the metallic nature of the iron species. Niemantsverdriet *et al.* [8] observed that with increasing reaction temperatures of the Fischer-Tropsch synthesis more χ-Fe_5C_2 is formed and eventually the most stable θ-Fe_3C results. These findings were confirmed for supported catalysts [10, 15]. In our experiments the relation between the nature of the iron carbide and the reaction temperature could not be established, since the catalysts were exposed to reaction conditions at only one temperature (623 K). It must be noted, however, that despite the relatively high reaction temperature, the most stable θ-Fe_3C was never observed (during Fischer-Tropsch synthesis). Moreover, the initially present cementite is converted to other carbides at 623 K and ambient pressure. Probably the formation of a mixed oxide of iron and the support plays an eminent role in the stability of the carbides. Raupp and

Delgass [15] studied a silica-supported and a magnesia-supported iron-based catalyst and observed – next to a temperature dependence on the nature of the carbide formed – a different behaviour during the reaction to iron carbides for iron particles of a similar size on different supports. The magnesia-supported catalyst having an average iron particle size of 6.1 nm exhibited predominantly χ-Fe_5C_2 after exposure to carbon monoxide and hydrogen, whereas the silica-supported system having a similar particle size exhibited predominantly the metastable ε'-$Fe_{2.2}C$. Iron particles of approximately 10 nm supported on silica mainly display the χ-carbide. These authors conclude that metastable carbides are stabilized on silica more effectively than on magnesia; the stabilizing effect of the support is attributed to an interaction between the support and the iron particles. Furthermore, it appears that ε'-carbide is preferably formed in small particles and that the Hägg carbide appears with increasing particle size and eventually only χ-Fe_5C_2 will be the predominant species [15-18]. In our experiments this relation between particle size and carbide species is not directly evident. In every experiment χ-carbide is the predominant phase. At elevated pressure at which large Fe^0 particles and superparamagnetic metallic iron are initially present in both catalysts, a relatively large amount of ε'-$Fe_{2.2}C$ is encountered. Although it is not unambiguously shown, these results point to the reported relation.

Furthermore, it was observed that cooling of an exposed catalyst to room temperature at 9.5 bar does not reveal any ε'-$Fe_{2.2}C$ despite the fact that this species is observed at reaction temperature (623 K). It is deduced that ε'-carbide is converted to either χ-Fe_5C_2 and to divalent iron. The latter conversion leads to the conclusion that the metastable carbide is oxidized while cooling to 300 K. This oxidation is (again) explained by the presence of water, which is a primary product in the Fischer-Tropsch synthesis. When the temperature is raised to its original reaction temperature, the same species (as observed prior to the cooling step) reappear in similar amounts. Clearly, the processes of oxidation to Fe^{2+} and conversion to χ-Fe_5C_2 are reversible.

It is further found that decarburisation of most of the carbides produced within the unpromoted catalyst during Fischer-Tropsch synthesis (at 1 bar) calls for a temperature of 773 K at ambient hydrogen pressure. The iron carbides produced within the unpromoted catalyst (Fe/ZrO_2) during Fischer-Tropsch synthesis at 9.5 bar are incompletely (and slowly) removed by thermal treatment with 9.5 bar hydrogen at 623 K. Only about 30 % of the iron carbides are reduced to metallic iron. In contrast, thermal H_2 treatment at 1 bar of the promoted $Fe/K/ZrO_2$ catalyst (which has been exposed to syngas at 9.5 bar) causes the carbide to lose its carbon

almost completely. Taking into account that the hydrogen pressure differs a factor 10 – a higher p_{H2} causes the gasification equilibrium ($C + 2H_2 \quad CH_4$) to shift to the methane side and hence increase the carbon removal rate – the carbon is (much) more strongly bound in the unpromoted Fe/ZrO_2 catalyst. It must further be noted that the reduction degree also appears to be an important factor in the regeneration reaction. A highly reduced potassium-promoted catalyst (having about 80% zerovalent iron) already loses its carbon at 623 K (at 1 bar), whereas the relatively lowly reduced $Fe/K/ZrO_2$ (having about 40 % zerovalent iron) is only substantially regenerated at 773 K. This observation may indicate that a larger amount of mixed oxide is able to stabilize χ-Fe_5C_2 to a higher extent. Our results further show that of the two carbides the ε'-carbide is more easily regenerated, since the Hägg carbide is generally observed last. This is in agreement with the reported stability of the carbides, which predicts that Hägg carbide is more stable than the metastable ε'-$Fe_{2.2}C$ [9, 10]. The higher resistance towards carbon removal of χ-Fe_5C_2 confirms this relative stability. Obviously, the stability of the carbide reported for its formation holds also for its decomposition reaction (*i.e.* regeneration).

In every experiment divalent iron species were present in both the unpromoted Fe/ZrO_2 and the potassium-promoted $Fe/K/ZrO_2$ catalyst. At ambient pressure a Fe^{2+} surface species is present as well as a Fe^{2+} mixed oxide species. At elevated pressures the Fe^{2+} surface species is reduced and converted to iron carbide species. A model as shown in Figure 5.7, in which the metal carbide completely (or partially) covers the mixed oxide, can explain the different reactivity of both Fe^{2+} species.

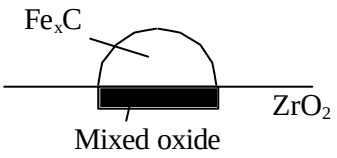

Figure 5.7 *A schematic model of the iron distribution during the Fischer-Tropsch synthesis when the contribution to the spectra of the Fe^{2+} present as a mixed oxide is relatively low.*

This model is quite similar to the model proposed for the reduction process of the unpromoted catalyst [11]. Taking into account that generally Fe^0, once

exposed to Fischer-Tropsch conditions, reacts completely to iron carbide and that the divalent oxidic species remains unaffected, the above proposed model seems acceptable.

5.6 Conclusions

It is demonstrated that the nature of the iron species during Fischer-Tropsch conditions can be measured both at ambient and elevated pressure by using in situ Mössbauer spectroscopy.

Upon exposure to carbon monoxide-hydrogen at ambient pressure the lowly reduced unpromoted Fe/ZrO_2 catalyst revealed only Hägg carbide, whereas two carbides, *viz.* ε'-$Fe_{2.2}C$ and χ-Fe_5C_2, are encountered in a highly reduced catalyst having a lower dispersion. These two carbides are also formed on potassium-promoted $Fe/K/ZrO_2$, which is profoundly reduced as well. The reduction degree, and consequently the particle size, appears to be a predominant factor in the carbide formation during Fischer-Tropsch synthesis.

Not only does a high reduction degree lead to both ε'- and χ-carbide at 1 bar, it also enables formation of the said carbides during Fischer-Tropsch synthesis at 9.5 bar. Surprisingly, it is observed that the ε'-$Fe_{2.2}C$ vanishes completely at room temperature due to conversion to χ-Fe_5C_2 and oxidation to Fe^{2+}. The latter process is enabled by a higher (oxidising) water content of the reaction gas due to a relatively high Fischer-Tropsch activity. Also at 300 K, the presence of water leads to oxidation of the divalent iron species. It is furthermore demonstrated that, when the reaction temperature is again increased to 623 K, the iron species present prior to cooling to 300 K are restored *i.e.* the oxidation of ε'-$Fe_{2.2}C$ and conversion to χ-Fe_5C_2 are reversible processes.

If both catalysts – after being exposed to synthesis gas – are regenerated in hydrogen, the carbides can be completely removed. It is generally observed that first the metastable ε'-$Fe_{2.2}C$ is hydrogenated and then the Hägg-carbide. The regeneration is observed to be substantially higher for the potassium-promoted catalyst compared to the unpromoted Fe/ZrO_2.

5.7 References

[1] M.E. Dry, *'The Fischer-Tropsch Synthesis'* (Catalysis Science & Technology, J.R. Anderson and M. Boudart, 1st ed.), Springer Verlag, 1981, Chapter 4.

[2] J.R. Reymond, R. Meriaudeau and S.J. Teichner, *J.Catal.* **75** (1982) 39.
[3] J.W. Niemantsverdriet, *'Spectroscopy in Catalysis'*, VCH Verlagsgesellschaft, Weinheim, Germany, 1st ed., 1993, Chapter 5, 127.
[4] Chapter 1 of this thesis.
[5] D.J. Dwyer and G.A. Somorjai, *J.Catal*. **56** (1979) 249.
[6] J.A. Amelse, G. Grynkewich, J.B. Butt and L.H. Schwartz, *J.Phys.Chem.* **82(5)** (1978) 558.
[7] G. Le Caër, J.M. Dubois, M. Pijolat, V. Perrichon and P. Bussière, *J Phys.Chem.* **86** (1982) 4799.
[8] J.W. Niemantsverdriet, A.M. van der Kraan, W.L. van Dijk and H.S. van der Baan, *J.Phys.Chem* **84** (1980) 3363.
[9] M.A. Vannice, '*Catalysis Science and Technology*', Vol.3, 1982, Springer-Verlag, Berlin, Germany, Chapter 3.
[10] J.A. Amelse, J.B. Butt and L.H. Schwartz, *J.Phys.Chem.* **82 (5)** (1978) 558.
[11] Chapter 3 of this thesis.
[12] A.M. van der Kraan, J.W. Niemantsverdriet, '*Industrial Applications of the Mössbauer Effect'*, G.J. Long, J.G. Stevens (eds), Plenum, New York, 1986, 609.
[13] A.M. van der Kraan, *Phys.Stat.Sol(A)* **18** (1973) 215.
[14] P.W. Selwood, *'Magnetochemistry'*, 1956, Interscience Publishers Inc., New York, Chapter XV.
[15] G.B. Raupp and W.N. Delgass, *J.Cat.* **58** (1979) 348.
[16] H. Jung and W.J. Thomson, *J.Cat*. **134** (1992) 654.
[17] J.A. Amelse, J.B. Butt and L.H. Schwartz, *J.Phys.Chem.* **85** (1981) 558.
[18] J. van de Loosdrecht, Thesis, Utrecht University, 1995, Chapter 6.

6

The Fischer-Tropsch Synthesis: an Activity Study

Abstract

In this chapter the catalytic activity during the Fischer-Tropsch synthesis of unpromoted Fe/ZrO_2 and potassium-promoted $Fe/K/ZrO_2$ were investigated at elevated pressure. For reason of comparison, both catalysts were measured in a nanoflow reactor. The unpromoted catalyst reveals a higher CO conversion. Furthermore, it exhibits a lower methane fraction together with a higher selectivity to light olefins with the exception that the ethene fraction is lower. For this reason, $Fe/K/ZrO_2$ was investigated on a larger scale in a microflow reactor.

From the experiments in the microflow reactor, it is established that the selectivity to olefins increases at low pressure, high temperature and low H_2/CO. In our experiments, variation of the gas hourly space velocity does not bring about changes in the product selectivity nor in the CO conversion. The space velocity not affecting the conversion and selectivity is attributed to a deactivation-reactivation cycle, wherein both deactivation and reactivation proceed within 6 hours. Deactivation proceeds via oxidation of the active carbide species resulting in a mixed oxide, which is inactive during the Fischer-Tropsch synthesis. This process is reversible. It is further demonstrated that only a small part of the catalyst bed is active.

6.1 Introduction

This chapter deals with an investigation of the catalytic properties of two zirconia-supported iron catalysts in the Fischer-Tropsch synthesis. One of the catalysts, Fe/ZrO_2, only contains iron oxide deposited on a zirconia support, the other catalyst, $Fe/K/ZrO_2$, contains beside iron oxide potassium oxide as a promotor. The objective was to study the behaviour of very small iron particles. The loading of the zirconia support was therefore low, *viz*., only 2.5 wt% metallic iron. In the previous chapters, we have described the chemical composition and the nature of the iron species within the catalyst during the pre-treatment and during exposure to the reactions conditions of the Fischer-Tropsch synthesis. The experiments have also been carried out at elevated pressures. Since iron catalysts perform much better at higher pressures, the total pressures during the Fischer-Tropsch reactions to be described in this chapter were 10, 11, and 24 bar and the temperatures were varied from 523 to 623 K.

In Chapter 3 it was shown that reduction of the unpromoted catalyst, Fe/ZrO_2, in a hydrogen flow of 1.8 bar at 573 K leads to reaction of 8 % of the iron species of the catalyst to very small, superparamagnetic iron particles. Reduction at 623 K for a long period of time resulted in 20 % of the iron species present as larger, ferromagnetic particles and no less than 25 % of the iron species as very small, superparamagnetic particles. More than 50 % of the iron species in the catalyst is present as Fe^{2+} after reduction at 623 K. The Fe^{2+} species is liable to react with water to Fe^{3+} upon decreasing the temperature to room temperature. Upon exposure to hydrogen and carbon monoxide of 9.5 bar the metallic iron particles react to iron carbides, such as, the Hägg carbide, χ–Fe_5C_2. Since the iron carbides involve about 54 % of the iron species present in the catalyst, some additional reduction of Fe^{2+} has proceeded. The resulting iron carbides are fairly stable; thermal treatment at 623 K in hydrogen of 9.5 bar for 52 to 72 hours results in only about 17 % of metallic iron, while still about 37 % is the iron is still present as iron carbides.

The potassium-promoted catalyst is more easy to reduce. Thermal treatment in hydrogen of 1.8 bar at 623 K leads to 75 % of larger, ferromagnetic iron particles and 11 % of very small, superparamagnetic particles. The fraction of very small, superparamagnetic iron particles is thus lower than that in the non-promoted catalyst. The catalytically active metallic iron surface area of the promoted catalyst is therefore likely to be smaller than that of the unpromoted catalyst. The iron carbides resulting from exposure of the catalyst to hydrogen and carbon monoxide is less stable. Upon exposure to hydrogen at 623 K, 78 % of the iron is present as metallic iron after treatment for 115 hours. It is remarkable that the iron carbide is liable to oxidation by water at low temperatures.

The Fischer-Tropsch synthesis involves the conversion of carbon monoxide and hydrogen to predominantly hydrocarbon products. These products can either be olefins or paraffins as is illustrated in Equations 6.1a, 6.1b, 6.2a, and 6.2b.

$$n\,CO + (2n+1)\,H_2 \longrightarrow C_nH_{2n+2} + n\,H_2O \qquad (6.1a)$$

$$n\,CO + 2n\,H_2 \longrightarrow C_nH_{2n} + n\,H_2O \qquad (6.1b)$$

$$2n\,CO + (n+1)\,H_2 \longrightarrow C_nH_{2n+2} + n\,CO_2 \qquad (6.2a)$$

$$2n\,CO + n\,H_2 \longrightarrow C_nH_{2n} + n\,CO_2 \qquad (6.2b)$$

Generally it is assumed that carbon monoxide dissociates on the surface of the catalytically active species to adsorbed carbon and oxygen atoms. The oxygen atoms can react either with hydrogen atoms generated by dissociation of molecular hydrogen on the catalytically active surface to water or with carbon monoxide to carbon dioxide. The carbon atoms remaining within the surface layer of the catalyst can either be hydrogenated to hydrocarbons or react with the catalytically active metal to a carbide. The rate of the dissociation of adsorbed carbon monoxide and the mobility of adsorbed hydrogen atoms determine the ratio of the reaction of the adsorbed oxygen atoms to carbon dioxide and to water.

The metal carbide can decompose to the metal and to graphitic carbon. Layers of graphitic carbon grow on the surface of the metal, which can completely encapsulate the catalytically active metal particles and thus deactivate the catalyst. Formation of graphitic carbon corresponds to the Boudouard reaction

$$2\,CO \rightleftharpoons CO_2 + C \qquad (6.3)$$

Since the Fischer-Tropsch synthesis also involves the reaction to water, the carbon monoxide shift conversion must be considered too. The carbon monoxide shift conversion is

$$CO + H_2O \rightleftharpoons CO_2 + H_2 \qquad (6.4)$$

Iron oxide-chromium oxide and copper-zinc oxide catalysts are known to catalyse the carbon monoxide shift reaction. The copper-zinc oxide catalyst is active at low temperatures, whereas the iron oxide-chromium oxide catalyst is known to become active only at temperatures above about 623 K. Since the maximum temperature of our experiments was at most 623 K, it is not likely that the carbon monoxide shift conversion significantly affects the results.

As mentioned above the reduced catalysts contain a considerable amount of Fe^{2+} species. In a previous study [1], it has been reported that a considerable fraction of the Fe^{2+} species is present as a mixed iron-zirconium oxide, which may influence the catalytic properties of the catalysts. In order to establish the catalytic properties and to assess the effect of the promotion with potassium oxide, the catalysts are studied and compared in a nanoflow reactor during Fischer-Tropsch synthesis. The potassium-rich catalyst is further investigated in a larger catalyst bed within a microflow reactor. The influence of several process variables, such as, pressure, temperature, gas hourly space velocity (GHSV), and H_2/CO ratio will also be assessed.

We will show that the catalysts under study are able to suppress the selectivity to methane and produce a high fraction of light olefins. It will further be demonstrated that – when using a relatively large volume of the potassium-promoted catalyst – only a fraction of the entire catalyst bed is active. Moreover, it will be shown that the catalyst can be deactivated and (re)activated upon variation of the GHSV during Fischer-Tropsch synthesis; this (de)activation process will be elucidated.

6.2 Experimental

6.2.1 Catalyst preparation

The catalyst was prepared by means of incipient wetness impregnation. The pre-shaped support used was zirconia (Norton XZ16075). The zirconia extrudates possessed a pore volume of 0.28 ml/g and a specific surface area of 49 m^2/g. Ammonium iron(III) citrate (Merck, 28% Fe) was employed as a precursor to achieve a calculated iron loading of 2.5 wt%. The potassium-promoted catalyst was prepared by co-impregnation of the above citrate and potassium carbonate. An atomic Fe/K ratio of 1 was applied. After impregnation the loaded supports were subsequently dried at 350 K under flowing air, and calcined at 623 K for 2 hours.

The citrate precursor left behind some carbon in the catalysts due to incomplete combustion. The amount of carbon within the calcined catalysts was assessed by thermogravimetry. The potassium-promoted catalyst contained significantly more carbon, *viz*., 2.09 wt.% than the Fe/ZrO_2 catalyst, which contained only 0.64 wt.% carbon.

6.2.2 Reaction conditions

6.2.2.1 Nanoflow experiments

The Fischer-Tropsch synthesis was carried out in a fixed-bed nanoflow reactor in downstream operation, in which about 40 mg of the catalyst diluted with silicon carbide was placed. A reductive treatment with hydrogen of 1.8 bar at 633 K preceded the synthesis. The catalysts were exposed for 24 hours to a carbon monoxide-hydrogen flow of a H_2/CO ratio of 0.5 and a pressure of 10 bar. The gas hourly space velocity was 2000 h^{-1}. Only the temperature was varied; measurements were executed at 523, 573, and 623 K.

The composition of the gas flowing out of the reactor was determined by gas-chromatography. The content of the different hydrocarbons was measured as well as the content of carbon dioxide, carbon monoxide, hydrogen and water.

6.2.2.2 Microflow experiments

With the potassium-promoted catalyst the Fischer-Tropsch synthesis was executed also in a fixed-bed microflow reactor in downstream operation, in which 8.5 g of a Fe/K/ZrO_2 catalyst diluted with silicon carbide was placed. A reductive treatment with hydrogen of 1.8 bar at 633 K preceded the synthesis. Several process variables were changed, *i.e.*, pressure, H_2/CO, and gas hourly space velocity (GHSV). Table 6.1 represents the different experimental conditions.

Table 6.1 Consecutively applied process conditions with the microflow experiments.

p (bar)	T (K)	H_2/CO	GHSV (h^{-1})	TOS (h)
11	548	1.0	1865	24
11	598	1.0	1865	24
11	623	1.0	1865	130
24	623	1.0	1865	48
24	623	1.0	750	48
24	623	1.0	1865	98
24	623	1.7	1880	71

TOS represents time on stream

Every 6 hours the product stream was analysed by gas-chromatography. The content of the different hydrocarbons was measured as well as the content of carbon dioxide, carbon monoxide, hydrogen and water.

6.3 Results and discussion

6.3.1 Nanoflow experiments

Table 6.2a and 6.2b tabulate the selectivities to C_1, C_2 and C_3 hydrocarbons together with the fraction of ethene (C_2=) and propene (C_3=) relative to the total amounts of C_2 and C_3 produced as observed for the Fe/ZrO_2 and $Fe/K/ZrO_2$ catalyst, respectively. In addition, the conversion of CO is represented.

Table 6.2a CO Conversion and selectivity to C_1-C_3 and olefin selectivity of Fe/ZrO_2 at different temperatures.

T (K)	C_1	C_2	C_3	$C_{2=}/(C_2+C_{2=})$	$C_{3=}/(C_3+C_{3=})$	Conversion
523	-	-	-	-	-	-
573	4.1	7.3	12.6	76.7	91.3	3.4
623	9.9	13.9	19.7	59.7	88.8	10.9

Table 6.2b CO Conversion and selectivity to C_1-C_3 and olefin selectivity of $Fe/K/ZrO_2$ at different temperatures.

T (K)	C_1	C_2	C_3	$C_{2=}/(C_2+C_{2=})$	$C_{3=}/(C_3+C_{3=})$	Conversion
523	-	-	-	-	-	-
573	7.7	5.2	7.9	90.4	84.8	1.6
623	24.6	7.4	10.0	82.4	83.0	2.4

After keeping the catalysts for 24 hours at 523 K in the carbon monoxide-hydrogen flow, no significant activity is detected for both catalysts. When the reaction temperature is increased, both Fe/ZrO_2 and $Fe/K/ZrO_2$ show a significant CO conversion. The unpromoted catalyst exhibits conversions of 3.4 and 10.9 % at reaction temperatures of 573 and 623 K, respectively. The potassium-promoted catalyst displays lower conversion levels of 1.6 and 2.4 % for both temperatures. The much higher conversion of the unpromoted catalyst, Fe/ZrO_2, is not unexpected, since the amount of very small superparamagnetic iron particles in this catalyst and, hence, the surface area of the iron particles is larger. Furthermore it is possible that potassium oxide is covering some of the active iron surface. The ratio of the conversions at 573 and 623 K of the promoted and unpromoted catalyst

indicates that the promoted catalyst exhibits a lower apparent activation energy than the unpromoted catalyst.

From Tables 6.2a and 6.2b it is apparent that the selectivity for methane is higher for the promoted catalyst. Beside the activity also the selectivity to methane increases with the temperature for both catalysts. However, for the promoted catalyst, $Fe/K/ZrO_2$, the increase in the selectivity for methane with the temperature is much larger. The methane selectivity for the catalyst Fe/ZrO_2 remains well below 10 % even at 623 K. In contrast, the catalyst $Fe/K/ZrO_2$ exhibits a much higher methane selectivity of 24.5 % at this temperature. Analogous to the selectivity for methane the selectivity for C_2 and C_3 hydrocarbons increases with temperature indicating that the average chain length of the products drops. A shortening of the chain length of the hydrocarbons can be a purely kinetic effect leading to a decrease of the chain growth probability α. The drop in chain growth probability may be caused, e.g., by the hydrocarbon intermediates present on the iron surface desorbing (and thus terminating) more readily at higher temperatures or by inhibition of the propagation reaction. Thermodynamics [2,3,4] predicts also formation of smaller hydrocarbons to be more favorable at higher temperatures. The higher selectivity for C_2 and C_3 hydrocarbons may therefore be due to a combination of a kinetic and a thermodynamic effect.

The effect of the temperature on the selectivities of the promoted and unpromoted catalyst is significantly different. While raising the temperature from 573 to 623 K increases the selectivity for methane by a factor of 2.4 with the unpromoted catalyst, the selectivity for methane with the promoted catalyst rises by a factor of 3.2. Comparing the selectivities for C_2 and C_3 hydrocarbons of both catalysts, higher selectivities are observed for the unpromoted catalyst. The selectivity of the promoted catalyst for C_2 and C_3 hydrocarbons increases by raising the temperature from 573 to 623 K by a factor of 1.4 for the C_2 hydrocarbons and a factor of 1.3 for the C_3 hydrocarbons. The corresponding factors for the unpromoted catalyst are 1.9 for the C_2 hydrocarbons and 1.6 for the C_3 hydrocarbons.

The selectivity to olefins is higher at 573 K than at 623 K for both the Fe/ZrO_2 and the $Fe/K/ZrO_2$ catalyst. The effect of the temperature on the olefin selectivity would suggest that kinetic effects determine the selectivity for olefins. Of the two catalysts, the potassium-promoted catalyst displays a higher selectivity to ethene. The selectivity for olefins of a short hydrocarbon chain is between 80 and 90 %, which is relatively high. Since the main objective of this research is to develop a catalyst and reaction conditions that selectively produce as much olefins of a short hydrocarbon chain as possible, the potassium-promoted catalyst was

studied more extensively in a microflow reactor, which will be described in the following section.

6.3.2 Microflow experiments

6.3.2.1 Fischer-Tropsch synthesis at 11 bar

In Figure 6.1a the conversion of CO is plotted as a function of time on stream. Three regions can be discriminated, each region representing CO conversion at different reaction temperatures, *viz.* 548, 598 and 623 K. The corresponding selectivity toward C_1-C_5 hydrocarbons is plotted in Figure 6.1b. Table 6.3 represents the amounts of carbon dioxide produced at different times-on-stream. To demonstrate that the carbon monoxide shift conversion does not proceed significantly on the promoted catalyst, the values for the equilibrium constant have also been calculated. The data are included in Table 6.3. For the thermodynamic equilibrium values of 59.6 [5] and 56.7 [6] are calculated at 548 K. The experimental values being much lower than the values corresponding to the thermodynamic equilibrium indicates that the carbon monoxide shift conversion does not proceed significantly at 548 K.

Table 6.3 *CO conversion to CO_2 and K_{WGS} at 548K*

Time-on-stream (h)	CO_2 (%)	K_{WGS}
6	36	1.43
12	32	1.00
18	24	0.52
24	22	0.42

At the lowest temperature, *viz.* 548 K, the conversion curve shows a decrease during the first 18 hours. According to literature, deactivation of the catalyst during Fischer-Tropsch reaction is caused by carbon deposition as it covers or inactivates the active site [7-10]. Eliason and Bartholomew [9] suggest this deactivation to proceed in two parallel steps, *viz.* crystallisation of polymeric β-carbon into graphitic δ-carbon and formation of more stable (less reactive and less carbon-rich) carbides. The deactivation rate decreases with prolonged time-on-stream [9, 10] and is larger at higher temperature [9].

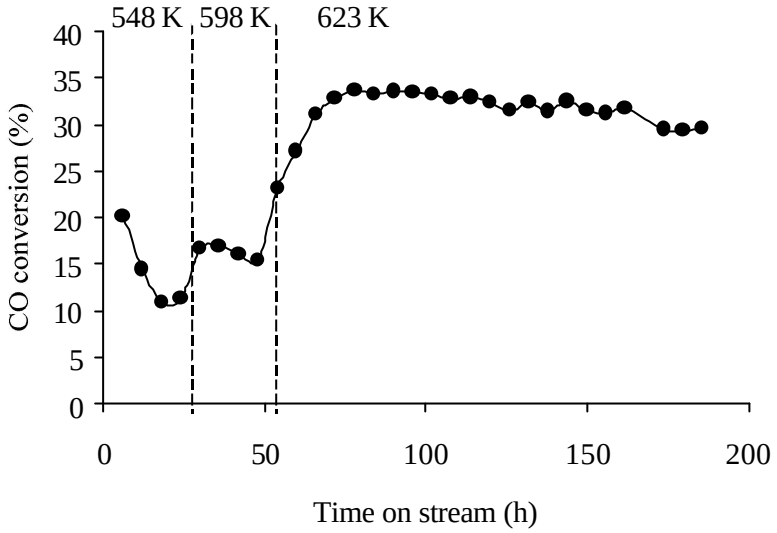

Figure 6.1a *CO conversion as a function of time on stream. FT synthesis conditions: 11 bar, 1865 h^{-1}, H_2/CO = 1.0. Dotted lines separate regions of different reaction temperatures.*

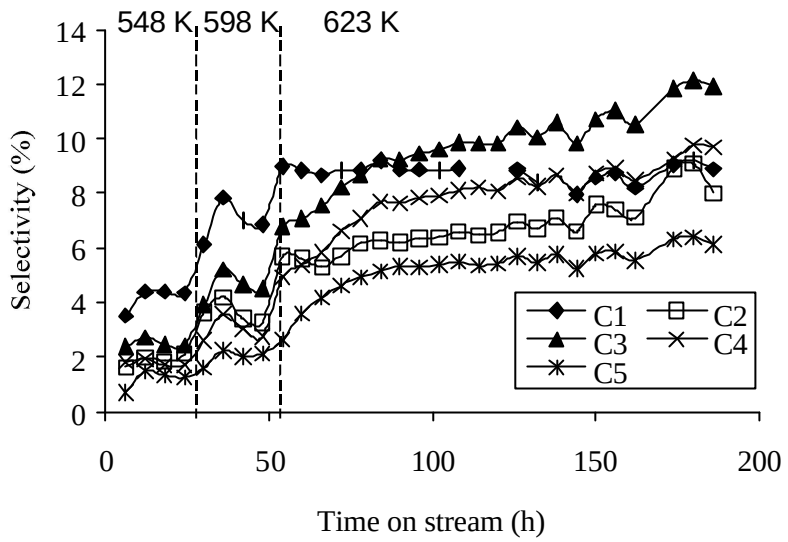

Figure 6.1b *Selectivity towards hydrocarbons as a function of time on stream. Conditions as in Figure 6.1a.*

However, the extensive Mössbauer experiments of the present research have shown that the iron particles of our catalysts react very rapidly upon exposure to carbon monoxide and hydrogen to iron carbides of a relatively high carbon content. Decomposition of the metal carbide to graphitic carbon and metallic iron would have been evident in the Mössbauer spectra. However, the spectra did not show any evidence for the decomposition to metallic iron at the maximum temperature of 623 K at which the catalysts were exposed to the carbon monoxide-hydrogen flow. At more elevated temperatures, above about 773 K, the metal carbide can decompose to graphitic carbon and the metal, which results in the graphitic layers encapsulating the metal particles provided the size of the metal particles is not too small. The deactivation exhibited in Figure 6.1a can therefore not be due to encapsulation by graphitic carbon layers.

Our extensive experiments on the Fischer-Tropsch synthesis at ambient pressure have demonstrated that at temperatures where the Fischer-Tropsch synthesis is usually performed the catalytically active surface is blocked by partially hydrogenated carbonaceous material. Switching off the supply of carbon monoxide and keeping the catalyst at the reaction temperature in the remaining hydrogen flow rapidly re-activates the catalyst. The experiment at 548 K represented in Figure 6.1a indicates that also at elevated pressures blocking of the surface by partially

hydrogenated carbonaceous material proceeds. As a result, the non-dissociative adsorption of carbon monoxide is blocked and the adsorbed oxygen atoms are removed by reaction with hydrogen atoms. Hydrogen molecules can still dissociate on the surface covered by partially hydrogenated carbonaceous material and the resulting adsorbed hydrogen atoms react with the adsorbed oxygen atoms to water. However, the dissociation of hydrogen molecules and the subsequent reaction of the resulting adsorbed hydrogen atoms with the carbonaceous material and the adsorbed oxygen atoms proceed more slowly. Consequently the rate of the overall reaction and, hence, the conversion of carbon monoxide drops. In this way, the build-up of partially hydrogenated carbonaceous material brings about a slowly developing drop in the production of carbon dioxide due to reaction of non-dissociatively adsorbed carbon monoxide with adsorbed oxygen atoms.

Another reason for deactivation of Fischer-Tropsch catalysts can be reaction of the catalytically active iron to an iron carbide that is stable under the conditions of the Fischer-Tropsch synthesis. Usually deactivation of iron catalysts in the Fischer-Tropsch synthesis is attributed to the formation of cementite, θ-Fe_3C. However, the experiments of Chapter 3 have unambiguously demonstrated that cementite is only observed at ambient hydrogen pressure. Exposure to a hydrogen pressure of 1.8 bar at elevated temperatures leads to complete hydrogenation of the carbon in the iron carbide resulting in immediate reduction to Fe^0 without cementite formation. Nevertheless the experiments of Chapter 5 have shown that the hydrogenation of the carbon in the less stable, more carbon-rich Hägg carbide, χ-Fe_5C_2, and ε'-$Fe_{2.2}C$ proceeds slowly and call for a long period of time. Almost complete hydrogenation of the carbon in the iron carbides present in the promoted catalyst $Fe/K/ZrO_2$, which is studied in the present microflow experiments, was observed in Mössbauer experiments to last from 19 to 115 hours. The slow hydrogenation of the iron carbides observed in previous Mössbauer experiments [11] may therefore account for the deactivation at 548 K. Since we feel that the non-dissociative adsorption of carbon monoxide and, hence, the reaction to carbon dioxide can still proceed on the surface of iron carbide, we prefer the deposition of a partially hydrogenated carbonaceous layer as the cause of the deactivation observed at 548 K.

The selectivity to hydrocarbons differs only slightly during the period of time the reaction was executed at 548 K. The C_{5+} fraction decreases from 91 to 89 %, whereas the selectivity to C_3 and C_4 remains constant, but the C_2 fraction increases. The C_1 fraction grows almost 1 %. Accordingly, the variation in the selectivity is small and is thus not significant.

By raising the reaction temperature to 598 K the conversion increases from 11 % at 548 K to 17 %. The first detection point is not relevant due to equilibration of the experimental conditions. The incomplete equilibration brings about that the measured selectivity towards C_1-C_4 hydrocarbons is lower than corresponds to the reaction temperature of 598 K. The increase of the reaction temperature also affects the selectivity to hydrocarbons. The selectivity towards C_1-C_4 rises and the C_{5+} fraction drops. Since shorter chains are thermodynamically more favourable at higher temperatures, the empirically recorded temperature effect was to be expected.

A slow deactivation of the catalyst is apparent from the fact that the conversion of carbon monoxide decreases by 1 % over a period of 18 hours. The deactivation is accompanied by an increase in length of the hydrocarbon chains, which is reflected by a decrease in the C_1-C_5 hydrocarbons and an increase in the C_{5+} hydrocarbons. The CO_2 fraction also diminishes from 32 % to 28 % indicating that – analogous to deactivation at 548 K – partially hydrogenated carbonaceous material is deposited on the iron surface, though to a more limited extent.

At the still higher temperature of 623 K a relatively slow increase in activity is observed. The activity reaches a steady state within 24 hours. The increase in activity is linked to a rise in CO_2 production. Table 6.4 shows the content of carbon dioxide of the gas flowing out of the reactor and the calculated values of the equilibrium of the carbon monoxide shift conversion, K_{WGS}, during the period in which the activity of the catalyst grows. At thermodynamic equilibrium the value for K_{WGS} is calculated to be 21.4 [5] and 19.9 [6] at 623 K. Also at 623 K the carbon monoxide shift conversion is thus far from equilibrium, and therefore does not proceed significantly. The more elevated production of carbon dioxide is due to the reaction of not dissociated carbon monoxide with the adsorbed oxygen atoms from previously dissociated carbon monoxide. The activation during the first 24 hours on stream at 623 K is likely to be due to the removal of the partially hydrogenated carbonaceous material present on the surface of the iron particles.

Table 6.4 CO conversion to CO_2 and K_{WGS} at 623 K during activation.

Time on stream (h)	CO_2 (%)	K_{WGS}
6	35	1.38
12	37	1.65
18	38	1.99
24	40	2.40
30	40	2.44

From previous experiments at lower temperatures it has been concluded that deposition of partially hydrogenated material is involved in the observed

deactivation. By hydrogenation of the deposited carbonaceous material, the active sites are regenerated. As the removal of the carbonaceous material by hydrogenation is competing with the deposition reaction [4], the rate of the hydrogenation must increase more rapidly than the deposition rate of the carbonaceous material. Van de Loosdrecht speculates that methane is formed upon regeneration of inactive carbonaceous material in hydrogen [10]. In our experiments, the selectivity to C_1 increases initially to about 9% and subsequently slightly drops with progressive time on stream. In contrast, the selectivity to C_3 to C_5 hydrocarbons rises gradually during the first 30 hours. Consequently relatively more methane is formed during the first 30 hours after raising the temperature to 623 K, which in turn suggests that the deposited carbon is removed during that initial period.

After 30 hours on stream, a very slow deactivation process sets on. The conversion of carbon monoxide decreases from 32% to 29% over a period of 110 hours. The deactivation is accompanied by a decrease in the C_{5+} hydrocarbons indicating that formation of hydrocarbons with shorter chains becomes more favourable. Consequently, the fraction of C_2-C_4 hydrocarbons rises from 23 to 31 %. The selectivity for the C_1 hydrocarbon and for carbon dioxide of 9 and 40 %, respectively, remains unchanged during this period of time.

The selectivity for olefins does not change for the C_2 hydrocarbon, *viz*., 84 %, but gradually increases slightly for the C_3 hydrocarbon from 91 to 92 % and for the C_4 hydrocarbon from 90 to 91 %. It is likely that hydrogenation of the partially hydrogenated carbonaceous species leads to methane, while the usual Fischer-Tropsch reaction proceeds on the remaining bare sites. Hydrogenation of the different surface species might suggest the presence of different sites on the iron surface [15, 16]. However, the presence of different sites on the iron surface does not agree with the dynamical state of the iron surface during the Fischer-Tropsch synthesis. Reaction of the iron to different iron carbides and reduction of the iron carbides as well as deposition of partially hydrogenated carbonaceous on the iron surface leads to a continuously changing, dynamic situation on the surface of the iron particles. It is important to note that the competition between hydrogenation and deposition of partially hydrogenated carbonaceous material – both processes take place simultaneously during the Fischer-Tropsch reaction [4] – shifts to the hydrogenation at more elevated temperatures.

6.3.2.2 Fischer-Tropsch reaction at 24 bar

The conversion of CO and the selectivity to C_1-C_4 hydrocarbons measured at 623 K and a pressure of 24 bar are plotted against the time-on-stream in Figure 6.2a and 6.2b. The figures indicate the effect of a change in space velocity from 1865 h^{-1} to 750 h^{-1} and back to 1865 h^{-1}. Two dotted lines separate the regions of different space velocity. From the Figures, it is apparent that the changes in space velocity do not affect the conversion level. This remarkable phenomenon will be discussed further on in this section. From Figure 6.2a a slow deactivation is evident, which eventually leads to a steady conversion of 39 %. Comparison of this conversion with that found at 11 bar (32%) leads us to conclude that an increase in pressure results in a higher CO conversion.

Although the shift of the space velocity does not influence the conversion, it does slightly affect the selectivity. The selectivity to C_1 and C_2 hydrocarbons gradually grow in the first two regions, but after the final change to the space velocity of 1865 h^{-1} the growth is slightly enhanced. The C_3 and C_4 fractions remain virtually equal and the selectivity to C_{5+} diminishes from 60 to 56 %. In other words, the hydrocarbon chains become shorter after prolonged time-on-stream, although the conversion of CO does not change. The olefin selectivity of the C_3 and C_4 fraction is not influenced by the variation in GHSV. The olefin fraction of C_2, however, declines very slowly in the first two regions, but more pronouncedly in the third region.

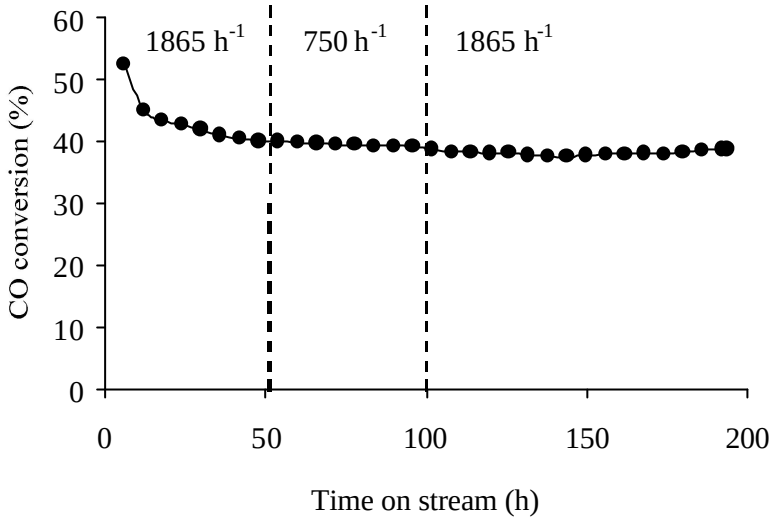

Figure 6.2a *CO conversion as a function of time-on-stream. FT synthesis conditions: 24 bar, 623 K, H_2/CO = 1.0. Dotted lines separate regions of different GHSV.*

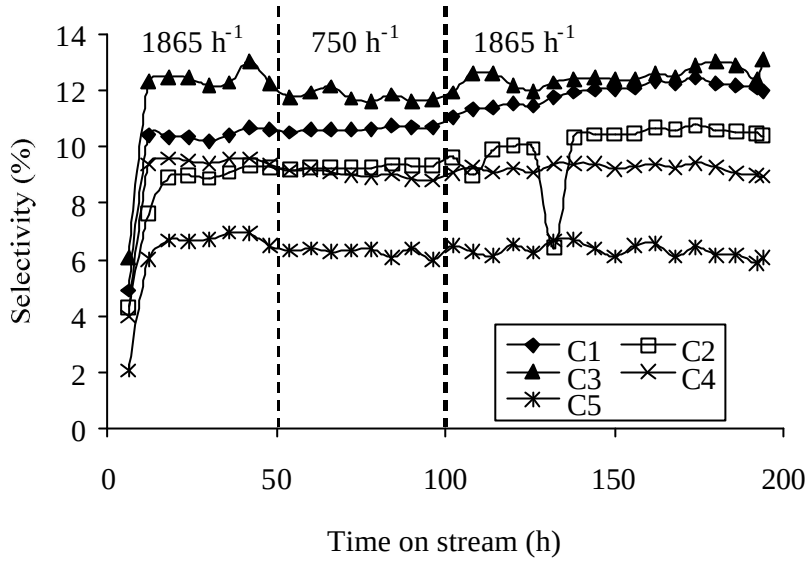

Figure 6.2b Selectivity towards hydrocarbons as a function of time on stream. Conditions as in Figure 6.2a.

Subsequent to the aforementioned experiments the catalyst was exposed to a higher H_2/CO ratio of 1.7. The conversion of carbon monoxide and the selectivity to C_1-C_4 as a function of time-on-stream are plotted in Figures 6.3a and 6.3b, respectively.

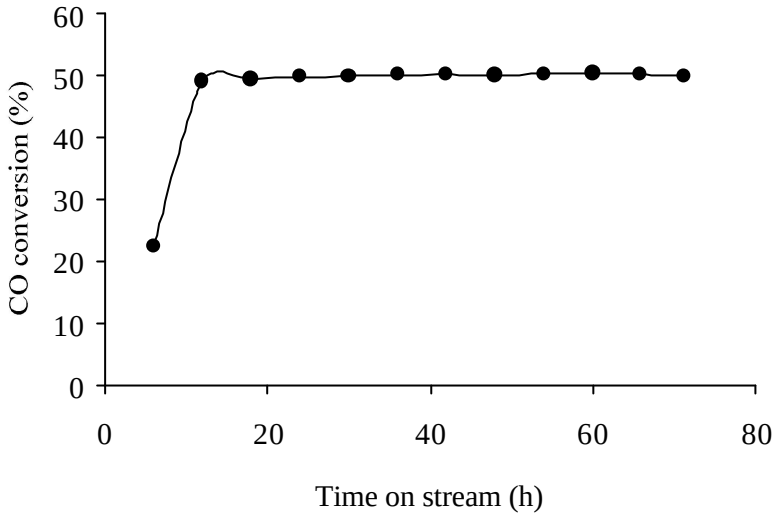

Figure 6.3a CO conversion as a function of time on stream. FT synthesis conditions: 24 bar, 623 K, 1880 h^{-1}, H_2/CO = 1.7.

Comparison of the experiments with a H_2/CO ratio of 1.0 with those with a ratio of 1.7 reveals an increase in CO conversion from about 40 % to 50 % by raising the H_2/CO ratio from 1.0 to 1.7. The selectivity to C_1 increases to 18 %, which is significantly higher than the value found at a H_2/CO of 1.0, *viz*., about 12 %. Moreover, all components of the C_2-C_4 fraction exhibit a higher selectivity, *viz.* 13, 15 and 9 % for C_2, C_3 and C_4, respectively. Overall, an increase in the H_2/CO ratio leads to a shortening of the hydrocarbon chain length and a decrease in α. This can be explained by a lower surface coverage of carbon (from the dissociation of CO), which is inversely proportional to α [3].

The selectivity to olefins also decreases as compared to that observed at a lower H_2/CO. For C_2 a value of 59 % was found, for C_3 86% and for C_4 84 %. With a more hydrogen-rich gas flow the rate of hydrogenation of the adsorbed carbon species increases markedly, resulting in lower olefin selectivity.

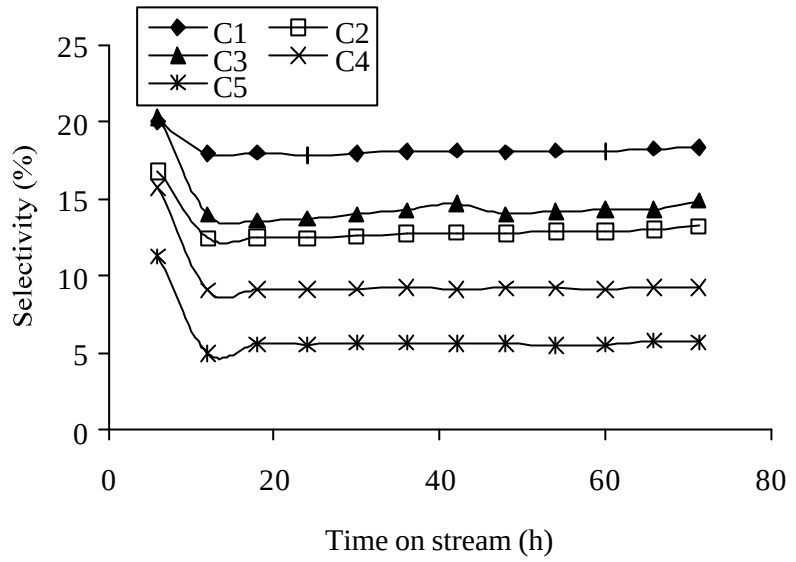

Figure 6.3b *Selectivity towards hydrocarbons as a function of time on stream. Conditions as in Figure 6.3a.*

The selectivity to CO_2 is 42 % and does not change during reaction. This value is slightly lower than was found at the lower H_2/CO ratio of 1.0. The lower level of carbon dioxide production can be understood from the higher partial pressure of hydrogen, which leads to more hydrogenation of adsorbed oxygen to water and less reaction of carbon monoxide with adsorbed oxygen. Under these reaction conditions all above-mentioned values remain constant over a period of 70 hours.

6.3.2.3 Anderson-Schulz-Flory (ASF) distribution

The ASF distribution for a measurement at 24 bar is plotted in Figure 6.4. Only one distribution is shown as an example, since the distributions measured under the applied reaction conditions all exhibit the same features.

On the promoted $Fe/K/ZrO_2$ catalyst the chain growth probability α is calculated to be 0.56. The value of the probability is relatively low and very close to the value for maximum C_2-C_4 yield ($\alpha \approx 0.5$). The experimentally observed selectivity to C_2-C_4 hydrocarbons is much lower than that predicted by the product distribution model, namely 31% *vs.* 53 %. As demonstrated by Figure 6.4 the

relatively low C_2 fraction leads to the difference. This phenomenon is often encountered in literature and is mainly attributed to secondary reactions, such as, hydrogenolysis to methane, rapid readsorption, and hydrogenation of ethene [17].

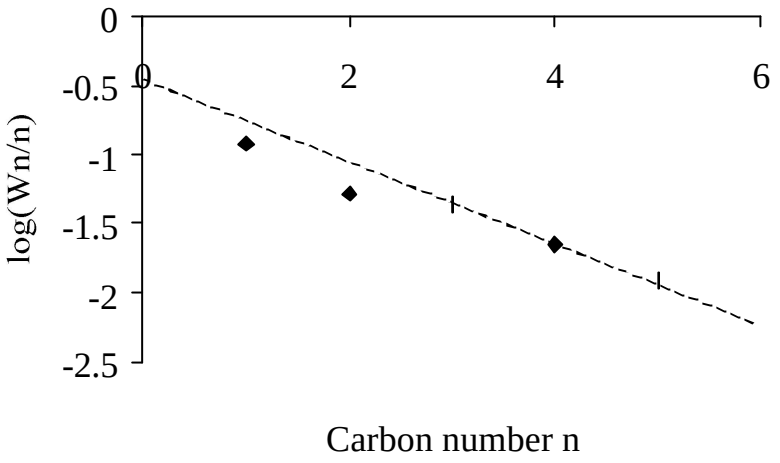

Figure 6.4 ASF distribution of Fischer-Tropsch reaction. Conditions: 24 bar, 1865 h^{-1}, 623 K, $H_2/CO=1$

According to experiments described in the literature the weight fraction of C_1 is always higher than that predicted by the ASF distribution. However, in our experiments the selectivity to methane is much lower than that predicted by the ASF model. Supported by quantum chemical calculations Koerts *et al.* [18] suggested a relation between carbon atoms more strongly adsorbed to the metal surface and the formation of higher hydrocarbons. The metal-carbon bond can be affected by the properties of the catalyst, *viz.* a promoter, the presence of more open metal surfaces, or an interaction of the metal phase with the support. Though the iron particles in the promoted catalyst, $Fe/K/ZrO_2$, are larger than the iron particles in the not promoted catalyst, Fe/ZrO_2, the relatively low temperature at which a high level of reduction to metallic iron was achieved with the promoted catalyst leads to relatively small iron particles. Accommodation of carbon atoms in between the metal surface atoms of small particles proceeds much more easily than that with larger metal particles containing a higher proportion of closely packed

planes. A sideways shift of metal atoms present in the small facets bounding small metal particles can take place smoothly.

6.3.3 Nanoflow *vs*. microflow experiments

In this section the relation between the conversion levels of the nano- and microflow experiments is considered. Although the exact reaction conditions (see Table 6.5) are not identical, the effectiveness of the catalyst bed in the microflow experiment can be evaluated from the experimental data.

Table 6.5 Reaction conditions at 623 K of the nano- and microflow experiments and their respective CO conversion level

Experiment	Weight (g)	p (bar)	GHSV (h^{-1})	H_2/CO	CO conv. (%)
nanoflow	0.040	10	2000	0.5	2.4
microflow	8.5	11	1865	1	30

Whether the conversion levels of the nanoflow and microflow experiments can be compared must be considered first. The pressure and the gas hourly space velocity are similar in both sets of experiments. Consequently, the H_2/CO ratio may lead to an erroneous comparison of the conversions. Considering the H_2/CO ratio, Figures 6.2a and 6.3a demonstrate that a lower H_2/CO ratio results in a lower conversion level at 24 bars. Taking the effect of the H_2/CO ratio into account, it is clear that the conversion of 40 mg catalyst under the reaction conditions of the microflow experiments is expected to be higher than 2.4 %. If, nonetheless, this conversion is accepted and it is further assumed that every 40 mg of catalyst converts the same amount of carbon monoxide, it is easily calculated that about 500 mg will convert 30 % of the admitted carbon monoxide. This means that only 5.8 % of the entire catalyst bed is responsible for the conversion measured in the microflow experiments of Table 6.5. Knowing that the accepted conversion of 2.4 % is a lower limit, the calculated fraction of the catalyst bed of 5.8 % is very likely to be even smaller. The fact that only a small fraction of the entire catalyst bed is active in the microflow experiments is confirmed by the other microflow experiments at 24 bar, in which the space velocity was varied. Measurements at a pressure of 24 bars displayed a CO conversion that did not change when the space velocity was decreased from 1865 to 750 h^1. This behaviour can be attributed to either mass transport limitations or changes of the active species. Mass transport limitations will be discussed in the next section, changes of the active species in the following.

6.3.4 Mass transport limitation

Two types of mass transport limitation are known, *viz.*, external and internal transport limitation [20]. External transport limitation can be established either by variation of the linear flow rate at constant space-time or by monitoring the conversion as a function of space-time. The former method should show a constant conversion level when diffusion limitation is absent. The latter should exhibit a linear relationship between conversion and space-time (x times lower space-time, x times lower conversion). In our experiments, the decrease in space velocity does not cause a change in conversion level. The absence of an effect of the space velocity could point in the direction of external transport limitation. However, Post *et al.* [21] determined experimentally under similar reaction conditions that significant transport limitations due to the resistance in the gas or liquid film around the catalyst particles are absent. Therefore, it is likely that external transport limitation does not explain the aforementioned behaviour.

Internal diffusion limitation can be assessed by changing the particle size and determining the effect of the size on the conversion or by calculating the Thiele modulus (ϕ) and the effectiveness factor (η). If ϕ and η are calculated according to Post *et al.* [21] using the same assumptions, the Fischer-Tropsch synthesis is under both conditions reaction driven (ϕ is smaller than 1 and, hence, η is 1). This can be easily understood considering that the process is only diffusion-limited when particles exceeding 1 mm are used. In our experiments much smaller particle sizes (100-200 mesh) are employed. In addition, the reaction rates for H_2 conversion, k_H, were higher than determined by Post *et al.*, namely 128 and $51 \cdot 10^{-4} m^3/m^3$ cat/s for 1865 and 750 h^{-1} respectively. It is obvious that internal diffusion limitation can be ruled out. Therefore, it is likely that the observed reaction behaviour must be attributed to changes of the catalyst during the variation of the space velocity.

6.3.5 Nature of deactivation

As argued above, other reasons must account for the constant level of conversion of carbon monoxide. Partial deactivation of the catalyst bed can account for the behaviour, i.e. at high contact times (low GHSV) 40% of CO is converted in the first section and the second part of the bed is completely inactive. In literature [4, 9] this deactivation is suggested to be due to: (i) poisoning of active sites by, *e.g.*, sulphur, (ii) a morphology change due to sintering and subsequent addition of carbon adlayers, (iii) transformation of reactive carbon into inactive carbon, (iv) formation of a less active carbidic species, *e.g.*, stable θ-Fe_3C, and (v) oxidation by

water creating an inactive oxide. In the following all five possible deactivation processes are discussed separately.

Contamination by sulphur is known to cause a complete loss in activity, which is not observed. Moreover, regeneration of an iron catalyst poisoned by sulphur by thermal treatment in pure hydrogen is not possible below 673 K. Consequently, the regeneration is not likely to occur under Fischer-Tropsch conditions [22]. This argument and the fact that our initial gas mixture does not contain sulphur-containing compounds exclude the poisoning option (i).

Formation of larger particles due to sintering generally gives rise to a different activity and selectivity. In addition, such restructuring of the active iron particles is not reversible. Option (ii) can therefore be excluded.

Option (iii) can also be eliminated. Only in hydrogen-lean atmospheres excessive carbon accumulation is most likely to occur [23]. In this experiment, the H_2/CO ratio was relatively low, which makes the deposition of inactive carbon feasible. If carbon would be deposited, the carbonaceous species can generally only be hydrogenated at higher temperatures than the reaction temperature employed [16, 24, 25]. It has been mentioned previously in this chapter that the activity rises only slowly (in about 30 hours on stream) after increasing the temperature to 623 K. Since carbon cannot be hydrogenated at 623 K, regeneration of the active phase by removal of carbon is not likely. Based on the above arguments, it is concluded that this deactivation option (iii) does neither explain our results.

The fourth process is only possible when cementite (θ-Fe_3C) is formed upon decarburization of the active ε'- or χ-carbides. In experiments previously carried out [11] θ-Fe_3C was never observed to be an end-product or even an intermediate product in the regeneration step with hydrogen. The active carbides appear to react directly to metallic iron. Additionally, cementite is a very stable carbide [5], which is observed to remain unaffected when exposed to H_2 at 823 K [1]. In view of the above, the formation of an inactive carbide can also be ruled out.

This discussion leaves the deactivation by oxidation as a possible candidate. The oxidation reaction depends on p_{H2O}/p_{H2} and on p_{CO2}/p_{CO} [22, 26]. If these ratios exceed certain critical values, oxidation of the active iron phase by water or carbon dioxide will proceed resulting in an inactive oxide. The H_2O-to-H_2 ratio at which reduction of FeO to metallic iron is thermodynamically possible depends on the temperature. In view of the entropy of steam being higher than that of hydrogen, the equilibrium shifts to metallic iron and water at more elevated temperatures. At 523 K the H_2O-to-H_2 ratio at which reduction to metallic iron is possible is 0.13, at 623 K this ratio is 0.30 and at 723 K the ratio is 0.56. Reaction of the hydrogen initially present in the feed to the catalyst to water will readily lead to conditions where the metallic iron is oxidised to iron(II) oxide. At a low(er) space velocity

more water and carbon dioxide will be produced in higher sections of the catalyst

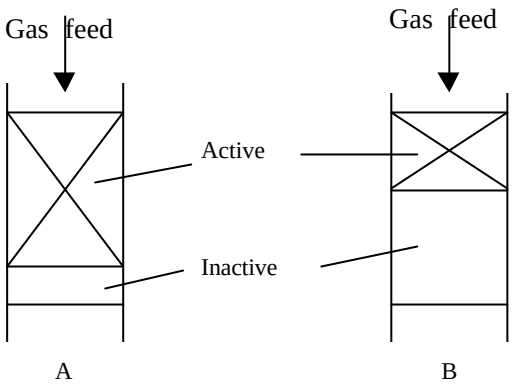

bed. Hence, the critical values for inactivation will be reached earlier in the catalyst bed.

Figure 6.5 Schematic representation of the active bed at different space velocity a) 1865 h^{-1} and b) 750 h^{-1}.

The oxidation and subsequent establishment of a steady state is a rather fast step, which takes place within 6 hours as can be concluded from the absence of a change in activity and selectivity. This process is reversed when the space velocity is restored to 1865 h^{-1}. At this space velocity p_{H2O}/p_{H2} and p_{CO2}/p_{CO} will both increase below the critical value leading to reduction of the oxidised iron species, after which it is carburised to the active species. The inactive region becomes smaller and its border is transferred closer to the exit of the catalyst bed. This (re-)activation also occurs within 6 hours. Satterfield *et al.* [26] also reported the regeneration to the original activity. These authors studied the effect of addition of water to the gas feed on the Fischer-Tropsch activity of an iron-based catalyst and found upon addition of 27 mol% water a decrease in activity which could be reversed.

6.3.6 Nature of iron species

In the last paragraph it is shown that oxidation of the active species explains the constant conversion level upon increasing and decreasing the space velocity. In the following the nature of the iron species and their change during the space velocity variation is elucidated. Based on previous Mössbauer experiments [26] it is assumed that in the active fraction of the catalyst bed the ε'-$Fe_{2.2}C$ and/or

χ-Fe_5C_2 are present as well as one or more divalent iron species. When the space velocity is changed from 1865 to 750 h^{-1}, the critical values for p_{H2}/p_{H2O} and p_{CO}/p_{CO2} for oxidation of the metallic iron will be reached earlier in the catalyst bed. The Mössbauer experiments discussed in Chapter 4 have shown that the two iron carbides present upon exposure to carbon monoxide and hydrogen are liable to oxidation to divalent iron species. Previous decarburization of the iron carbides is therefore not required to get oxidation of iron carbides by water. Earlier it has been observed that only the Hägg carbide is liable to decarburization at the employed reaction temperature of 623 K, whereas the ε'-carbide looses its carbon only at 773 K [26]. However, the iron carbides resulting from exposure of the catalysts investigated here did not exhibit such behaviour. Hydrogenation of the carbon present in the iron carbides proceeded only slowly, while the Hägg carbide appeared to be relatively more stable.

The catalytically active iron carbides are oxidised by H_2O and/or CO_2, which results in an inactive oxidised iron species. Previously it was observed that keeping the catalyst at room temperature after a thermal treatment does not oxidise the metallic iron phase [22]. However, it is likely that the metallic iron surface is very rapidly oxidised already during cooling down to room temperature, which brings about that at room temperature no drop in the spectral contribution of metallic iron is evident.

It must further be noted that one of the divalent iron species present is probably a mixed oxide species with the ZrO_2 support [22, 26]. This species is easily oxidised when exposed to oxidising conditions. In a subsequent reducing step it is also easily re-converted to the divalent species.

The behaviour of the active particles upon exposure to water vapour and upon regeneration by carbon monoxide-hydrogen is represented in Figure 6.6. As the double arrows in Figure 6.6 indicate the Figure can also be read from right to left, in such case representing the restoring of the space velocity from 750 to 1865 h^{-1}.

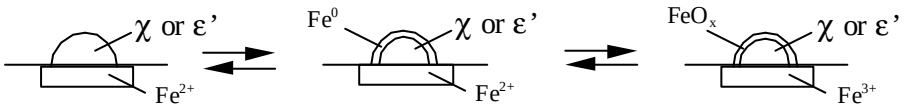

Figure 6.6 *A possible oxidation process during space velocity variation demonstrating that only `the outer surface is decarburised and subsequently oxidised*

6.4 Conclusions

Comparison of the potassium-promoted and the not promoted catalyst unambiguously shows that the not promoted catalyst is more active. Although the not promoted catalyst produces more propene, the selectivity to ethene is lower. Because of the higher selectivity for ethene of the promoted catalyst, this catalyst was studied in a microflow reactor.

In the microflow reactor the effect of process variables (as observed for the potassium-promoted catalyst) on the olefin selectivity and the selectivity to hydrocarbons were observed to be similar to those described in literature. The only exception is the influence of variation of the space velocity, which hardly affects the conversion and the selectivity. The lack of an effect of the space velocity is attributed to oxidation of the active iron carbides leaving at lower space velocity a smaller fraction of the catalyst bed available for the Fischer-Tropsch reaction. Increasing the space velocity to its original value shows that the oxidation process is reversible and consequently no change in activity and selectivity is observed.

The selectivity of the zirconia-supported iron catalysts to methane is well below the expected ASF distribution. Under all reaction conditions the fraction of C_2-C_4 products lies below the maximum value of 56 %, which can be ascribed to the relatively low C_2 fraction. With the highly dispersed promoted iron catalyst the selectivity for olefins of the C_3-C_4 hydrocarbons is relatively high (around 90 %). For the C_2 fraction the olefin content is, however, always lower.

At a pressure of 11 bar a deactivation process is encountered, the rate of which strongly depends on the temperature. Whereas the rate of deactivation at 548 K is appreciable, at 598 K the rate is small and at 623 K very small, hardly noticeable. The deactivation is related to deposition of partially hydrogenated carbonaceous material on the iron carbide surface. Experiments at 24 bar reveal an initial deactivation, which gradually changes into a steady activity. Increasing the H_2/CO ratio does not change the behaviour of the catalyst.

6.5 Literature

[1] Chapter 3 of this thesis.

[2] R.B. Anderson, *'The Fischer-Tropsch Synthesis'* (Academic Press, Inc. Orlando, 1984)

[3] R. Snel, *Catal.Rev.-Sci.Eng.* **29(4)** (1987) 361.

[4] M.E. Dry, in '*Catalysis Science and Technology*', eds. J.R. Anderson and M. Boudart, Vol. 1, Springer Verlag, 1981, Chapter 4.
[5] Thermodynamic calculations with HSC Chemistry, Version 3.02, Outokumpu Research Oy, Pori Finland.
[6] G.H.Graaf, P.J.J.M. Sijtsema, E.l. Stamhuis, G.E.H. Joosten, *Chem.Eng.Sci.* **41** (1986) 2883.
[7] D.J. Dwyer and G.A. Somorjai, *J.Catal.* **56** (1979) 249.
[8] J.A. Amelse, G. Grynkewich, J.B. Butt and L.H. Schwartz, *J.Phys.Chem.* **82(5)** (1978) 558.
[9] S.A. Eliason and C.H. Bartholomew, *Appl.Cat.A:General* **186** (1999) 229.
[10] J. van de Loosdrecht, Ph.D. thesis, Utrecht University, 1995, Chapter 6.
[11] Chapter 5 of this thesis.
[12] D.S. Newsome, *Catal.Rev.-Sci.Eng.* **21** (1980) 25.
[13] E.S. Lox and G.F. Froment, *Ind.Eng.Chem.Res.* **32** (1993) 61.
[14] D.G. Rethwisch and J.A. Dumesic, *J.Catal.* **101** (1986) 35.
[15] V. Ponec, *Catal.Rev.-Sci.Eng.***18** (1978) 151.
[16] F. van Looij and J.W. Geus, *Catal.Lett.* **45** (1997) 209.
[17] G.P. van der Laan and A.A.C.M. Beenackers, *Catal.Rev.-Sci.Eng.* **41(3-4)** (1999) 255.
[18] T. Koerts and R.A. van Santen, *Catal.Lett*, **6** (1990) 49.
[19] V. Ponec, in '*Metal Support and Metal-Additive Effects in Catalysis*', eds. B.Imelik et al., Elsevier Sci.Publ.Comp., Amsterdam, 1982, 63.
[20] G.F. Froment and K.B. Bischoff, *'Chemical Reactor Analysis and Design*', 2nd ed., John Wiley & Sons, New York, 1990.
[21] M.F.M. Post, A.C. van 't Hoog, J.K. Minderhoud and S.T. Sie, *AlChe.J.* **35(7)** (1987) 1107.
[22] M.E. Dry, *Catal.Lett.* **7** (1990) 241.
[23] M.S. Hoogenraad, Ph.D. thesis, Utrecht University, 1995, Chapter 2.
[24] J.G. McCarthy and H. Wise, *J.Catal.* **57** (1979) 406.
[25] F. van Looij., Ph.D. thesis, Utrecht University, 1994, Chapter 6.
[26] C.N. Satterfield, R.T. Hanlon, S.E. Tung, Z.Zou and G.C. Papaefthymiou, *Ind.Eng.Chem.Prod.Res.Dev.* **25** (1986) 407.
[27] C.K. Rofer-De Poorter, *Chem.Rev.* **81** (1981) 447.
[28] M. Janardanarao, *Ind.Eng.Chem.Res.* **29** (1990) 1735.

7

Summary and Concluding Remarks

It is very attractive to directly and selectively produce light olefins, especially ethene and propene, via the Fischer-Tropsch synthesis, since light olefins are an important feedstock to produce polyethylene and polypropylene, for example. In producing such small-chain hydrocarbons, formation of the thermodynamically favourable methane is inevitable. The methane selectivity should therefore be reduced as much as possible. Moreover, two unwanted reactions may also occur, *viz.* the Boudouard reaction ($2\ CO \rightarrow CO_2 + C$) and the water gas shift reaction ($CO + H_2O \rightarrow CO_2 + H_2$). Both reactions produce undesirable carbon dioxide. Especially, the Boudouard reaction may furthermore lead to severe deactivation through deposition of carbon. The extent of the above undesired reactions depend on the reaction conditions and on the catalyst properties.

In this thesis both properties will be dealt with. It must be noted that the catalyst properties are more difficult to control, since they depend *e.g.* on the active metal, the support, the dispersion of the active metal and the promotor employed. Iron is chosen as active metal for its ability to dissociatively adsorb CO faster than H_2, hence producing olefins selectively. However, this ability makes iron also liable to deactivate faster. This deactivation problem is addressed by a high dispersion of the active iron species on which carbon deposition is enormously reduced. The support must be able to stabilise the high dispersion and moreover should not interact with an applied promotor. For this reason, a ZrO_2 support is screened for suitability. Finally, a potassium promotor is chosen since it is reported that potassium enhances the formation of unsaturated hydrocarbons and decreases the hydrocarbon chain size.

In view of the above, two highly dispersed catalysts were prepared, *viz.* an unpromoted Fe/ZrO_2 and a potassium-promoted $Fe/K/ZrO_2$ catalyst, which is described in **Chapter 2**. Subsequent to preparation and prior to the Fischer-Tropsch reaction, the catalysts are reduced. Their reduction behaviour was investigated at ambient and elevated pressure, and described in **Chapter 3**. In **Chapter 4** the effect of a H_2/H_2O treatment on the reduction behaviour of the unpromoted Fe/ZrO_2 catalyst is unveiled. Following reduction, the catalytic properties during Fischer-Tropsch reaction at 1 bar and elevated pressure were extensively studied. The nature of the iron species present during Fischer-Tropsch synthesis were studied using *in situ* Mössbauer spectroscopy, the results are presented in **Chapter 5**. Finally, their activity and selectivity were monitored during reaction at elevated pressure, and described in **Chapter 6**.

The unpromoted and potassium-promoted catalysts were prepared using the incipient wetness impregnation and an organic chelating citrate complex. The advantage of such a precursor is the steep viscosity increase already in the initial stage of drying. In this way the precursor is not mobile leading to a homogeneous distribution of the citrate over the zirconia support. After calcination at relatively low temperature (723 K), a thin amorphous iron oxide layer (having a thickness of about 1 nm) remains on the support. A high calcination temperature (generally reported in literature) results in undesired bimodal particle size distributions. It is established that the catalysts under study comprise a highly dispersed iron(III) oxide species which is, moreover, monodisperse. It is further found that carbon is also present, which is a remainder of the citrate precursor. It is established that $Fe/K/ZrO_2$ contains more carbonaceous deposit than the unpromoted Fe/ZrO_2.

This carbon influences the reduction at 1 bar at which pressure cementite (θ-Fe_3C) is encountered. The larger carbon fraction of the promoted $Fe/K/ZrO_2$ catalyst is confirmed by the larger amount of θ-carbide. However, reduction at 1.8 bar does not reveal this carbide. This is due to the higher hydrogen pressure which enables the removal of the carbonaceous deposit already at relatively low temperature – that is before metallic iron is formed, a process being thermodynamically driven. Although it is observed that the presence of carbon leads to θ-Fe_3C at 1 bar, the carbon is readily removed when exposed to a H_2/H_2O mixture. In this way, analogous to high-pressure reduction highly dispersed (superparamagnetic) Fe^0 is also observed at ambient pressure.

The potassium-rich catalyst is more easily reduced than the unpromoted Fe/ZrO_2. This higher reduction degree can either be explained by the presence of the carbon species or by the potassium species. As it is observed that both at ambient and elevated pressure $Fe/K/ZrO_2$ reduces more easily, and considering that at 1.8 bar the carbon has vanished, the potassium species itself enhances the reduction.

In the reduction process, divalent iron plays an eminent role. Two divalent species are encountered, of which one relates to a lowly ordered Fe^{2+} which is situated at the surface, and the other relates to a well-ordered Fe^{2+} species which is involved in a mixed oxide with the support. Due to the (intimate) interaction with the support, the formation of magnetite (Fe_3O_4) is prevented. The presence of the mixed oxide is also a prerequisite in maintaining a high dispersion. The formation of this 'mixed' Fe^{2+} is enhanced by a H_2/H_2O treatment resulting in a higher resistance towards reduction. Although trivalent iron is completely reduced to (the stable) Fe^{2+} before metallic iron is formed, (re-)oxidation of the divalent species to Fe^{3+} proceeds already at room temperature.

During Fischer-Tropsch synthesis the mixed oxide species is always encountered, which again stabilises a high dispersion. Upon exposure to a H_2/CO mixture, the θ-carbide is readily converted to more carbon-rich carbides, *i.e.* Hägg carbide (χ-Fe_5C_2) for Fe/ZrO_2, and χ-Fe_5C_2 and ε'-$Fe_{2.2}C$ for Fe/K/ZrO_2. The unpromoted catalyst is relatively lowly reduced exhibiting only χ-Fe_5C_2, whereas a more profoundly reduced catalyst reveals both ε'- and χ-carbide. Fischer-Tropsch synthesis at 9.5 bar reveals the two carbides for both unpromoted and potassium-promoted catalysts. These carbides species are believed to remain within the boundary and on top of the mixed oxide layer.

For the unpromoted Fe/ZrO_2 catalyst the decarburization rate is observed to be lower relative to the rate for Fe/K/ZrO_2. It is further found that the metastable ε'-carbide is faster decarburized in a hydrogen environment than the Hägg carbide. The lower stability of ε'-$Fe_{2.2}C$ is also evident when the catalyst is – following Fischer-Tropsch synthesis at 623 K at 9.5 bar – cooled to 300 K. At this temperature, ε'-carbide vanishes completely, it is converted to χ-carbide and oxidized to Fe^{2+}. This process is observed to be reversible. Water – being a primary product of the Fischer-Tropsch reaction – is thought to be responsible for the oxidation. This is confirmed in experiments on a microflow reactor (8.5 g of catalyst). By decreasing the space velocity, the CO conversion and product selectivity do not change. Restoring the original space velocity shows the same indifference. This phenomenon could not be explained by external diffusion limitation. However, it is explained by oxidation of the active carbide, and consequently formation of an inactive iron species. This oxidation process is reversible.

Comparison of the activity and selectivity of Fe/ZrO_2 and Fe/K/ZrO_2 during Fischer-Tropsch synthesis at 10 bar (in a nanoflow reactor), shows that the unpromoted catalyst is much more active, which is explained by a higher reduction degree of the potassium-promoted catalyst leading to large iron particles having less active sites. Moreover, the olefin selectivity is generally higher and the methane fraction lower for the Fe/ZrO_2 catalyst. Despite these good catalytic properties of Fe/ZrO_2, it was chosen to investigate the potassium-rich catalyst on a larger scale due to its higher ethene selectivity. These experiments demonstrate that the catalyst is rather stable and still reveal a relatively high selectivity towards olefins together with a low methane fraction. However, it also produces a large amount of CO_2. It is furthermore established that only part of the catalyst bed is active, the rest of the bed is oxidised to an inactive species due to the relatively high H_2O concentration.

In conclusion, it is shown that a highly disperse iron-based catalyst can be prepared, which is moreover monodisperse. This iron in combination with the ZrO_2 support is able to form a mixed oxide. This mixed oxide plays an important role in stabilising the iron dispersion during the reduction and also during the Fischer-Tropsch synthesis. Another key player is water which is hardly removed out of the pores of the support. It is further shown that the catalysts under study are able to selectively produce ethene and propene without severe deactivation.

Samenvatting

Het is zeer aantrekkelijk lichte olefinen, zoals etheen en propeen, te produceren via een directe route volgens de Fischer-Tropsch reactie. Voor de productie van korte koolwaterstoffen is de vorming van methaan, dat thermodynamisch zeer gunstig is, onvermijdelijk. Aangezien methaan geen wenselijk product is, moet de selectivitiet naar methaan zo laag mogelijk zijn. Bovendien, zijn er nog twee onwenselijke reacties namelijk de Boudouard reactie ($2\ CO \rightarrow CO_2 + C$) en de water gas shift (evenwichts)reactie ($CO + H_2O \leftrightarrow CO_2 + H_2$). Via beide reacties wordt kooldioxide gegenereerd. De Boudouard reactie kan bovendien tot deactivatie leiden door koolstofafzetting op de actieve plaatsen. De mate waarin bovenstaande reacties plaatsvinden hangt af van de reactiecondities en de eigenschappen van de katalysator.

In deze dissertatie zullen zowel de reactiecondities als de katalysatoreigenschappen aan bod komen. De laatste is moeilijker instelbaar, aangezien ze afhankelijk is van onder meer het type actieve metaal, de drager, de deeltjesgrootte en de promotor. Als actief metaal is ijzer gekozen daar ijzer in staat is beter koolmonoxide dan waterstof dissociatief te adsorberen, waardoor meer olefinen geproduceerd kunnen worden. Echter, door deze eigenschap zal een ijzerkatalysator ook sneller deactiveren. Dit pleit voor het gebruik van zeer kleine ijzerdeeltjes, omdat dergelijke deeltjes aanzienlijk langzamer inkolen. Een

geschikte drager moet in staat de kleine deeltjes te stabiliseren en moet bovendien geen interactie aangaan met een eventuele promotor. Om deze reden is gekozen voor zirconiumdioxide (ZrO_2). Verder is een kaliumverbinding genomen als promotor, aangezien kaliium de selectiviteit naar olefinen vergroot en de vorming van korte koolwaterstofketens bevordert.

Het bovenstaande in acht nemende werden twee katalysatoren met zeer kleine ijzeroxidedeeltjes bereid, te weten een ongepromoteerde Fe/ZrO_2 en een met kalium-gedoteerde $Fe/K/ZrO_2$ katalysator. De bereiding en bijbehorende karakterisering staat beschreven in **hoofdstuk 2**. Na de bereiding wordt de katalystor gereduceerd. Een uitgebreide studie bij zowel 1 bar als verhoogde druk wordt behandeld in **hoofdstuk 3**. In **hoofdsuk 4** wordt de invloed van een H_2/H_2O behandeling op de reductie van Fe/ZrO_2 beschreven. Na reductie worden de katalysatoren blootgesteld aan koolmonoxide en waterstof bij verschillende drukken. Een *in situ* Mössbauer studie van de ijzerverbindingen die gevormd worden tijdens de Fischer-Tropsch synthese staat beschreven in **hoofdstuk 5**. **Hoofdstuk 6** handelt over de katalytische activiteit en selectiviteit tijdens de Fischer-Tropsch reactie.

Beide katalysatoren zijn bereid middels de ‘net niet nat’ impregneermethode met een organische citraat precursor. Het voordeel.van deze methode is de verhoging van de viscositeit in de beginperiode van het droogproces. Hierdoor is de precursor niet meer mobiel in de poriën van het dragermateriaal met als gevolg een zeer homogene verdeling van het citraat. Na calcinatie bij 723 K, hetgeen relatief laag is, ontstaat een zeer dunne amorfe ijzeroxidehoudende laag, waarin ook koolstof opgesloten zit. Deze katalystor kent geen verschillende deeltjesgrootteverdeling, louter zeer kleine deeltjes. Zoals gezegd bevat de dunne laag ook koolstof dat is overgebleven van de citraat-precursor na calcinatie. De kalium-gedoteerde katalysator bleek meer koolstof te bevatten.

Deze koolstof beïnvloedt de reductie bij 1 bar, hetwelk cementiet (θ-Fe_3C) voortbrengt. De grotere koolstoffractie op $Fe/K/ZrO_2$ wordt bevestigd door de grotere hoeveelheid cementiet. Echter, deze ijzercarbide wordt niet gevonden tijdens reductie bij 1,8 bar. Dit wordt verklaard door de hogere partiaaldruk van waterstof, waardoor de initieel aanwezige koolstof al bij lage temperaturen (voordat metallisch ijzer gevormd wordt) verwijderd wordt; deze reactie wordt gedreven door thermodynamica. Ondanks dat θ-Fe_3C bij 1 bar reductie gevonden wordt, wordt de initiële koolstof door een H_2/H_2O voorbehandeling bij 1 bar verwijderd. Dientengevolge, wordt, net als bij hoge druk, kleine (superparamagnetische) Fe^0 deeltjes gevonden.

De kalium-gedoteerde katalysator wordt gemakkelijker gereduceerd dan Fe/ZrO_2. De gevonden hogere reductiegraad kan verklaard worden door de aanwezigheid van koolstof of van kalium. Ook tijdens reductie bij hogere druk wordt $Fe/K/ZrO_2$ sneller gereduceerd. Dit feit en het gegeven dat bij hogere druk geen koolstof aanwezig is, laten zien dat kalium de reductie bevordert.

Tijdens de reductie speelt tweewaardig ijzer een vooraanstaande rol. Twee typen Fe^{2+} zijn geanalyseerd, namelijk een slecht geordende Fe^{2+}, dat zich aan het oppervlak bevindt en een goed geordende Fe^{2+}, dat onderdeel uitmaakt van een gemengd oxide met de drager. Deze laatste ijzervorm draagt zorg voor een goede stabiliteit en voorkomt de vorming van magnetiet (Fe_3O_4). Bovendien wordt de hoge dispersie van ijzer gehandhaafd. Een H_2/H_2O behandeling bevordert de vorming van het gemengde Fe^{2+} met als gevolg dat Fe/ZrO_2 (iets) minder goed reduceert. Alhoewel driewaardig ijzer eerst volledig reduceert naar Fe^{2+} zonder dat Fe^0 gevormd wordt, blijkt het stabiliserende Fe^{2+} reeds bij kamertemperatuur snel geoxideerd te worden.

Tijdens de Fischer-Tropsch synthese wordt de gemengde Fe^{2+} species altijd aangetroffen. Zodra θ-Fe_3C blootgesteld wordt aan koolmonoxide en waterstof bij 1 bar, wordt het eenvoudig omgezet in de meer koolstofrijke carbides: Hägg carbide (χ-Fe_5C_2). in het geval van Fe/ZrO_2 en χ-Fe_5C_2 en ε'-$Fe_{2.2}C$. in het geval van $Fe/K/ZrO_2$. Op de relatief laag gereduceerde Fe/ZrO_2 wordt alleen χ-Fe_5C_2 gevormd, terwijl op de meer gereduceerde $Fe/K/ZrO_2$ zowel χ-Fe_5C_2 als ε'-$Fe_{2.2}C$ aangetroffen worden. Deze laatste twee carbides worden ook gevonden tijdens fischer-tropsch synthese bij 9,5 bar. De carbides zouden zich bevinden bovenop een stabiliserende gemengde oxide laag.

Het verwijderen van koolstof uit de carbides op Fe/ZrO_2 is moeilijker in vergelijking tot $Fe/K/ZrO_2$. Bovendien wordt van de beide carbiden de ε'-carbide het eerst ontdaan van koolstof. Deze lagere stabiliteit wordt bevestigd doordat dit carbide verdwijnt nadat de katalysator afgekoeld wordt naar 300 K (volgend op Fischer-Tropsch synthese bij 623 K en 9.5 bar). Op deze temperatuur wordt het ε'-carbide omgezet in het χ-carbide en geoxideerd naar tweewaardig ijzer. Dit proces is reversibel. De oxidatie wordt verklaard door de aanwezigheid van water, dat een primiar product is van de Fischer-Tropsch reactie. Dit wordt bevestigd door experimenten in een microflow reactor (ca. 8,5 g katalysator). Door verhoging van de contacttijd blijven de CO conversie en de productselectiviteiten onveranderd. Het opnieuw instellen van de originele contacttijd laat geen verandering zien. Dit fenomeen kan niet verklaard worden door externe diffusielimitering. Echter, het is

het gevolg van oxidatie van de actieve ijzercarbide, waardoor een inactieve oxide gevormd wordt. Ook hier blijkt het oxidatieproces omkeerbaar te zijn.

Als de activiteit en de selectiveit tijdens de Fischer-Tropsch synthese bij 10 bar van Fe/ZrO_2 en $Fe/K/ZrO_2$ vergeleken worden, blijkt dat de ongepromoteerde Fe/ZrO_2 veel actiever is. Dit wordt verklaard door de hogere reductiegraad van de $Fe/K/ZrO_2$ resulterend in meer grote ijzerdeeltjes, waardoor het aantal actieve plaatsen lager is. Bovendien laat de ongepromoteerde katalysator in het algemeen een hogere selectiviteit naar olefinen en een lagere methaanfractie zien. Desalniettemin is gekozen om $Fe/K/ZrO_2$ te bestuderen in een microflowreactor, doordat de selectiviteit naar etheen hoger is. Deze experimenten demonstreren dat $Fe/K/ZrO_2$ stabiel is en dat deze katalysator een hoge olefine selectiviteit en een lage methaanfractie genereert. Echter, er wordt een grote hoeveelheid kooldioxide gevormd. Verder wordt aangetoond dat slechts een deel van het gehele katalysatorbed actief is, het resterende inactieve deel is geoxideerd als gevolg van een hoge waterpartiaaldruk.

Concluderend, het is aangetoond dat hoog disperse ijzerkatalystoren bereid kunnen worden, die bovendien monodispers zijn. Verder is duidelijk geworden dat ijzer een sterke interactie met de ZrO_2 drager kan aangaan door vorming van een gemengd oxide. Dit gemengde oxide vervult een prominente rol tijdens de reductie en de Fischer-Tropsch synthese. Ook water speelt een sleutelrol daar het moeilijk uit de dragerporiën te verwijderen is. Het wordt verder aangetoond dat de bestudeerde katalysatoren selectief etheen en propeen kunnen produceren zonder ernstige deactivering.

Dankwoord

Met een voldaan gevoel ontdek ik dat ik toe ben gekomen aan mijn dankwoord. Beseffende dat een dankwoord nooit volledig kan zijn, wil ik hierbij iedereen bedanken die heeft bijgedragen tot de totstandkoming van mijn dissertatie. Iedere positieve bijdrage, hoe klein ook, heb ik zeer gewaardeerd. Bedankt.
Er zijn een aantal mensen die ik in het bijzonder wil bedanken. Allereerst natuurlijk mijn promotor John Geus. John, ik wil je bedanken voor de grote vrijheid tijdens mijn promotie-onderzoek en je nooit aflatende enthousiasme. Vooral in de laatste spannende weken voor het gereedkomen van dit boekje is onze relatie enorm geïntensiveerd. Ik denk dat ik me later nog eens zal afvragen, hoe we uiteindelijk zoveel werk hebben kunnen verzetten in zo'n korte tijd.
Mijn boekje kan alleen zulke prachtige Mössbauer metingen bevatten door de noeste arbeid van Adri van der Kraan en Menno Crajé. Menno, fantastisch dat je zelfs de avond voor je vakantie nog tijd vond om plaatjes voor mijn boekje te maken. Adri, ik zal me je altijd herinneren als mijn grote stimulans, een doortastende wetenschapper en kritisch docent. Ik ben blij dat jij mijn co-promoter bent.
Natuurlijk wil ik ook Michiel Huisman, Hans Geerlings, Peter van de Brink en Martijn van Hardeveld van Shell Research and Technology Centre Amsterdam bedanken. Ik heb onze samenwerking altijd als zeer prettig ervaren en vooral de discussies en mijn korte verblijf in Amsterdam waren zeer inspirerend.
Speciale dank ben ik Patricia Kooyman verschuldigd. Patricia, ik stond versteld hoe snel jij met de electronenmicroscoop mooie plaatjes tevoorschjn kunt toveren. Twee van zulke plaatjes staan in hoofdstuk 2.
Ik wil alle (ex)collega's en studenten bedanken voor de vele interessante discussies, gezellige eetfestijnen en fanatieke sportwedstrijden. In het bijzonder wil ik Tias en Bok noemen. Onze gesprekken, volleybalwedstrijden, fiets- en skatetochten zijn mij het meest bijgebleven. Ook de laatste marathonzit voor de (drukkers)deadline zal ik niet snel vergeten. Bedankt dat jullie mijn paranimfen willen zijn.
Ook wil ik mijn vrienden bedanken voor de vele ontspannende momenten en blijvende interesse.
Zonder mijn ouders had ik nu niet dit dankwoord kunnen schrijven: pa en ma bedankt. In het bijzonder wil ik mijn schoonouders bedanken. Ricky en Marius, jullie hartelijkheid en steun zijn voor mij van onschatbare waarde. En natuurlijk

Mariuske, jij hebt mij laten inzien dat de macht der kennis ondergeschikt is aan de kracht van de liefde.
Ik draag dit proefschrift op aan mijn twee grote liefdes: Elize en Gioia. Mijn kleine Gioia, al sinds je geboorte geef je mij inspiratie en kracht.
Elize,ik zou je tekort doen als ik probeer te verwoorden wat jij voor mij betekent. Queste parole dicono tanto…e più: ti amo per sempre.

Frans

Curriculum Vitae

Frans van den Berg werd geboren op 14 mei 1972 te IJsselmuiden. In juni 1990 behaalde hij het VWO diploma aan het Almere College te Dronten/Kampen. In datzelfde jaar begon hij met de studie Scheikunde aan de Universiteit Utrecht. In augustus 1991 werd het propedeutisch examen afgelegd. In het kader van het bijvak Infrarood Spectroscopy heeft hij 3 maanden aan The University of Southampton onderzoek gedaan. Vervolgens is hij begonnen met het hoofdvak Anorganische Chemie en Katalyse. In aansluiting daarop heeft hij 5 maanden stage gelopen bij de Nederlandse Gasunie in Groningen. In mei 1995 werd het doctoraalexamen behaald.
Op 1 juni 1995 trad hij in dienst als assistant-in-opleiding bij de vakgroep Anorganische Chemie en Katalyse van de Universiteit Utrecht. Onder leiding van prof.dr.ir. J.W. Geus is het in dit proefschrift beschreven onderzoek verricht. Vanaf 1 maart 2000 is hij werkzaam bij ASM Lithography B.V. in Veldhoven.